Synthesis and Analysis of Amino-Functionalised Mesoporous Silica

---

Dissertation

zur

Erlangung der naturwissenschaftlichen Doktorwürde (Dr. sc. nat.)

vorgelegt der

Mathematisch-naturwissenschaftlichen Fakultät

der

Universität Zürich

von

Hanna Taina Katariina Ritter

aus Finnland

Promotionskomitee

Prof. Dr. Heinz Berke (Vorsitz)

Dr. Dominik Brühwiler (Leitung der Dissertation)

Zürich, 2009

Synthesis and Analysis of Amino-Functionalised Mesoporous Silica

---

Dissertation

zur

Erlangung der naturwissenschaftlichen Doktorwürde (Dr. sc. nat.)

vorgelegt der

Mathematisch-naturwissenschaftlichen Fakultät

der

Universität Zürich

von

Hanna Taina Katariina Ritter

aus Finnland

Promotionskomitee

Prof. Dr. Heinz Berke (Vorsitz)

Dr. Dominik Brühwiler (Leitung der Dissertation)

Zürich, 2009

Abstract

The regularly ordered pore arrangement and the narrow pore size distribution of mesoporous silica offer possibilities for several applications such as drug delivery and controlled release. A successful implementation requires methods that allow the selective functionalisation of external and internal surfaces. A convenient and scale-up friendly procedure for synthesising high quality mesoporous silica MCM-41 at room temperature was developed. Amino-functionalised samples were analysed using several methods to understand the grafting behaviour of aminopropylalkoxysilanes. The distribution of amino groups on mesoporous silica surfaces was evaluated by analysing textural properties and amino group loadings, as well as by labelling the amino groups with fluorescein isothiocyanate (FITC) for photoluminescence spectroscopy. A reliable method to determine the amount of grafted amino groups over a wide range of loadings was developed. The functionalisation of mesoporous silica by vapour phase deposition was studied as an alternative to the common solvent based techniques. The accessibility of amino groups anchored on selected mesoporous silicas was investigated by FITC coupling. One-dimensional channel systems with small pores (3.1 nm and 3.9 nm) and large pores (7.6 nm) as well as three-dimensional channel systems were compared to non-porous silica. Several methods for the selective functionalisation of the external surface of mesoporous silica were critically evaluated.

Kurzfassung

Die regelmässige Anordnung der Poren und die schmale Verteilung der Porengrössen von mesoporösem Silica bieten eine Vielzahl von Anwendungsmöglichkeiten, wie Wirkstofftransport und kontrollierte Abgabe. Eine erfolgreiche Umsetzung verlangt nach Methoden, die die selektive Funktionalisierung von äusseren und inneren Oberflächen ermöglichen. Es wurde eine einfache und in grossem Ansatz durchführbare Raumtemperatur-Synthese für qualitativ hochstehendes mesoporöses Silica MCM-41 entwickelt. Aminofunktionalisierte Proben wurden mit verschiedenen Methoden analysiert, um das Reaktionsverhalten von Aminopropylalkoxysilanen zu verstehen. Die Verteilung von Aminogruppen auf der Oberfläche des mesoporösen Silicas wurde durch Analyse von strukturellen Eigenschaften und Aminobeladungen evaluiert. Aminogruppen wurden mit Fluoresceinisothiocyanat (FITC) gekoppelt und mittels Lumineszenzspektroskopie analysiert. Ein verlässliches Verfahren zur Bestimmung der Aminogruppenbeladung wurde entwickelt. Als alternative Methode zur Lösungsmittel-basierten Synthese wurde die Funktionalisierung von mesoporösem Silica durch Abscheidung aus der Gasphase untersucht. Die Zugänglichkeit von oberflächengebundenen Aminogruppen, wurde durch FITC Kopplung bestimmt. Eindimensionale Porensysteme mit kleinen (3.1 nm und 3.9 nm) und grossen Poren (7.6 nm), sowie dreidimensionale Porensysteme (MCM-48) wurden mit nicht-porösem Silica verglichen. Mehrere Methoden für die selektive Funktionalisierung der äusseren Oberfläche von mesoporösem Silica wurden kritisch evaluiert.

Tiivistelmä

Mesohuokoisen silikan säännöllisesti järjestäytyneet huokoset sekä niiden suppea huokoskoon jakauma mahdollistavat useita käytännän sovelluksia kuten lääkeaineiden kuljetuksen ja kontrolloidun vapauttamisen. Menestyksekäs toteutus vaatii menetelmän, joka sallii silikan ulko- ja sisäpintojen funktionalisoinnin erikseen. Tässä työssä kehitettiin käyttäjäystävällinen ja silikamäärän säätelemisen mahdollistava menetelmä, jolla voidaan syntetisoida huoneenlämmössä erittäin laadukasta mesohuokoista silikaa MCM-41. Aminoryhmillä muokattuja silikanäytteitä analysoitiin useilla eri menetelmillä, jotta ymmärrettäisiin aminopropyylialkoksisilaanien käyttäytymistä reaktio-olosuhteissa. Aminoryhmien jakautumista mesohuokoisen silikan pinnalla tutkittiin analysoimalla rakennetta, aminoryhmien määrää sekä merkitsemällä aminot fluoresiini-isotiosyanaatilla (FITC) fotoluminesenssi-spektroskopiaa varten. Työssä kehitettiin luotettava menetelmä aminoryhmien määrän analysoimiseksi. Kaasufaasireaktioiden soveltumista mesohuokoisen silikan pinnoittamiseksi tutkittiin korvaamaan perinteisiä liuotinmenetelmiä. Animoryhmien saavutettavuutta valikoiduissa huokoisissa silikoissa tutkittiin FITC reaktioiden avulla. Erilaisia silikoita, joilla on yksidimensionaalinen huokosrakenne pienin huokosin (3.1 nm ja 3.9 nm), isoin huokosin (7.6 nm) tai kolmiuloitteinen huokossysteemi, verrattiin ei-huokoisen silikaan. Tutkimuksessa kokeiltiin useita menetelmiä selektiivisesti ulkopinnan muokkaamiseksi aminoryhmillä.

Acknowledgement

Experimental work of this thesis was carried out during the years 2005 - 2008 at the Institute of Inorganic Chemistry, University of Zürich.

I am very grateful to my supervisor, Dr. Dominik Brühwiler, for his continuous support and encouragement. His genuine interest and advice have been a big contribution to my work.

Prof. Dr. Heinz Berke is acknowledged for chairing my defence and for financial support. Swiss National Science Foundation and the European Commission through the Human Potential Program (Marie-Curie RTN Nanomatch) provided financial support.

I am thankful to Dr. Minna Nieminen and Prof. Dr. Maarit Karppinen (Laboratory of Inorganic Chemistry, Helsinki University of Technology, Finland) for giving me the possibility to do the vapour phase experiments in the spring 2007. It was a pleasure to enjoy “the old times” for a while.

I want to thank sincerely all of the group members, Le-Quyenh Dieu, Jan Hinrich Ramm, Dr. Christophe Bauer, Dr. Igor Dolamic and Nando Gartmann, for help and discussions as well as the good atmosphere in the lab. Also the former group members are thanked. The entire personnel of ACI are thanked for pleasant working environment and for their practical advices whenever needed.

My parents are warmly acknowledged for their loving encouragement during my studies. My brother, Jussi, and his family, Jessica and Ukko, are thanked for helping me to look things from another view.

Loving thank you is dedicated to my husband, Stefan, for his continuous support and understanding. Now it is time to start our adventure.

Zürich, January 2009

Hanna Ritter

List of Abbreviations and Acronyms

ALD	Atomic layer deposition
APAS	Aminopropylalkoxysilane
APDIPES	3-Aminopropyldiisopropylethoxysilane
APDMMS	3-Aminopropyldimethylmethoxysilane
APTES	3-Aminopropyltriethoxysilane
APTMEES	3-Aminopropyltrimethoxyethoxyethoxysilane
APTMS	3-Aminopropyltrimethoxysilane
BET	Brunauer-Emmett-Teller
BJH	Barrett-Joyner-Halenda
BTESPA	Bis(triethoxysilyl)propylamine
BTMSPA	Bis(trimethoxysilyl)propylamine
CTAB	Cetyltrimethylammonium bromide
DFT	Density functional theory
DRIFTS	Diffuse reflectance infrared fourier transform spectroscopy
FITC	Fluoresceinisothiocyanate
FMOC*	2,7-di-tert-butyl-9-fluorenylmethylchloroformate
HT-MCM-41	High temperature MCM-41
MAPMDMS	[3-(Methylamino)propyl]methyldimethoxysilane
MAPTMS	[3-(Methylamino)propyl]trimethoxysilane
LCT	Liquid crystal templating
PL	Photoluminescence
PSD	Pore size distribution
RT-MCM-41	Room temperature MCM-41
SDA	Structure directing agent
SEM	Scanning electron microscopy
TEOS	Tetraethoxysilane
XRD	Powder X-ray diffraction

Table of Contents

1. Introduction

The discovery of the M41S[1] family of materials in the early 1990s offered new possibilities in the field of silicate-based molecular sieves. Potential applications of these highly ordered mesoporous materials are manifold, including photonics[2], drug delivery[3] and nanotechnology[4] as well as catalysis[5] and adsorption[6]. The definition of IUPAC divides porous materials in three classes according to their pore size (Figure 1.1)[7].

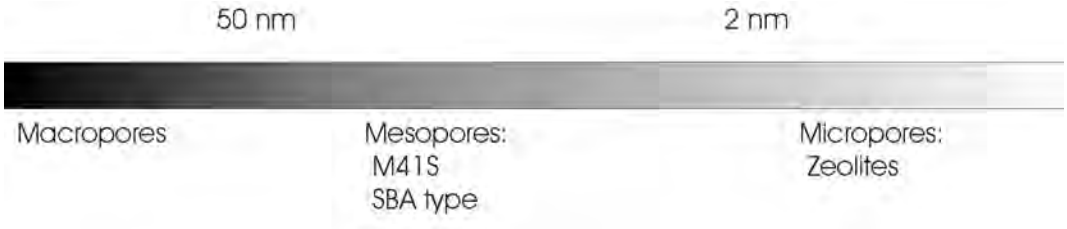

Figure 1.1. Definition of micro-, meso- and macroporous materials with examples.

MCM-41 (Mobil Composition of Matter) is a member of the M41S family and consists of hexagonal arrays of non-intersecting, uniform channels of narrow pore size distribution. High surface area (900 m^2/g) and large pore volume (0.75 cm^3/g) are additional properties of MCM-41. The mesoporous class includes other materials such as MCM-48 with cubic structure and SBA-15 with a hexagonal structure which can be prepared with larger pore diameter than MCM-41. The synthesis of MCM-41 is accomplished by liquid crystal templating (LCT)[8], also referred to a soft-templating[9]. The method (Figure 1.2) is based on the formation of micellar rods from the structure directing agent (SDA). Addition of a silica source to the solution leads to the condensation of silica around the rods which arrange in a hexagonal pattern. The pores become accessible after the SDA is removed by calcination or extraction.

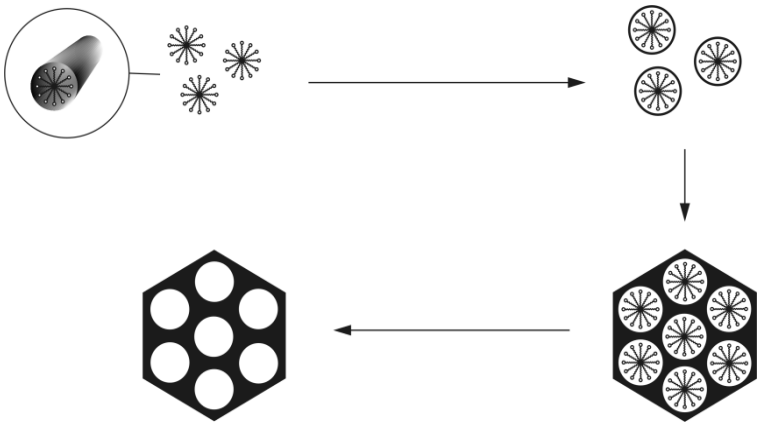

Figure 1.2. Liquid crystal templating method for synthesising MCM-41.

The properties of the mesoporous silica can be changed by binding functional groups to the surface silanols. Amine modified mesoporous silicas are of interest in the fields of analytical chemistry[10], materials chemistry[11], biochemistry[12], catalyst technology[13] and chromatography[14]. Functionlisation of the surface is possible via two different methods (Figure 1.3). In the postsynthetic modification method (also known as grafting), the silica surface is functionalised after the complete formation of the mesoporous structure. Grafting yields and functional group distributions are affected by the reactivity of the molecule containing the functional group as well as steric factors and diffusion limitations. The most readily accessible sites on the outer surface and close to the pore entrances are modified preferentially, while internal sites may remain unreacted[15]. The co-condensation method is a one-pot procedure where molecules containing the desired functional groups are added during the synthesis of the mesoporous silica. These molecules must contain a group which enables condensation with the silica source. This single step modification method is believed to result in an even distribution of the functional groups. However, silane inclusion into the pore walls can occur. Co-condensation synthesis yields thicker walls but the hydrothermal stability is often not as good as for the postsynthetically modified mesoporous silica[16].

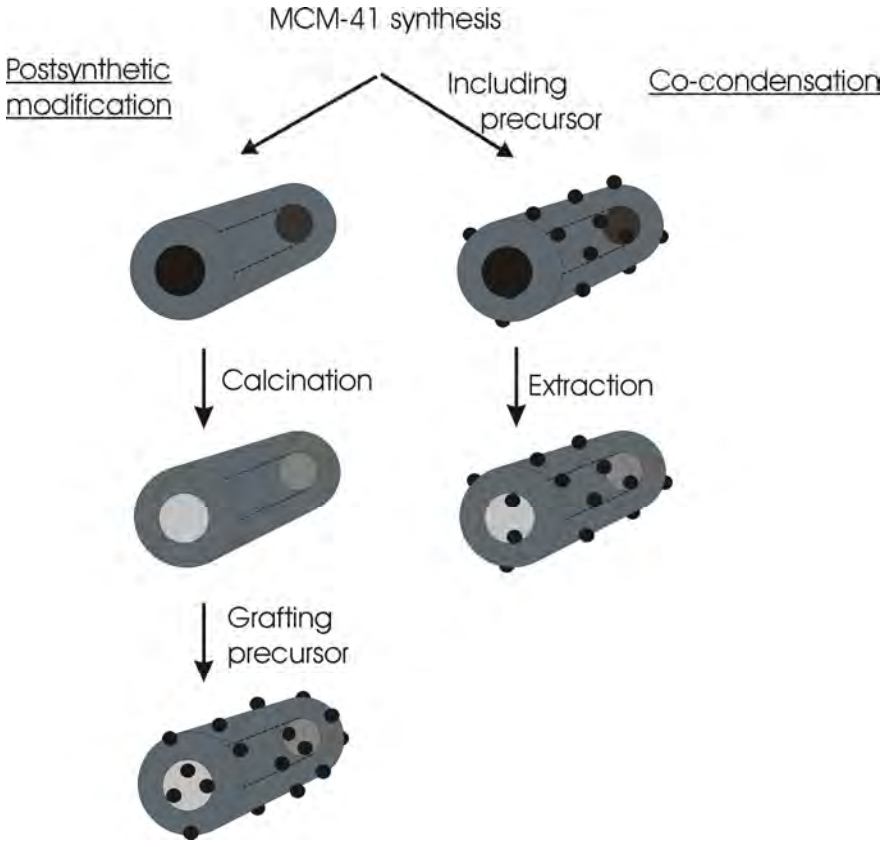

Figure 1.3. Two different modification methods, grafting and co-condensation.

The motivation for this work is the potential application of non-toxic and biocompatible mesoporous silica as a drug delivery device. The size of particles injected into the human circulatory system has to be less than 300 nm[17] and this can be achieved with mesoporous silica[18]. The large surface area enables efficient drug adsorption. Controlled drug loading and release can be achieved by appropriate functionalisation. [3]

Although non-modified mesopores are also adequate for drug release, amino-functionalised MCM-41 and SBA-15 have shown an even more effective controlled release of ibuprofen[19,20]. For ideal drug delivery, mesoporous particles need to have differently modified outer and inner surface. The pore surface adsorbs the drug molecules whereas the pore entrance is modified with gate molecules for accurate release. The outer surface has to be appropriately modified for compatibility with blood and for directing the drug carriers to the target cells.[3]

Controlled grafting on outer and inner surfaces was one goal of this work. The research further focused on the analysis of the functional group distribution on the mesoporous silica surface, which is also important for developing and evaluating new functionalisation methods. The amino group distribution, influence of water, pore blocking and deposition from the vapour phase have been studied in detail.

2. General Background to Materials and Experiments

The main features of materials, surface modification methods and some of the applied characterization methods are introduced in the following. Synthesis methods of different mesoporous silicas are described and compared.

2.1 Materials

2.1.1 MCM-41

MCM-41 used in this work has been synthesised according to literature[21]. The synthesis started with dissolving 2.2 g of hexacetyltrimethylammonium bromide (CTAB) in a mixture of 52 ml of distilled water and 24 ml of 25 % NH_3 under slight heating. Tetraethoxysilane (TEOS, 10 ml) was added dropwise to the clear solution at room temperature. The obtained white gel was further stirred for 3 h and afterwards transferred to an autoclave for aging at 110 °C for 48 h. After cooling, the gel was filtered and the product was washed with at least 800 ml of distilled water. Removal of the SDA was performed at 550 °C for 12 h. The heating rate was 2 °C/min and the temperature was held at 300 °C for 2 h. The maximum yield was 2.6 g of calcined MCM-41.

SDA removal can be followed by infrared spectroscopy (IR). Figure 2.1 shows the IR spectra of MCM-41 before and after calcination. The absence of bands at 2925 cm^{-1} and 2850 cm^{-1} ($\nu(CH_2)$) as well as 1460-1475 cm^{-1} ($\delta_s(CH_2)$) confirms the removal of the SDA. The hexagonal structure can be detected by powder X-ray diffraction (XRD).

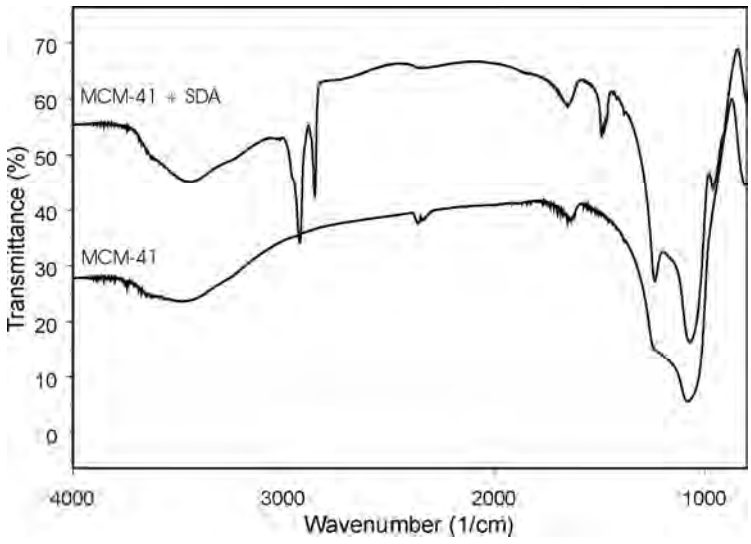

Figure 2.1. IR spectra of MCM-41 in a KBr pellet before and after SDA removal.

It is possible to synthesise high quality MCM-41 without using an autoclave. Two slightly different methods were developed. Room temperature MCM-41 (RT-MCM-41) was synthesised following the procedure for high temperature MCM-41 (HT-MCM-41) aged at high temperature with the difference that the white gel was aged at room temperature for 24 h. An even faster method, which included filtering the white gel immediately after TEOS addition was also evaluated (Fast RT-MCM-41). Calcination was performed as described above. Pore size distributions (PSDs) of these three samples are shown in Figure 2.2. XRD patterns (Figure 2.3) are similar for both MCM-41 syntheses. The shift to smaller angles is due to the slightly smaller pores of RT-MCM-41. The relative changes in total pore volume upon stirring in water for 24 h reveal the excellent stability of RT-MCM-41 and indicate the importance of aging (comparison with Fast RT-MCM-41). Table 2.1 compares textural and stability data of the HT- and RT-MCM-41 samples.

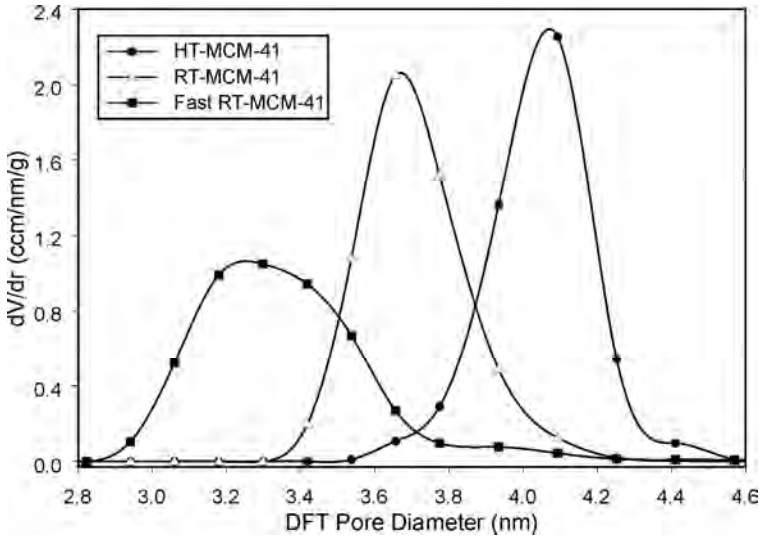

Figure 2.2. PSDs of HT-, RT- and Fast RT-MCM-41 analysed by DFT (adsorption).

The advantage of the RT-MCM-41 synthesis is that there is no need for an autoclave and therefore scaling up the synthesis is straightforward. Scale up to ten times the standard procedure was performed, resulting in high quality RT-MCM-41.

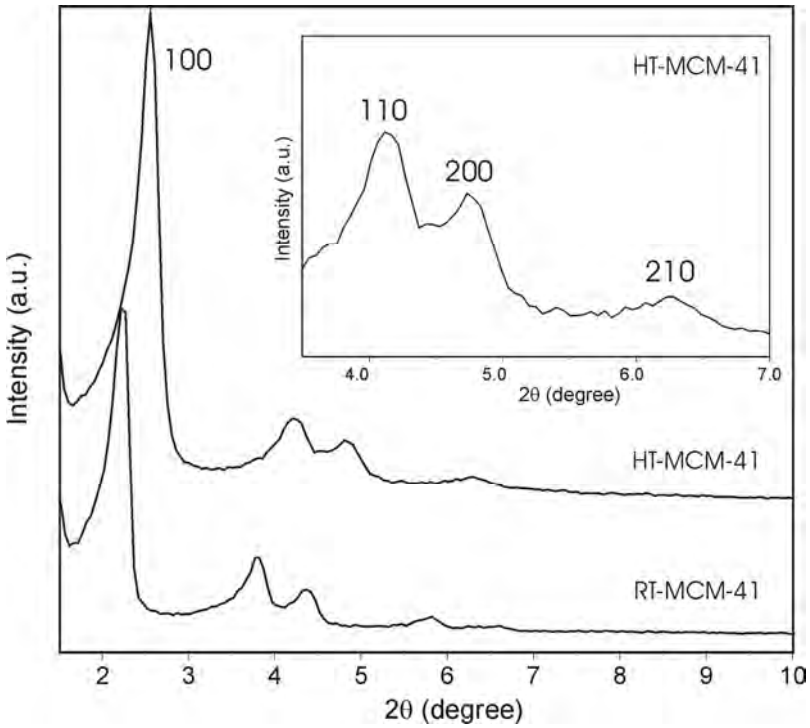

Figure 2.3. XRD of HT-MCM-41 and RT-MCM-41.

Table 2.1. Textural and stability data of HT- and RT-MCM-41 samples.

	HT-MCM-41	RT-MCM-41	Fast RT-MCM-41
Pore size (DFT) (nm)	4.1	3.7	3.3
BET (m^2/g)	896	957	976
External Surface (m^2/g)	67	93	104
Total Pore Volume (cm^3/g)	0.76	0.78	0.69
Primary Mesopore Volume (cm^3/g)	0.69	0.66	0.54
Stability in H_2O after 24 h (Total Pore Volume) %	88	84	70

2.1.2 Other Mesoporous Silica Types

Apart from MCM-41, mesoporous silica MCM-48 and SBA-15 were used in this work. MCM-48 has (for a given SDA) a pore diameter similar to MCM-41, but the pores are connected to each other three-dimensionally (Figure 2.4). Like MCM-41, SBA-15[22] features a hexagonal pore structure, but with thicker walls and typically larger pores. Intrawall porosity, which can be as high as 30 % of the total porosity[23], is often observed for SBA-15, depending to a certain extent on the synthesis temperature[24]. Intrawall pores include micropores[25], which provide connectivity between the primary mesopores.[26]

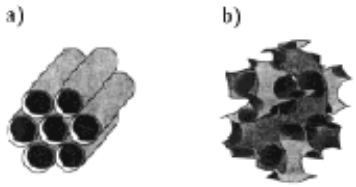

Figure 2.4. Different pore structures, (a) MCM-41 and (b) MCM-48[27]

As an example of pore diameter tuning, MCM-41(12) was synthesised with a SDA featuring a C_{12}-chain instead of the standard C_{16}. We have also investigated nano-MCM, which has a hexagonal mesoporous structure, even though the particle size is only 50 nm[28]. Fumed silica was used as a non-porous reference. Figure 2.5 shows the corresponding PSDs. Powder XRD measurements of MCM-48 and MCM-41(12) are given in Figure 2.6.

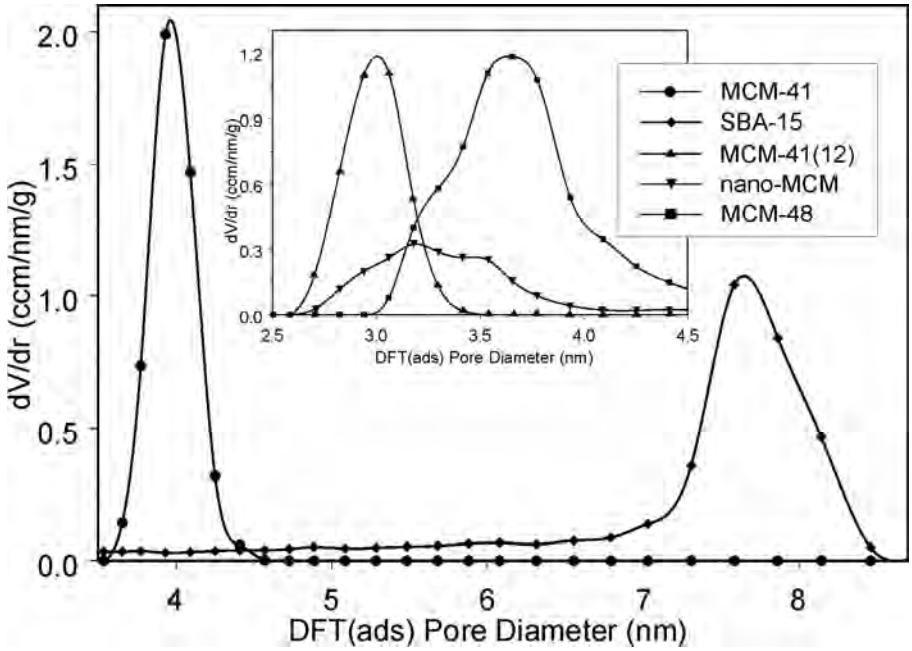

Figure 2.5. Typical DFT pore size distributions of mesoporous silicas used in this work. Calculations are based on the adsorption isotherms.

Table 2.2 compares the textural properties of the different silica types. The rather large total pore volume of nano-MCM is due to the interparticle spaces[28]. As a consequence of the small particle size, the external surface is significantly larger compared to the other silicas. The primary mesopore volume corresponds to the uniform mesopore volume, whereas the total pore volume additionally includes disordered secondary mesopores and interparticle spaces.

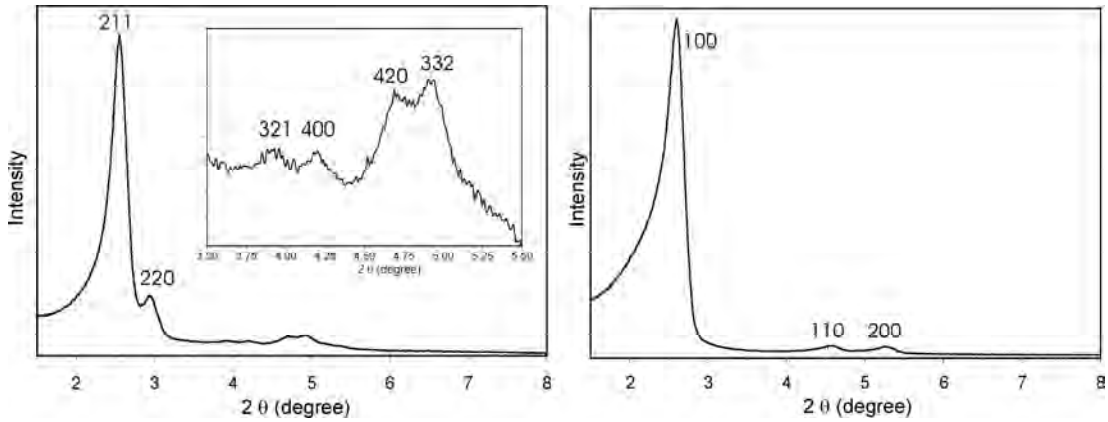

Figure 2.6. XRD of MCM-48 (left) and MCM-41(12) (right).

Table 2.2. Comparison of different silica types.

	MCM-41	MCM-41(12)	MCM-48	SBA-15	Nano-MCM	Fumed Silica
Particle size (µm)	1-2	1-2	1-2	1-2	0.02-0.05	0.014
DFT Pore size (nm)	3.93	3.06	3.66	7.59	3.18	-
BET (m^2/g)	900	1000	1100	860	600	200
External surface (m^2/g)	67	35	173	55	340	200
Primary Mesopore Volume (cm^3/g)	0.69	0.44	0.81	1.07	0.17	-
Total Pore Volume (cm^3/g)	0.76	0.48	0.98	1.15	0.81	-

MCM-48 was synthesised according to the literature[29], dissolving CTAB (8.8 g) in 80 ml of water under slight heating. After the solution was cooled to room temperature, 10 ml of 2 M aqueous solution of NaOH was added followed by dropwise addition of 10 ml of TEOS. The mixture was stirred for 30 min before aging in an autoclave at 100 °C for 72 h. The product was filtrated, washed with 2 l of H_2O and left to dry under ambient conditions. Calcination was carried out as reported for MCM-41[2]. 2.0 g of calcined MCM-48 was obtained.

SBA-15 was synthesised as follows[22]; 2.2 g of Pluronic P123 $EO_{20}PO_{70}EO_{20}$, 49 ml of H_2O and 31 ml of 4 M aqueous HCl was stirred with slight heating until a clear solution was obtained. 5 ml of TEOS was added slowly and the mixture was stirred for 20 h at room temperature. After aging in an autoclave at 100 °C for 24 h, the product was obtained by filtration and washed with 1 l of H_2O. After drying under ambient conditions, the material was calcined at 500 °C (with a heating rate of 1.2 °C/min) for 16 h, yielding 2.8 g of product.

Nano-MCM[28] synthesis starts with dissolving 7.8 g of cetyltrimethylammonium chloride and 6.0 g of Pluronic F127 $EO_{106}PO_{60}EO_{106}$ into 90 ml of 0.8 M aqueous HCl under stirring. TEOS (11.1 ml) was added dropwise to the clear solution and stirred for 20 h at room temperature. 11.1 ml of 25 % NH_3 was slowly added and the mixture was aged at room temperature for 44 h. The product was dried at 70 °C for 72 h and the surfactants were removed by calcination at 600 °C (heating rate of 2 °C/min) for 3 h. 2.8 g of nano-MCM was obtained.

MCM-41(12) is synthesised according to the method reported for MCM-41 but using 1.86 g dodecyltrimethylammonium bromide as SDA. The yield was 2.0 g of calcined material.

2.1.3 Aminopropylalkoxysilanes

Different aminopropylalkoxysilanes (APASs) were used for surface modification. Several types of APASs with interesting properties are commercially available (Figure 2.7). The purpose of the first part of this work was to compare the grafting behaviour of these silanes.

(3-Aminopropyl)dimethylmethoxysilane (APDMMS, Acros), (3-aminopropyl)di-isopropylethoxysilane (APDIPES, Gelest), (3-aminopropyl)trimethoxysilane (APTMS, Fluka), [3-(methylamino)propyl]trimethoxysilane (MAPTMS, Gelest), (3-amino-propyl)triethoxysilane (APTES, Fluka), bis(trimethoxysilyl)propylamine (BTMSPA, Fluka), bis(triethoxysilyl)propylamine (BTESPA, Gelest), and [3-(methylamino) propyl]methyldimethoxysilane (MAPMDMS, Gelest) were used as received and stored under dry conditions.

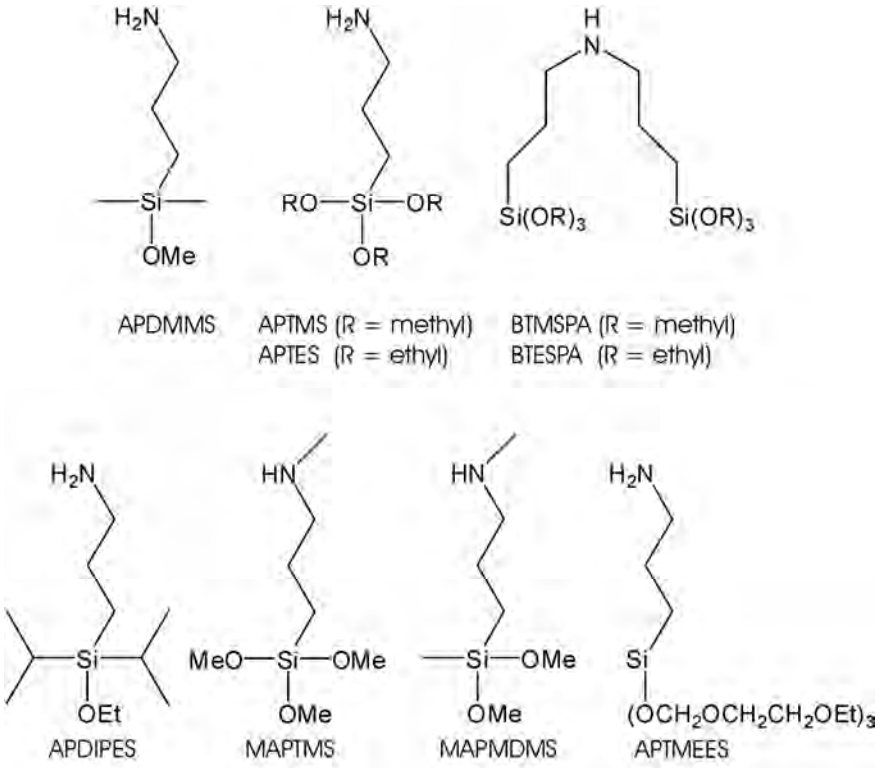

Figure 2.7. APASs for the functionalisation of mesoporous silica.

2.2 Surface Modification

Postsynthetic modification is a common method to prepare functionalised mesoporous silica using the silanol groups on the surface. Approximately 3 silanol groups per nm^2 are found on the surface of mesoporous silica, depending to a certain extent on the silica type and the calcination or extraction method.[30] Figure 2.8 shows the grafting mechanism of APTMS with self-catalysis [31].

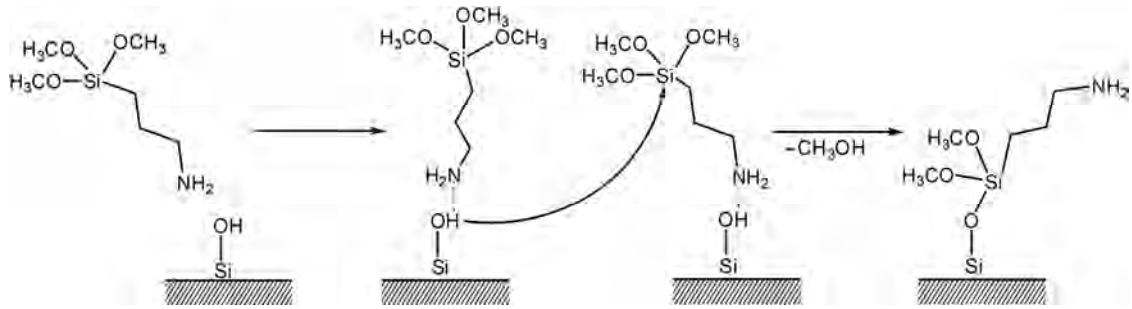

Figure 2.8. Postsynthetic surface modification with APTMS.

2.2.1 Reactions in Solution

Reactions are generally conducted in an organic solvent. In a typical grafting experiment, 500 mg of oven-dried (80 °C, 1 h) silica was dispersed in 30 ml of solvent. After APAS addition, the suspension was refluxed for 3 h including 15 min for the suspension to warm up to the required temperature. The suspension was allowed to cool to room temperature for 30 min. The product was recovered by filtration, washed with 100 ml of ethanol and oven-dried at 80 °C for 1 h.

2.2.2 Vapour Phase Reactions

In order to eliminate the effect of trace water, we have also investigated vapour phase reactions. Vapour phase reactions were made using an atomic layer deposition (ALD) reactor (F-120 ASM Microchemistry Ltd., Espoo, Finland). ALD was developed for surface coating and is based on cycles of vapour phase reactions. The surface of the substrate controls the growth of the film[32]. It is known that vaporised precursor molecules are deposited in a highly reproducible and homogeneous manner on open surface[33].

Reactions were carried out at pressure of 35-50 mbar. MCM-41 (2.1 g) was preheated at 180 °C for 2 h to remove physisorbed water. APTMS (2.5 ml) was vaporised at 100 °C and deposited onto the MCM-41 bed at a reaction temperature of 150 °C. Physisorbed APTMS molecules were then purged from the surface with nitrogen gas. A 0.5 cm thick layer (ca. 0.3 g) from the top of the silica bed was removed and the remaining sample was analysed.

2.2.3 Fluorescein Labelling

FITC (fluorescein 5-isothiocyanate, isomer I from Fluka, purity > 97.5 % or from Sigma-Aldrich, purity > 90%) is a common labelling reagent for biomolecules. It has further been used to prepare mesoporous thin films with pH-sensing abilities[34]. FITC forms a thiourea linkage in the reaction with a primary or secondary amine, as shown in Figure 2.9.

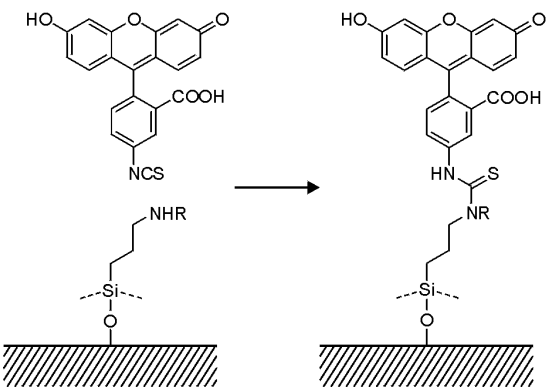

Figure 2.9. Reaction of FITC with a surface-grafted amino group.

FITC coupling amplifies the PSD differences between amino-functionalised mesoporous silicas with different amino group distributions. Depending on the intermolecular distance, fluorescein undergoes self-quenching due to resonance energy transfer. The Förster radius of fluorescein is 42 Å[35]. This opens possibilities to investigate the amino group distribution on the silica surface by photoluminescence (PL) spectroscopy for samples with identical FITC loadings. High intensity indicates a uniform distribution, while low intensity suggests clustering of amine sites.

Fluorescein is a dark red brownish solid, whereas FITC is dark orange. FITC coupled samples with low FITC loadings are bright and pale yellow. Upon increasing the loading, the colour becomes more intense and comparable to solid FITC. High luminescence intensity increases the brilliance of the colours. Figure 2.10 shows examples of FITC coupled amino-functionalised MCM-41 samples with different FITC loadings.

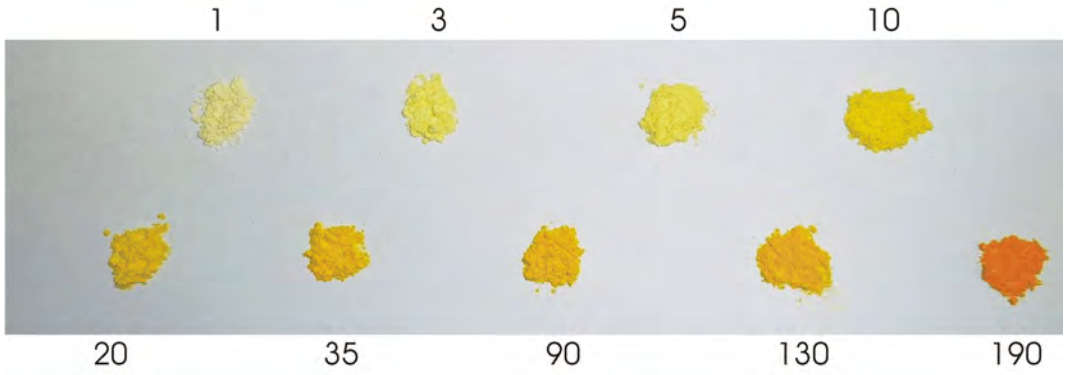

Figure 2.10. Different shades of yellows of FITC coupled MCM-41 samples. The numbers refer to the respective FITC loading in nmol/mg.

FITC coupling was achieved as follows; a 1.5-fold excess (calculated from the amino loading) of FITC dissolved in ethanol was mixed with either 100 mg or 250 mg of silica and stirred for 24 h in the dark. The product was obtained by filtration and washed with 50 ml of ethanol. For complete removal of unreacted FITC, the product was dispersed in 50 ml of ethanol, stirred for 20 min and washed with 50 ml of ethanol

after filtration. The product was oven-dried at 80 °C for 1 h. The amount of FITC used in the reaction was calculated from the theoretical amino loading (in the case of low functionalisation degree) or from the analysed NH_2 content (for highly functionalised samples).

The FITC loading was analysed by dissolving 15 mg of amino-grafted silica in 25 ml of a 0.2 M aqueous solution of NaOH. A clear solution was typically obtained after 3 h. The concentration was determined by UV-vis at 490 nm. Water was employed as a reference. An extinction coefficient of 88000 M^{-1}/cm[36] or 75000 M^{-1}/cm was used. The latter value was determined based on a stock solution prepared as follows: FITC was coupled to APTMS in a 1:1 molar ratio by stirring in ethanol for 15 h at room temperature. After removal of the ethanol by evaporation, a weighed amount of the dry residue was dissolved in 50 ml of 0.2 M aqueous NaOH containing 50 mg of dissolved silica.

2.3 Characterisation Techniques

Textural properties such as pore diameter, surface area and pore volume were analysed by nitrogen sorption at 77 K. The periodic arrangement of the pores was determined by XRD. Particle size and morphology were investigated by scanning electron microscopy (SEM).

UV-vis was used for analysing FITC loadings after dissolving the samples in NaOH solution. Photoluminescence (PL) spectroscopy was used for solid, dispersion and solution samples to evaluate the amino distribution on the silica surface as well as the amount of grafted amino groups. Infrared (IR) spectroscopy was used to analyse SDA removal and binding modes. Qualitative analyses of surface species on silica were made by diffuse reflectance infrared fourier transform spectroscopy (DRIFTS).

A Quantachrome Nova 2200 was used for all N_2 sorption measurements. Samples were vacuum-degassed at 80 °C for 3 or 5 h. Nitrogen sorption as well as the amino group analysis for mesoporous silica based samples, which was specifically developed for this work, are discussed in more detail in the next chapters.

2.3.1 N_2 sorption

N_2 sorption was used to determine the textural properties of the mesoporous materials i.e. the surface area and pore size distribution. The sample has to be

degassed and weighed precisely for N_2 sorption studies. The measurement is made at 77 K. Nitrogen is adsorbed or desorbed until a predetermined relative pressure p/p_0 is achieved. Isotherms are obtained by plotting the relative pressure against the adsorbed N_2 volume. IUPAC has defined six different types of isotherms (Figure 2.11)[7]. Selected MCM-41, MCM-48, SBA-15 and fumed silica isotherms are shown in Figure 2.12.

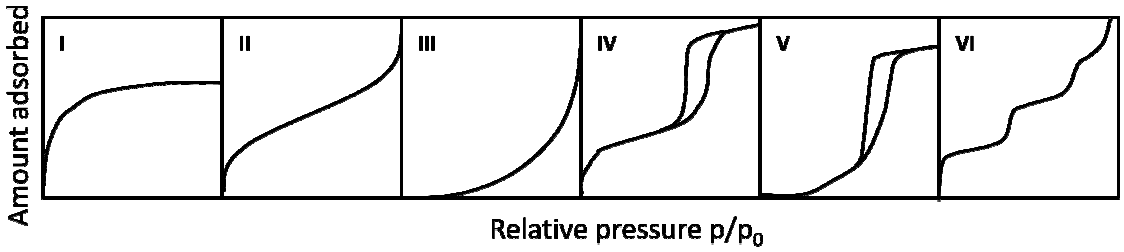

Figure 2.11. Isotherm types I-VI according to IUPAC[7].

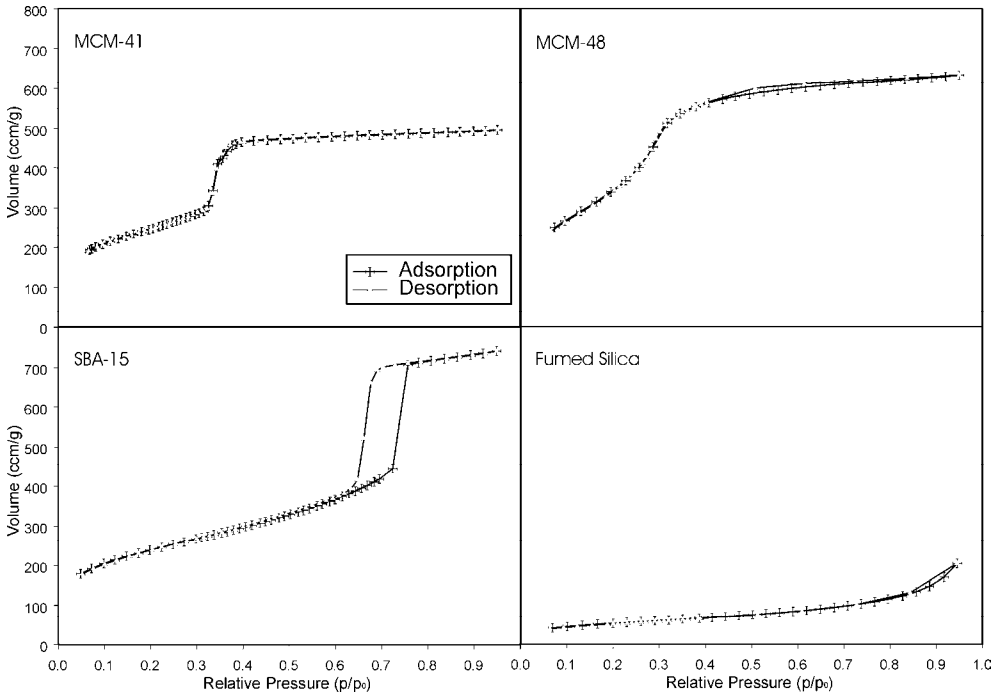

Figure 2.12. N_2 sorption isotherms of MCM-41, MCM-48, SBA-15 and fumed silica.

The nearly linear low-pressure part of the adsorption isotherms is due to monolayer/multilayer formation. Capillary condensation is observed as an almost vertical section of the isotherm. For most type IV isotherms, desorption from mesopores does not appear at the same relative pressure as adsorption, thereby causing hysteresis. MCM-41 is typically characterised by a type IV isotherm without hysteresis.[7]

There are several methods to analyse the isotherms. The Brunauer-Emmett-Teller (BET) method is the standard procedure to determine the surface area[37]. The method is based on a simplified model of monolayer-multilayer adsorption. BET uses the low-pressure part of the adsorption isotherm.

$$\frac{p}{n^a(p_0-p)} = \frac{1}{n_m^a C} + \frac{(C-1)p}{n_m^a C p_0}, \qquad (1)$$

where n^a is the amount adsorbed at the relative pressure p/p_0, n^a_m is the monolayer capacity and C is related exponentially to the enthalpy of adsorption in the first adsorbed layer. To calculate the BET surface area, the average molecular area (a_m) occupied by a single N_2 molecule ($a_m(N_2)$=0.162 nm^2) in the complete monolayer needs to be known

$$a_s(BET) = \frac{n_m^a \cdot L \cdot a_m}{m}, \qquad (2)$$

where L is the Avogadro constant and m is the mass of the sample. BET should not be applied to materials containing micropores[7].

Barrett, Joyner and Halenda developed a method[38] (BJH) for evaluating the pore size distribution by modifying the Kelvin equation. It is common practice to calculate the PSD using the data from the desorption isotherm although use of adsorption data is possible as well.

Density functional theory (DFT)[39] is often employed for analysing the pore size distributions of pure silica materials. DFT calculates the ideal isotherm from the ideal pores of fixed sizes needed to match the experimental results. NOVAWin2 (version 2.2 from Quantachrome Instruments) was used for the calculations. Figure 2.13 shows the pore size distribution of MCM-41 calculated by BJH and DFT.

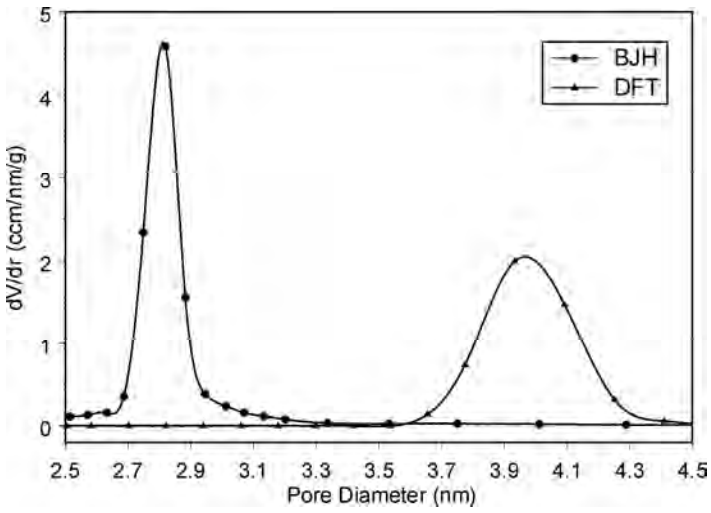

Figure 2.13. Comparison of BJH and DFT methods in the case of MCM-41.

Whereas BJH underestimates the pore size[39,40], DFT probably overestimates it slightly. There is a further method to determine the average pore size, taking into account data from XRD. This method was proposed by Kruk et al.[41] and is referred to as the "geometrical method".

$$w = 1.2125 d_{100} \sqrt{\frac{\rho V_p}{1+\rho V_p}}^{2} \quad (3)$$

where d_{100} is the lattice spacing from the XRD data, ρ is the density of the pore walls (=2.2 g/cm^3) and V_p is the primary mesopore volume. Table 2.3 compares the different methods used to analyse the pore size of MCM-41.

Table 2.3. Comparison of different pore size estimation methods.

	Average pore size (nm)	Wall thickness (nm)
BJH	2.8	1.7
DFT	3.9	0.6
Geom. Method	3.6	0.9

The total pore volume was calculated from the amount of nitrogen adsorbed at a relative pressure of 0.95. The external surface area and the primary mesopore volume (the volume of the uniform mesopores) can be determined using the α_s-plot method[42,43]42. This method makes the assumption that the course of adsorption in mesopores and macropores of the sample is the same as the adsorption for a nonporous reference material with similar surface properties. Therefore, a direct proportionality is expected between the adsorption on both the sample and the reference material when α_s >1

$$v = v_p + \eta_2 \alpha_s, \quad (4)$$

where η_2 is the slope, v_p is the intercept of the linear part of the plot in the high pressure region and

$$\alpha_s = \frac{v_{\mathrm{ref}}(\mathrm{p})}{v_{ref,0.4}}. \quad (5)$$

The external surface can be calculated as follows

$$S_{ex} = \frac{\eta_2 S_{BET,ref}}{v_{ref,0.4}}, \quad (6)$$

where $S_{BET,ref}$ is the BET surface area for the reference and $v_{ref,0.4}$ is the adsorbed amount for the reference at p/p_0=0.4[42,44].

We have used the t-plot method to analyse the microporosity of the samples. The experimental volume of adsorbed N_2 is plotted as a function of the statistical thickness of the adsorbed N_2 layer. When a multilayer is formed unhindered on a solid surface, the t-curve is a straight line passing through the origin. Micropores are present if the t-curve intercepts the y-axis at a positive value.[24,45]

2.3.2 Analysis of Amino Groups on Mesoporous Silica

For analysing the amino group content, experiments were made with ninhydrin (Kaiser test[46]), but the obtained data was unsatisfactory and difficult to reproduce. Samples with identical amounts of amino groups but different distributions of grafting sites (external surface vs. pore surface) produced different results in terms of the actual amount of detected amino groups. The reason for this could be the diminished accessibility of the sites deep inside the mesopores. This kind of problem is often encountered when functionalised mesoporous silicas are analysed. We have developed a method based on the fluorometric quantitation of primary amines with fluorescamine[47,48]. To eliminate the effect of the grafting site distribution, the mesoporous framework is decomposed before the addition of fluorescamine. Reaction of the non-fluorescent fluorescamine with the now fully accessible primary amines yields a fluorescent derivative (Figure 2.14). The fluorescence intensity is then used to determine the amino group content by means of a calibration line.

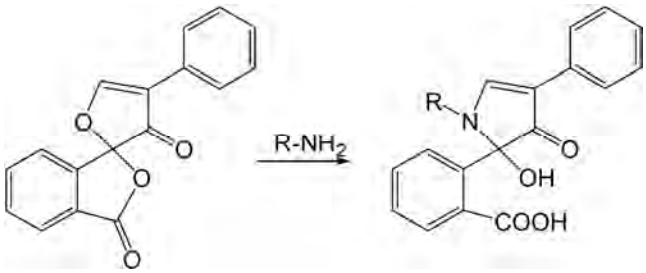

Figure 2.14. Reaction of fluorescamine with a primary amino group.

Amino analysis is conducted as follows: 15 mg of APTMS-functionalised silica was dissolved under stirring in 30 ml of a 0.02 M aqueous solution of NaOH. To 100 µl aliquots of this solution, 2 ml of 0.2 M phosphate buffer (pH 8) and 1 ml of 1 mM fluorescamine solution (dissolved in acetone) was added. The calibration line was made accordingly using different aliquots of a 75 mM APTMS solution (including 15 mg of silica in 0.02 M aqueous NaOH) which were diluted to 100 µl. Fluorescence was measured at 480 nm with the excitation wavelength set at 366 nm. For silanes other than APTMS, calibration lines were made with the respective silane.

3. Silane Distribution on MCM-41

The distribution of grafted amino groups after submonolayer deposition of APASs was investigated. Different silanes were used and the effect of the polarity of the solvent was studied. A summary of the results of the publication "Distribution of amino groups on a mesoporous silica surface after submonolayer deposition of APASs from an anhydrous liquid phase" is reported in chapter 3.1, whereas the published paper is attached in the Appendix. Further results on the topic are presented in chapter 3.2.

3.1 Main Results

The different grafting properties of silanes were studied using APDMMS, APTMS and BTMSPA (see Figure 2.7). Grafting the same molar amount of mono-, tris- and bis-tris-alkoxysilanes on MCM-41 and subsequently coupling FITC yielded different FITC loadings, generally increasing with the number of alkoxy groups per silane molecule. Comparison of samples with the same FITC loading (20 nmol/mg) revealed clear differences concerning PSDs and PL spectra. Figure 3.1 shows APDMMS, APTMS and BTMSPA grafted samples with similar FITC loadings under normal light and near UV-irradiation.

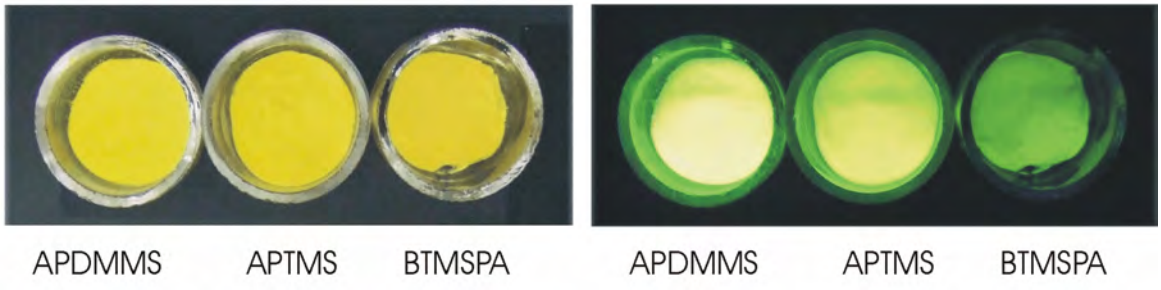

Figure 3.1. APDMMS, APTMS and BTMSPA grafted samples with FITC loadings of 20 nmol/mg under normal (left) and near UV-irradiation (right).

The samples were investigated by PL spectroscopy, revealing that APDMMS grafts more evenly over the whole MCM-41 surface, which is evident from the intense PL (Figure 3.2). BTMSPA, on the other hand, produces a highly non-uniform distribution. The grafting behaviour of APTMS is intermediate between APDMMS and BTMSPA. Figure 3.3 schematically depicts the distributions generated by these APASs.

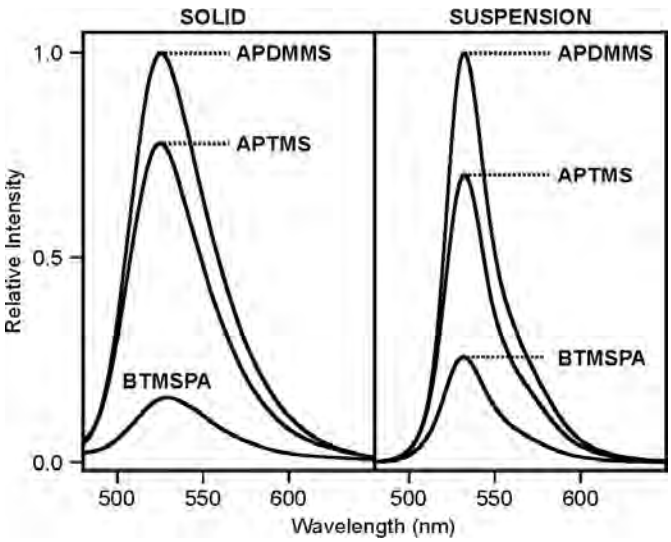

Figure 3.2. PL spectra of APDMMS, APTMS and BTMSPA grafted MCM-41 after FITC coupling (loading 20 nmol/mg) measured as a dry powder and in toluene suspension containing triethylamine. The excitation wavelength was set at 470 nm.

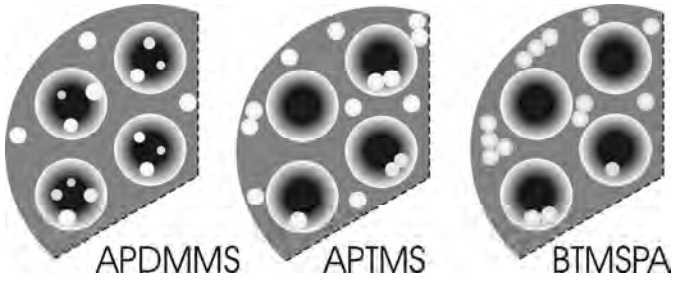

Figure 3.3. Distribution of different alkoxysilanes on mesoporous silica.

Methoxysilanes are generally more reactive than the corresponding ethoxysilanes[49]. The comparison of APTMS/APTES and BTMSPA/BTESPA pairs showed only minor differences in PSD. Ethoxysilanes had a slightly higher tendency to graft into the pores and the FITC coupled samples showed slightly stronger luminescence.

Monoalkoxysilane APDMMS was found to be the most efficient in terms of grafting to sites deep inside the pores. However, stability tests in 0.2 M sodium phosphate buffer (pH 7.5) showed relatively high fluorescein leaching (53 % after 24 h). Protecting the surface siloxane bond improves the stability. Fluorescein leaching of a corresponding APDIPES grafted sample indeed was only 18 % after 24 h.

A higher FITC coupling yield was observed for BTMSPA samples when compared to the respective APTMS and APDMMS samples. Reaction of the secondary amine MAPTMS was compared to BTMSPA and APTMS. PSDs are shown in Figure 3.4. Due to the strong hydrogen-bonding interaction with the surface silanol groups, the mobility of

secondary amines is lower, which is why they preferentially graft to the more accessible outer surface. As a consequence, the grafted amino groups are highly accessible, resulting in high FITC coupling yield. Table 3.1 summarises the results.

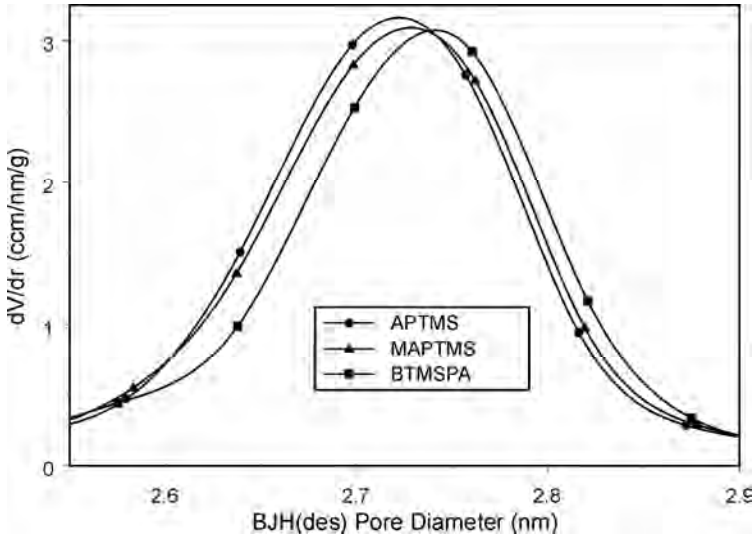

Figure 3.4. PSDs of MCM-41 grafted with APTMS, MAPTMS and BTMSPA with FITC loadings of 20 nmol/mg.

Table 3.1. Comparison of the grafting behaviour of different APASs. Samples were refluxed in toluene containing 100 µmol of silane per g of MCM-41.

Silane	Methoxy #	Amino group	FITC coupling yield	Cross-linking	Distribution
BTMSPA	6	Sec.	55 %	High	Non-uniform (external)
MAPTMS	3	Sec.	55 %	Medium	Intermediate
APTMS	3	Prim.	35 %	Medium	Intermediate
APDMMS	1	Prim.	25 %	Low	Uniform

Anhydrous toluene is the most frequently used solvent in mesoporous silica modification reactions. We have also tested THF, where the distribution was more uniform because of the increased mobility of the silanes. FITC loadings of BTMSPA grafted samples were similar in toluene and THF. However, a shift to smaller pore sizes was observed when using THF.

3.2 Additional Experiments

3.2.1 Quenching of Coupled FITC by Methylviologen and Tb^{3+}

Quenching is a process of non-radiative deactivation of a fluorescent species by another species. Concentration quenching causes the remarkable difference in terms of PL of BTMSPA and APDMMS grafted samples. Quenching by methylviologen is due to electron transfer and quenching by Tb^{3+} is due to the heavy atom effect[50].

In fluorescein/methylviologen electron transfer quenching, the electron donor (fluorescein) and acceptor (methylviologen) form a complex where the excited state of the donor is deactivated due to an electron transfer from the donor to the acceptor. No photon emission will be detected when the complex returns to the ground state.

For estimating the amount of coupled FITC on the outer surface of MCM-41, methylviologen (Figure 3.5) and terbium quenchers were used. Terbium is small and fits into the pores of mesoporous MCM-41 whereas bulkier methylviologen should be able to quench only fluorescein moieties on the outer surface.

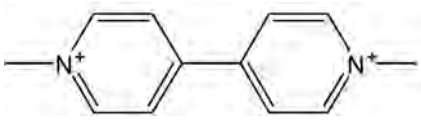

Figure 3.5. Methylviologen.

Figure 3.6 shows the time-dependent quenching of a FITC coupled sample (6 nmol/mg of coupled FITC) using methylviologen and terbium in n-butanol. The sample (2.5 ml) contained 10 nmol/ml of fluorescein moieties. 400 µl of a 6 mM methylviologen solution and a 3 mM terbium solution in n-butanol were used. Both quenchers were very efficient.

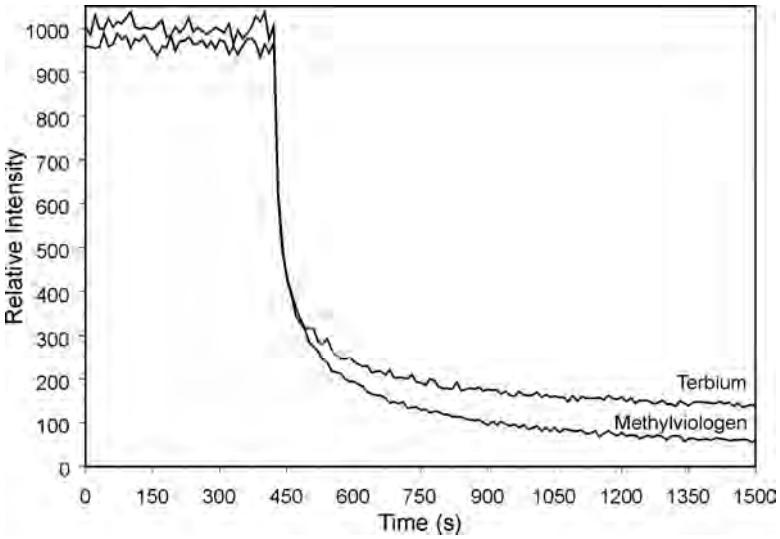

Figure 3.6. Time-dependent quenching of an APDIPES grafted and FITC coupled sample in n-butanol using methylviologen and terbium. Emission was set at 520 nm and excitation at 470 nm. The quencher was added after 450 s.

According to the results of Gartmann[51], the quencher has to be attached to a larger molecule for achieving selective outer surface quenching. The best results were obtained using the amine terminated dendrimer PAMAM-G3 in combination with surface grafted pyrene groups.

3.2.2 Cross-linking of Aminosilanes

Cross-linking occurs in the presence of water with silanes that have more than one alkoxy group. Mesoporous silica is hydrophilic and therefore it is difficult to exclude trace water effects. Figure 3.7 shows the mechanism of cross-linking of surface bound APTMS.

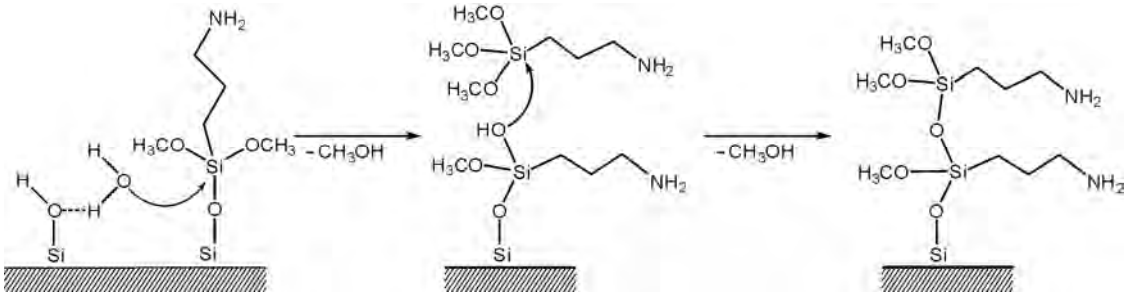

Figure 3.7. Cross-linking of APTMS on the surface of silica in the presence of trace water.

To obtain a uniform distribution of grafted functional groups, cross-linking is not desirable as this can lead to pore blocking. When amino groups are too close to each other, they are not accessible for further modification with bulky molecules such as

FITC. Site isolation (no cross-linking) is also required for the modification with luminophores[34], because otherwise self-quenching can occur. Luminescent mesoporous materials are of interest for applications in the field of biological labelling and imaging[52]. Islands of surface grafted functional groups are ideal for binding biomolecules with more than one binding site per molecule[53].

The effect of water in reactions between surface silanol groups and APASs is discussed in more detail in chapters 4 and 6.

4. Comparison of Vapour Phase and Liquid Phase Deposition Techniques

Postsynthetic functionalisation of MCM-41 is usually made via deposition of an organoalkoxysilane from a solvent. Trace water is relevant even when using dry solvents as the mesoporous silica surface adsorbs water efficiently, leading to a higher probability of cross-linking and hydrolysis of the organoalkoxysilanes[54,55].

Reactions in the vapour phase were investigated for their ability to eliminate trace water and produce a more uniform distribution of grafted amino groups. Reactions were made using an ALD reactor. Vapour phase experiments for comparative studies require large batches of silica. MCM-41 synthesised at room temperature was therefore used for all experiments in this chapter. A short summary and additional details of the publication "A comparative study of the functionalisation of mesoporous silica MCM-41 with 3-aminopropyltrimethoxysilane by deposition from toluene and from the vapour phase" are reported in the following. The corresponding publication can be found in the Appendix.

4.1 Main Results

The reaction temperature (see chapter 4.2.2 for more details) for vapour phase deposition has to be kept at 150 °C or lower. At higher temperatures, Si-NH-C bonds form. 2.5 ml (14 mmol) of APTMS deposited on 2.1 g of MCM-41 yielded 0.73 NH_2 per nm^2 (analysed by fluorescamine reaction assuming uniform distribution). Comparing samples deposited from the vapour phase and from solvent requires similar functionalisation degrees, which in this case was 1.2 mmol/g. Samples were either grafted at 150 °C (vapour phase) or under reflux (solvent).

The vapour phase deposited sample has a narrower PSD than the toluene deposited sample. To exclude possible APTMS oligomers, freshly distilled APTMS was deposited from toluene. The resulting PSD was slightly more uniform and narrower compared to the sample without distillation, but not as narrow as the vapour phase sample. Figure 4.1 shows the PSDs of samples with amino loadings of 1.2 mmol/g after APTMS deposition from the vapour phase and toluene (with and without distillation).

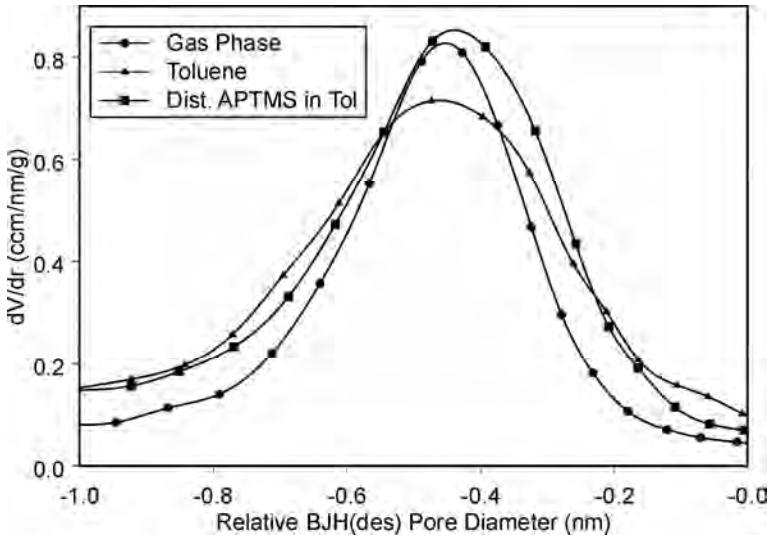

Figure 4.1. PSD of samples after deposition of APTMS from the vapour phase and from toluene. The pore diameter is given relative to the corresponding blind sample.

What is the influence of water on the reaction? To investigate this in more detail, samples were prepared as described in chapter 2.2.1 with H_2O addition and stirring for 15 min prior to APTMS grafting. There was no effect on the FITC loadings but broadening and a shift of the PSD to large pore diameters was noticed (Figure 4.2). We attribute this effect to cross-linking of APTMS and partial hydrolysis of the MCM-41 framework.

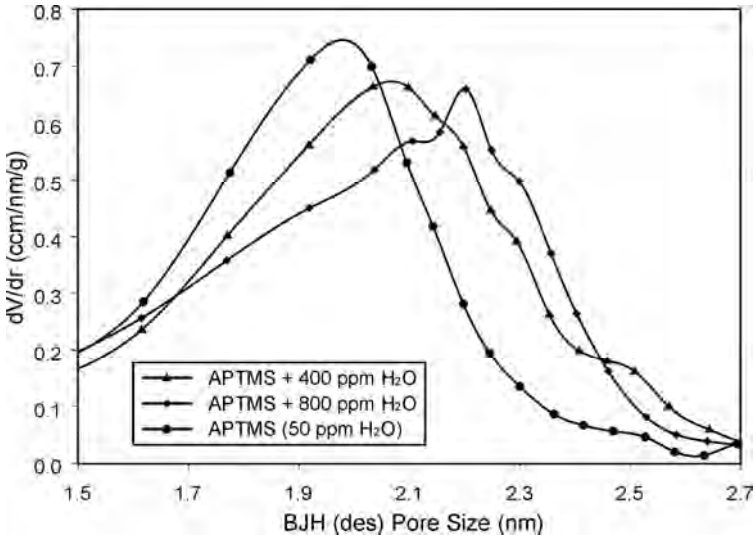

Figure 4.2. PSD of MCM-41 after APTMS grafting from dry toluene compared to PSDs of samples after grafting APTMS with additional water (400 ppm and 800 ppm).

The benefits of grafting from the vapour phase are considerable especially for large scale synthesis. The possibility to functionalise without solvents is an advantage in terms of environmental aspects.

4.2 Additional Experiments in the Vapour Phase

The influence of several reaction parameters was studied i.e. deposition temperature, precursor amount, evaporation temperature, reaction time. Similar experiments have already been conducted for silica gel[56].

4.2.1 Pretreatment of MCM-41 at Different Temperatures

Modification of the surface of MCM-41 is based on reactions with the surface silanol groups. Silica has different surface silanol species, shown in Figure 4.3. It is possible to control these surface sites by heat treatment. At high temperatures, the relative amount of isolated silanols increases.

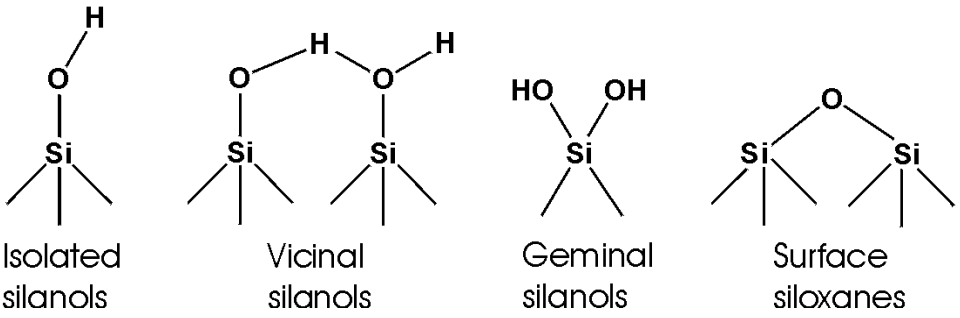

Figure 4.3. Surface groups of silica[57].

MCM-41 is calcined at 550 °C for complete removal of the SDA. For many silica types, higher temperatures are applicable and pretreatment temperatures at 1000 °C have been used. The framework of MCM-41 is, however, not stable at temperatures above ca. 600 °C (Figure 4.4)[58]. Kim et al.[59] have reported that, according to XRD studies, MCM-41 is stable up to 710 °C in dry air whereas Chen et al.[60] observed sufficient stability up to 850 °C in dry conditions.

In spite of the partial decomposition of the MCM-41 framework at higher temperatures, some experiments were made using batches treated at temperatures of 850, 700 and 550 °C. FITC loadings varied strongly depending on the pretreatment temperature. FITC coupling produced loadings of 40, 80 and 120 nmol/mg of FITC, respectively. This shows that at higher temperatures the amount of silanol groups is reduced. The sample treated at 850 °C also featured the smallest pore diameter which causes increased pore blocking upon FITC coupling.

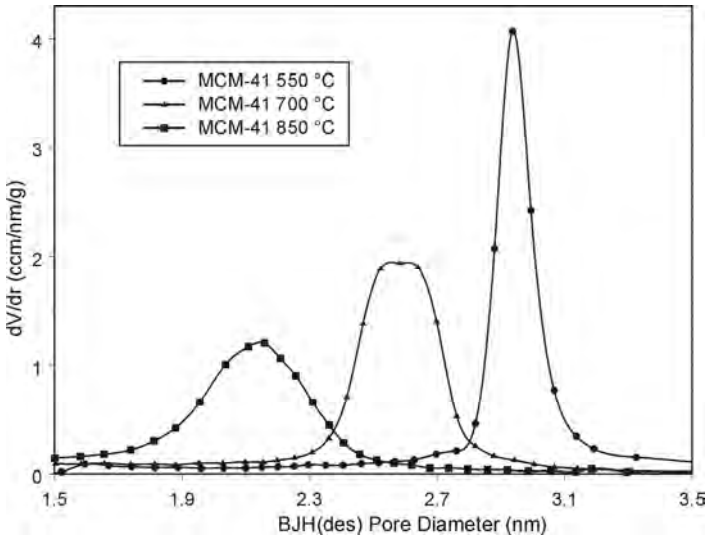

Figure 4.4. PSD of MCM-41 samples treated at the indicated temperature for 16 h in air.

4.2.2 Reaction Temperature

Grafting APTMS at higher temperatures increases the tendency of a reaction between surface silanol groups and amino groups, leading to Si-NH-C moieties, which can be detected by DRIFTS at 3437 and 3470 cm^{-1} (secondary amino groups). Stretching frequencies of the primary amino groups are observed at 3305 and 3373 cm^{-1}. [61] Figure 4.5 shows DRIFTS measurements of samples deposited at different temperatures as well as the corresponding FITC loadings.

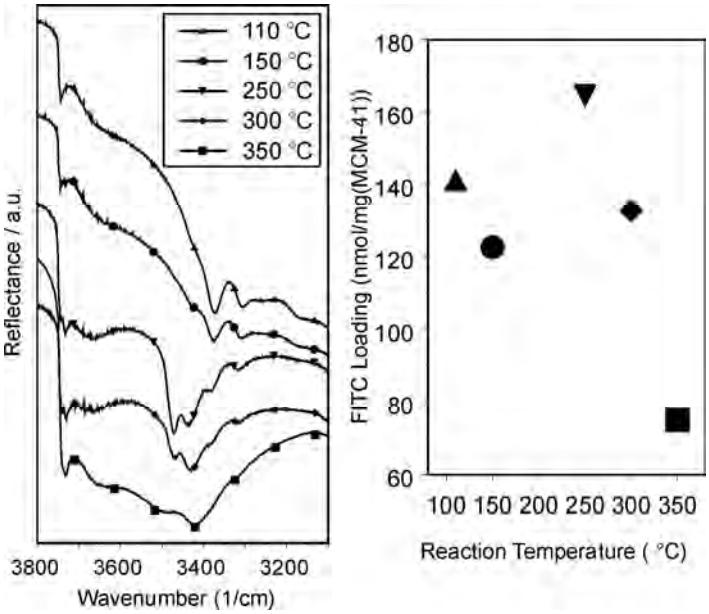

Figure 4.5. DRIFTS measurements (left) and FITC loadings (right) at different reaction temperatures.

At high temperatures, less FITC can be coupled to the modified MCM-41 surface. Large amounts of coupled FITC are found on samples deposited at 250 °C, despite the decreased primary amino stretching vibrations in the corresponding DRIFT spectrum. It is apparently possible to couple FITC to the secondary amine, although it might be sterically hindered. Figure 4.6 shows the different reactions at low and high temperatures. It is not possible to analyse amino loadings from these samples by means of the fluorescamine analysis, because primary and secondary amino groups need different references.

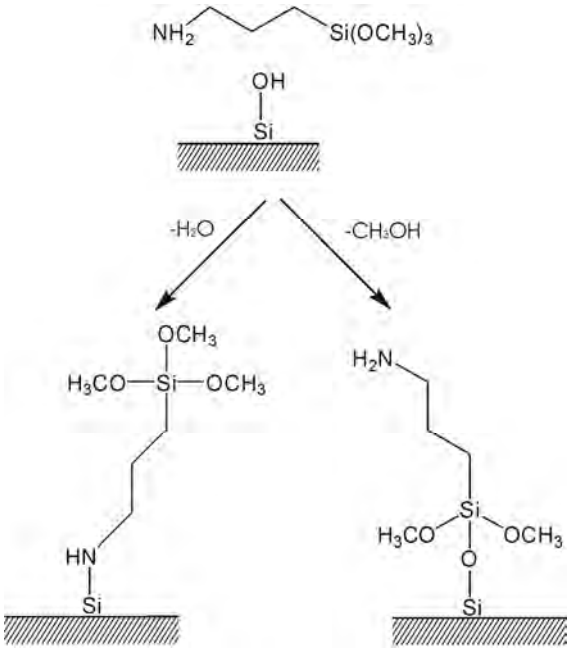

Figure 4.6. APTMS can react in the vapour phase at high temperatures by forming a Si-NH-C or a Si-O-Si bond[61].

4.2.3 Variation of Precursor Amount

The precursor amount was varied at a reaction temperature of 150 °C. Table 4.1 shows that the FITC loading increases slightly when 4 ml of APTMS is deposited whereas the use of 5.5 ml leads to a decrease. The differences in the FITC loadings are considered not significant. It is interesting to note that the amino loading stays at the same level in all samples.

Table 4.1. Effect of APTMS amount on FITC and NH_2 loadings.

V (APTMS) ml	c (APTMS) mmol/g MCM-41	FITC nmol/mg	NH_2 nmol/mg
2.5	6.7	123	1200
4.0	10.8	163	1229
5.5	14.8	146	1222

The amino loading of 1200 nmol/mg corresponds to a surface coverage of 0.73 NH_2 per nm^2. We can assume that maximum coverage with amino groups was obtained. Interestingly, it is possible to achieve loadings of up to one amino group per nm^2 (see chapter 5) in solvent grafting. This is most likely due to cross-linking of the silane precursor.

4.3 Additional Experiments in Solvent

This chapter includes experiments made in solvent for a more detailed study of water effects as well as a comparison of mono- and trialkoxysilanes.

4.3.1 Reactions in Other Solvents (THF)

In a previous experiment (Chapter 3.1) it was noticed that grafting from THF has an effect on the distribution of APASs over the silica surface. To achieve identical FITC loading as in the samples deposited from toluene, 10 % more APTMS is needed. This is due to the increased grafting into the pores when depositing from THF, leading to partially hindered FITC coupling. At high amino functionalisation degrees (>1000 nmol/mg), even a larger excess (50 %) is required when depositing from THF.

Comparing samples with similar FITC loadings is not conclusive, as they typically feature different amino loadings. It is important to compare samples with similar amino loadings. Figure 4.7 compares two amino-functionalised samples with a loading of 1650 nmol/mg, deposited from toluene and THF. The difference in primary mesopore volume is significant. For the THF sample, the pore volume is 0.26 cm^3/g, whereas 0.32 cm^3/g was measured for the toluene sample.

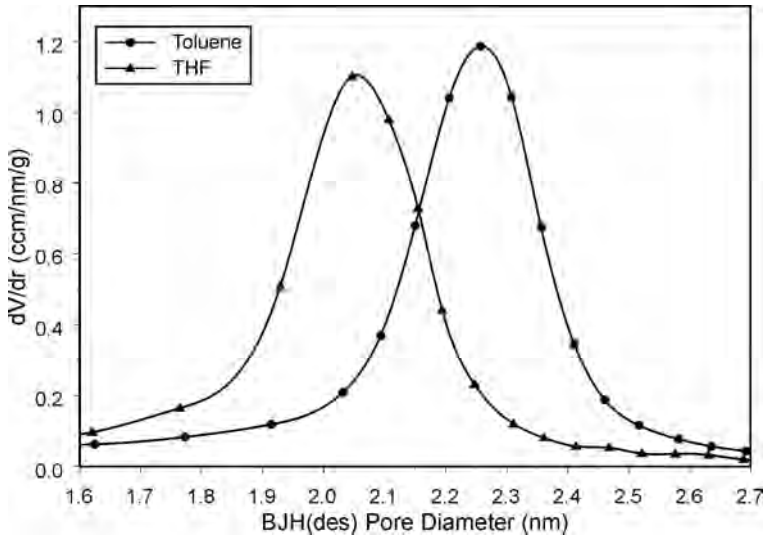

Figure 4.7. PSDs of samples deposited from toluene and THF. Each sample contains 1650 nmol/mg of grafted amino groups.

4.3.2 APDMMS vs. APTMS

Kallury et al.[62] have reported that APASs with one alkoxy group form exclusively monolayers or submonolayers. Comparing the grafting of APDMMS and freshly distilled APTMS reveals the clearly different behaviour of these two silanes (Figure 4.8). Results are in agreement with our observations concerning samples with low amino contents (Appendix).

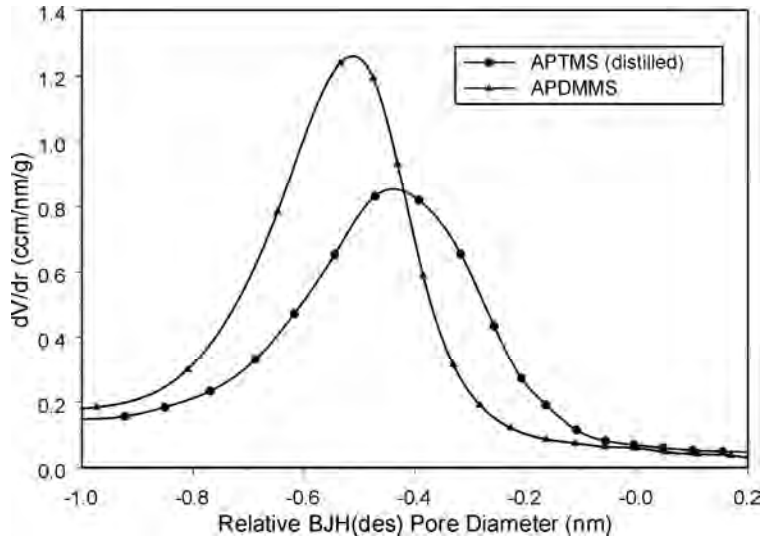

Figure 4.8. Relative PSDs of RT-MCM-41 after deposition of APDMMS and freshly distilled APTMS from toluene. Amino group contents are 1200 nmol/mg.

4.3.3 Effects of Water Addition

Water addition to the grafting suspension has an effect on the resulting PSD. It was investigated whether the difference is due to cross-linking of the silane or hydrolysis of the silica framework. Samples were grafted with 1.8 mmol of APTMS per 1 g of MCM-41 in toluene in the presence of <50 or 400 ppm of water. PSDs of samples were measured after modification as well as after calcination at 550 °C for 16 h (Figure 4.9).

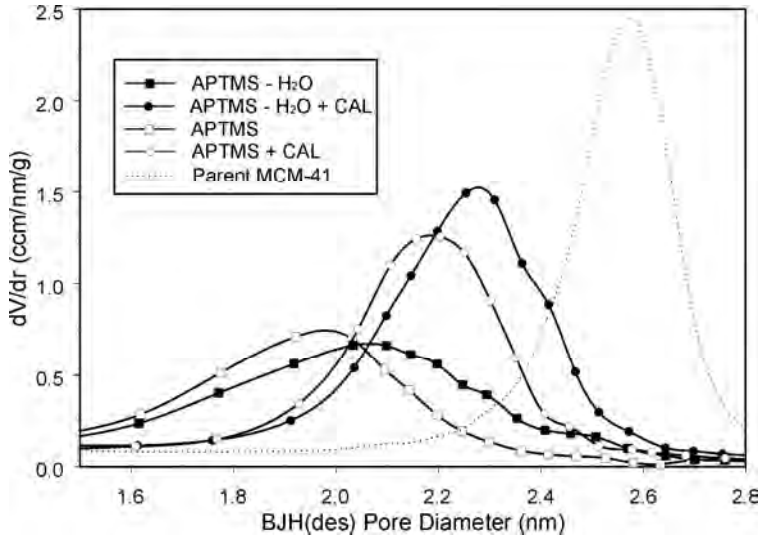

Figure 4.9. Effect of calcination on the PSDs after APTMS grafting from toluene in presence and absence of water.

After calcination of the amino modified samples, the organic species are removed, leaving an inorganic layer on the original pore surface. Samples show a slight difference in PSDs. As already shown in paragraph 4.1, water addition leads to a broader PSD and larger pore diameters. Full width at half maximum after calcination for the sample deposited without water is 0.32 nm compared to 0.34 nm for the sample prepared with water, leading to the conclusion that hydrolysis of the silica framework is unlikely in this case.

5. Pore Blocking in Postsynthetic Functionalisation

Accessibility of the pore surface binding sites is an important parameter of postsynthetic functionalisation of mesoporous silica. Combining amino grafting and FITC coupling, one-dimensional and three-dimensional pore systems of various pore sizes were compared to non-porous silica.

In the following paragraph, the results of the publication “Accessibility of grafting sites in postsynthetically modified mesoporous silica” (Appendix) are briefly discussed.

5.1 Comparison of Mesoporous Silicas

Three samples per silica type were functionalised with amounts of APTMS between 0.05 and 1.20 mmol per 1 g of silica. The samples are denoted A-x for low amino content, whereby x identifies the silica type. B-x and C-x represent intermediate and high amino loading, respectively. Samples were compared by how much FITC was coupled relative to the amount of grafted amino groups, taking into account the different surface areas of the silicas. Each data point corresponds to the average of three independent syntheses. MCM-41(16) was compared to MCM-41(12), nano-MCM (nanoparticles of MCM-41) and SBA-15 (one-dimensional pore system), as well as to MCM-48 (three-dimensional pore system) and non-porous fumed silica.

Figure 5.1 shows the FITC coupling yield as a function of the amino content for each silica type. Fumed silica exhibits rather constant FITC coupling yield, whereas MCM-41(16) features a strong dependence on the amino content. The FITC coupling yield of MCM-48 with similar pore diameter is slightly less dependent on the amino loading.

SBA-15, nano-MCM and MCM-41(12) have rather constant FITC coupling yields. Nano-MCM surprises with its high overall yield, while MCM-41(12) with similar PSD produces comparatively low yields. The reason for this is the much larger external surface area of nano-MCM, providing abundant binding sites with high accessibility.

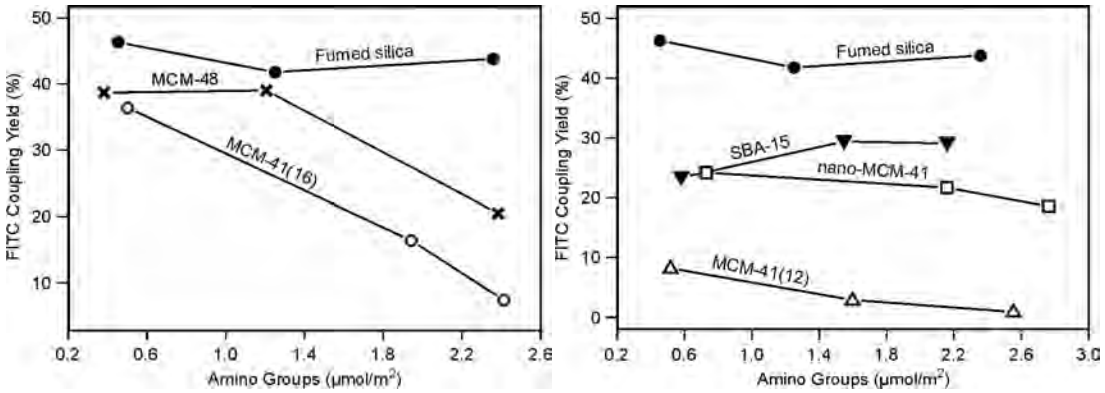

Figure 5.1. FITC coupling yield as a function of the amino group content.

Analysis of the nitrogen sorption isotherms reveals that some samples feature non-closing isotherms at low relative pressure (Figure 5.2). This is interpreted as bottlenecking (grafting to the pore surface close to the entrance and leaving the rest of the pore free)[63,64]. Table 5.1 summarises the course of the isotherms for all mesoporous silicas. It can be concluded that significant bottlenecking occurs in the case of MCM-41(16) and MCM-41(12).

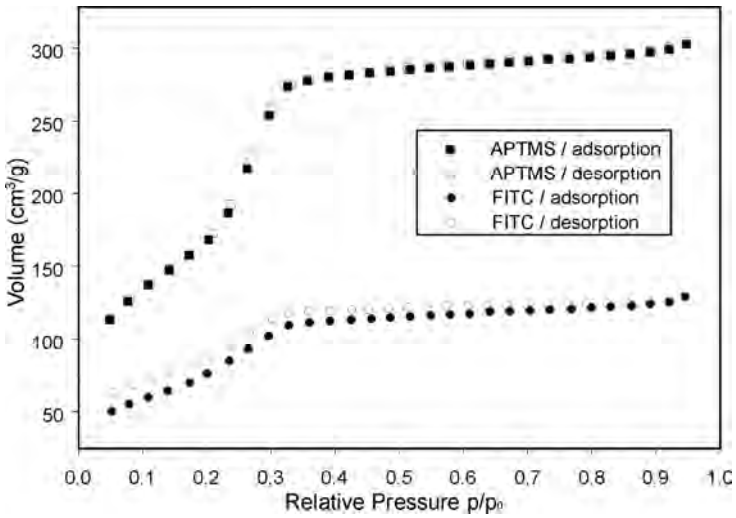

Figure 5.2. Isotherms of amino-functionalised MCM-41(16) before and after FITC coupling (B-MCM-41(16)). The amino content is 1930 nmol/mg and the FITC content is 450 nmol/mg.

Table 5.1. Course of the N_2 sorption isotherms, c indicates closed, o indicates open adsorption/desorption isotherms.

	A-x		B-x		C-x	
	NH_2	FITC	NH_2	FITC	NH_2	FITC
MCM-41(16)	c	c	c	**o**	c	**o**
MCM-41(12)	c	c	**o**	**o**	**o**	**o**
SBA-15	c	c	c	c	c	c
MCM-48	c	c	c	c	c	c
Nano-MCM	c	c	c	c	c	c

Figure 5.3 shows the possible amino group and FITC distribution for three different hexagonal mesoporous materials with high amino content. Trace water in the grafting suspension increases the cross-linking tendency of APTMS and leads to increased pore blocking in the case of silicas with small pore diameters.

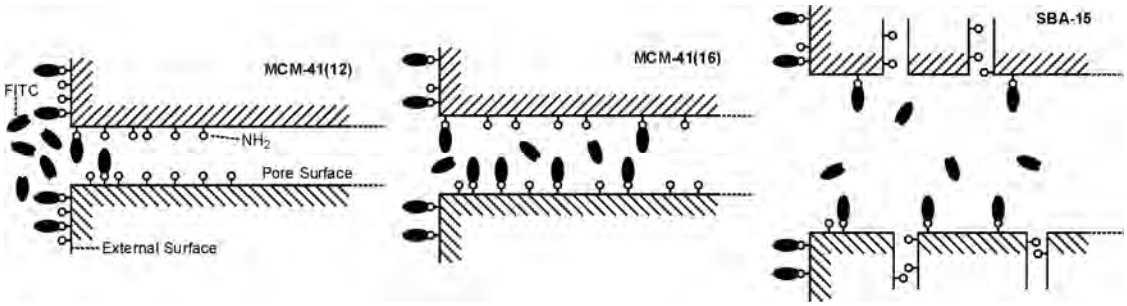

Figure 5.3. Schematic NH_2 and FITC distribution on MCM-41(12), MCM-41(16) and SBA-15.

A test of confinement was performed by physisorption of fluorescein on the amino modified samples. Due to the low pK_a values of neutral fluorescein (4.4) and fluorescein monoanion (6.7), it is expected that the surface amino groups are protonated with subsequent electrostatic interaction with fluorescein mono- and dianions. The fluorescein loading analysed after washing (Table 5.2) showed a trend similar to the one observed for the FITC coupled samples.

Table 5.2. Loadings (nmol/mg) of fluorescein in amino modified mesoporous silica samples.

	A-x	B-x	C-x
MCM-41(12)	1.6	2.0	2.0
MCM-41(16)	8.3	91	184
MCM-48	4.1	48	175
SBA-15	1.2	46	82
Nano-MCM	1.5	23	40
Fumed silica	0.9	9.0	46

MCM-41(16) features the highest confinement, as the fluorescein molecules are efficiently adsorbed in the channels and protected during washing. In silicas with smaller pore diameters, the fluorescein molecules are located close to the pore entrances or on the external surface. In the case of SBA-15 and MCM-48, removal of fluorescein is efficient due to the large pores and three-dimensional channel system, respectively. Interestingly, fumed silica samples achieve far higher fluorescein loadings than MCM-41(12). In the case of MCM-41(12), fluorescein cannot enter the pores due to pore blocking and is thus adsorbed predominantly on the outer surface. A large fraction of the amino groups is unavailable for fluorescein adsorption as the pore surface grafted amino groups are not accessible.

The larger pores of SBA-15 are functionalised in a more uniform fashion because of the unhindered diffusion into the pores, whereas sterical hindrance is more evident in MCM-41(16), especially when larger silanes are used. This problem can be overcome by using a three-dimensional pore structure such as MCM-48.

5.2 Microporosity of SBA-15

SBA-15 contains intrawall pores, which may constitute up to 30 % of the total porosity[23]. The amount and sizes of micropores depend on the synthesis conditions of the parent SBA-15. It was mentioned above that the FITC coupling yield is rather constant at 20-30 % for high amino loadings. Grafting a small amount (100 µmol per 1 g of SBA-15) of APTMS led to a FITC coupling yield of only 15 %. From this we can conclude that APTMS to some extent prefers to graft into the micropores.

The amount of free micropores can be analysed by the t-plot method[25]. Figure 5.4 compares SBA-15 samples of different amino contents. When the linear fit of the low pressure isotherm crosses the y-axis at zero, micropores are absent. It can be seen that the microporosity decreases to zero at an amino content of 400 µmol/g. At an amino content of 100 µmol/g, free micropores are still detected.

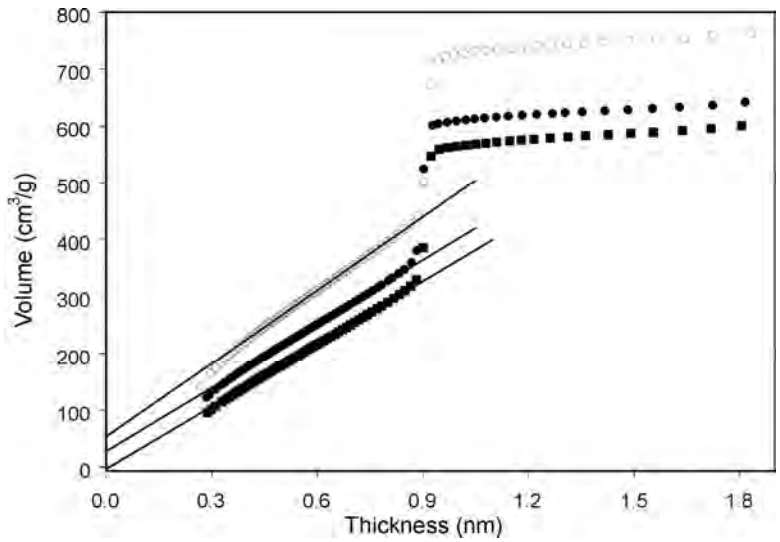

Figure 5.4. t-plots of samples containing 0 (open circles), 100 (black circles) and 400 µmol (black squares) of grafted amino groups per 1 g of SBA-15.

It is obvious that APTMS can fill the micropores. The question remains whether it is possible to find bulky silanes which would not fit into these micropores. This was investigated by grafting APTMS, APTMEES and BTESPA using a silane concentration of 400 µmol/g. Figure 5.5 shows the corresponding t-plots. APTMS is the smallest of these silanes, therefore leading to extensive micropore filling. APTMEES reacts rather well with the pore surface silanol groups, whereas BTESPA reacts to a larger extent with the outer surface silanols. For this reason, the BTESPA sample has a larger pore volume after grafting than the APTMEES sample. The formation of less than 3 surface bonds in the absence of hydrolysis leads to bulky surface anchored species in the case of APTMEES which ultimately results in to an unusually small pore volume.

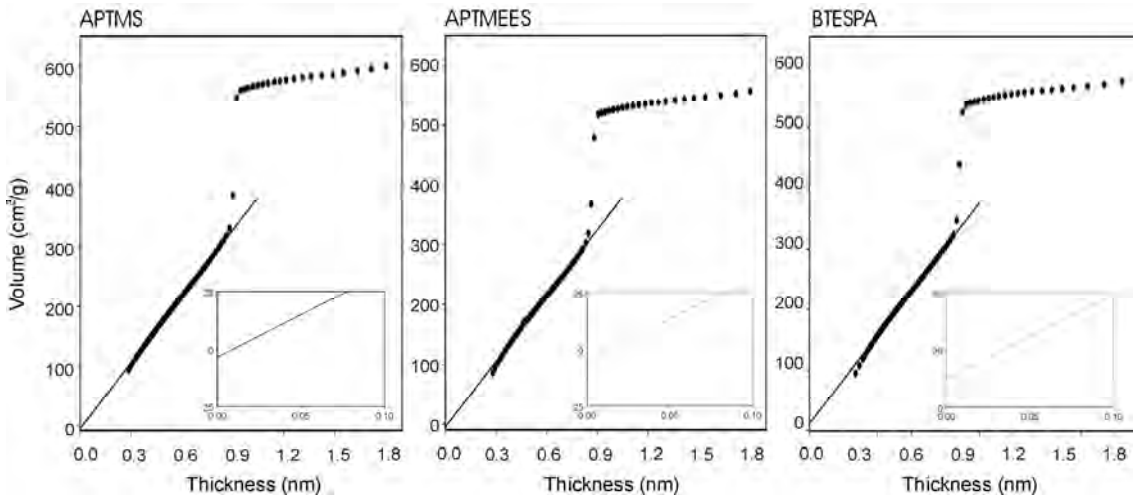

Figure 5.5. t-plots measured from samples grafted with 400 µmol/g APTMS, APTMEES and BTESPA in toluene.

It was further studied how water affects micropore grafting. The amount of water corresponding to one theoretical monolayer on SBA-15 was added to the suspension

before APTMS addition (400 µmol/g). As can be seen in Figure 5.6, some of the micropore volume is still available.

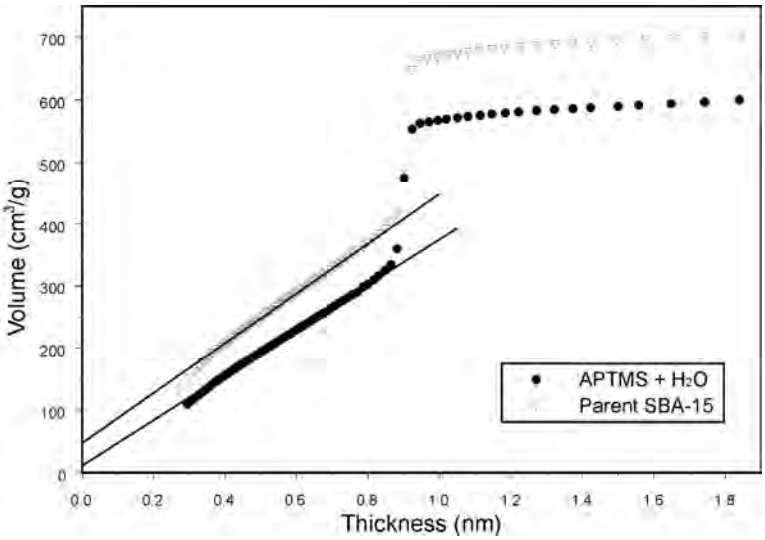

Figure 5.6. t-plots measured from a sample synthesised with addition of water before APTMS grafting. The corresponding t-plot of the parent SBA-15 is shown for comparison.

It is reasonable to assume that the micropores stay free of grafted amino groups in case of larger amounts of preadsorbed water, although this might lead to an uncontrolled cross-linking of APTMS. Further experiments are required to fully understand the relationship between micropore and mesopore grafting in SBA-15.

6. Studies on the Effect of Water

As shown in chapters 4 and 5, trace water can have a considerable effect on the grafting of aminopropylalkoxysilane[65,66]. The grafting behaviour of APTES was investigated in toluene, ethanol and water. All experiments were made at 80 °C and 3 h, if not indicated otherwise.

6.1 Grafting in Toluene in Presence of Water

In these experiments, water was added to the grafting suspensions in quantities corresponding to ½ or one theoretical monolayer with respect to the BET surface area. These samples were compared to samples which were grafted without water addition. 0.4 mmol of APTES was grafted per 1 g of MCM-41. Figure 6.1 shows that water affects the PSDs by shifting them to slightly larger diameters. This effect might be due to the partial hydrolysis of the MCM-41 silica framework, cross-linked silanes which do not fit into the mesopores and/or non-uniform grafting of the silanes.

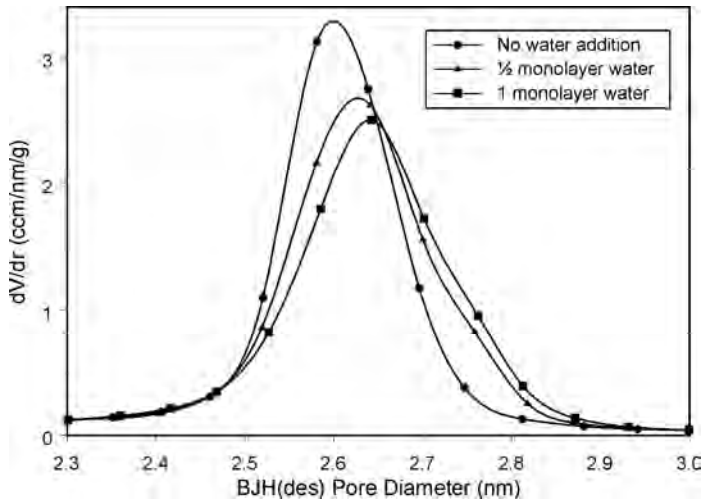

Figure 6.1. PSDs of APTES-grafted samples prepared by deposition from toluene containing various amounts of water.

The BET surface area increased with additional water (Table 6.1). Similarly, the total pore volume and the primary mesopore volume increased. While the FITC coupling yield decreased with increasing water content, the amino loading remained constant (Table 6.2). A decreasing FITC coupling yield, similar pore volume and large pore sizes with broad distribution indicates pore blocking.

Table 6.1. Effect of water on the BET surface area, total pore volume and primary mesopore volume when APTES was grafted from toluene.

Water (monolayer)	S_{BET} (m^2/g)	V_{tot} (cm^3/g)	V_p (cm^3/g)
0	796	0.68	0.57
½	779	0.67	0.56
1	768	0.67	0.55

A possible reaction mechanism for APTES in toluene with trace water might be that APTES cross-links and the resulting clusters do not fit into the pores. This mechanism is, however, very unlikely, as the APTES cross-linking reaction does not take place in solution, but rather on the silica surface. However, grafting to the pore entrances may slow down the diffusion of other precursor molecules leading to an inhomogeneous distribution of amino groups[16].

6.1.1 APTES vs. APDIPES

Figure 6.2 shows the effect (which is rather minimal) of water addition on APDIPES grafting. Contrary to APTES, PSDs of APDIPES grafted samples tend to shift to smaller values in presence of water.

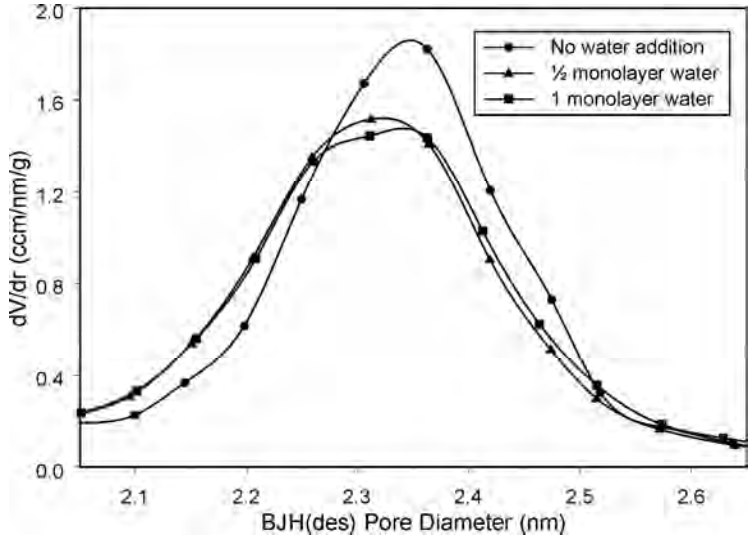

Figure 6.2. PSDs of APDIPES-grafted samples prepared by deposition from toluene containing various amounts of water.

With higher water concentrations, the FITC coupling yield is decreasing for APTES and APDIPES (Table 6.2). Water addition does not have an influence on the amino group loading, whereas a clear decrease of the FITC coupling yield is observed for APTES

grafted samples. This is a result of silane cross-linking leading to pore blocking. Due to the single ethoxy group in APDIPES, cross-linking is not possible. In presence of water it seems that APDIPES grafts more effectively to the pore surface leading to lower FITC coupling yields due to sterical reasons. Water screens the interaction of amino and surface silanol groups which ultimately leads to less hydrogen bonding between APDIPES and the silica surface. As a consequence APDIPES has a higher mobility which enables grafting to sites deep inside the pores. FITC loadings of APDIPES modified samples are slightly lower compared APTES samples, which is in agreement with our previous results (Chapter 3.1).

Table 6.2. Comparison of FITC and amino loadings (nmol/mg) of grafted (400 µmol/g MCM-41) APTES and APDIPES in toluene.

Water (monolayer)	APTES			APDIPES		
	NH_2	FITC	Yield %	NH_2	FITC	Yield %
0	357	134	37.5	380	112	29.5
½	354	112	31.6	376	107	28.5
1	352	106	30.1	362	94	26.0

6.1.2 Silica Framework Hydrolysis

APTES was replaced with propylamine to probe the effect of the amino group in terms of promoting the hydrolysis of the silica framework. Figure 6.3 shows the PSD of a sample reacted with propylamine and water. The divided peak could be due to a partial hydrolysis of the mesoporous silica framework. No amino groups were detected by the fluorescamine analysis. Unlike APTES, propylamine does not react with the surface silanol groups forming covalent bonds and therefore has a higher mobility which might promote the framework hydrolysis.

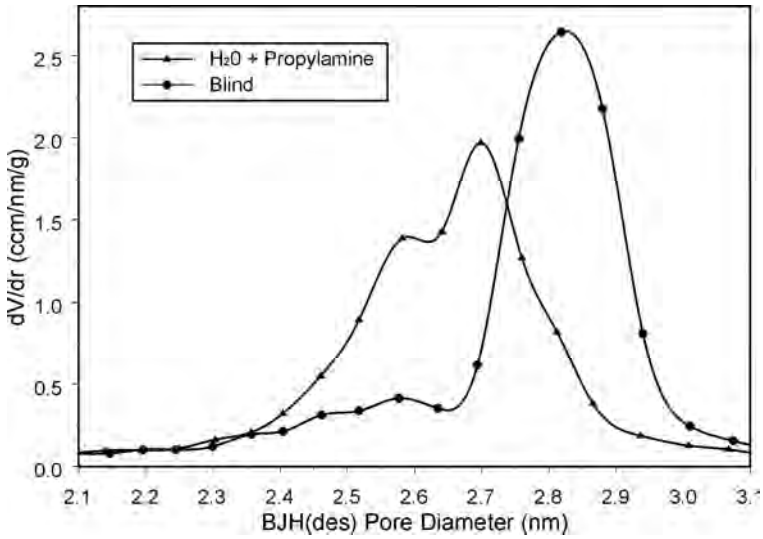

Figure 6.3. PSDs after deposition of propylamine (400 nmol/mg) in toluene in presence of a theoretical monolayer of H_2O. The blind sample was prepared according to the propylamine sample without propylamine addition.

6.1.3 Effects of Grafting vs. Time

APTES grafting in toluene at room temperature was studied as a function of time. A reaction conducted at 80 °C instantly produces covalent surface bonds. The amino group loading was constant after 20 minutes. Deposition at room temperature, washing with ethanol and drying (80 °C, 1 h) yielded the same result. It has already been reported that APASs instantly adsorb on the silica surface by forming hydrogen bonds and electrostatically bound species[67]. To remove these species, the sample is washed by stirring in 0.04 M HCl solution in ethanol for 5 min. Afterwards, the sample was washed with ethanol and oven-dried at 80 °C for one hour.

Figures 6.4 and 6.5 show the primary mesopore volume changes and amino loading changes vs. time with and without water addition. In absence of water, the maximum amino loading is achieved after two hours, whereas in presence of one theoretical monolayer of water, the maximum is achieved after 20 min. The decreasing amino loading in the presence of water is most likely due to the slow leaching of the grafted silanes. Table 6.3 shows the pore volume in percentage of the original value for both experiments. After three hours, the primary mesopore volume has decreased in both cases to 70 % of the original value.

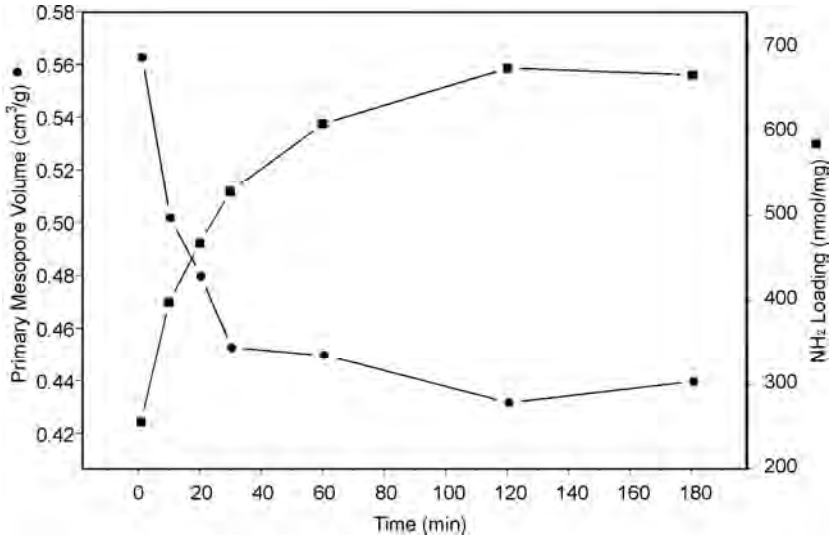

Figure 6.4. Development of the primary mesopore volume (circles) and amino loading (squares) upon deposition of APTES from dry toluene.

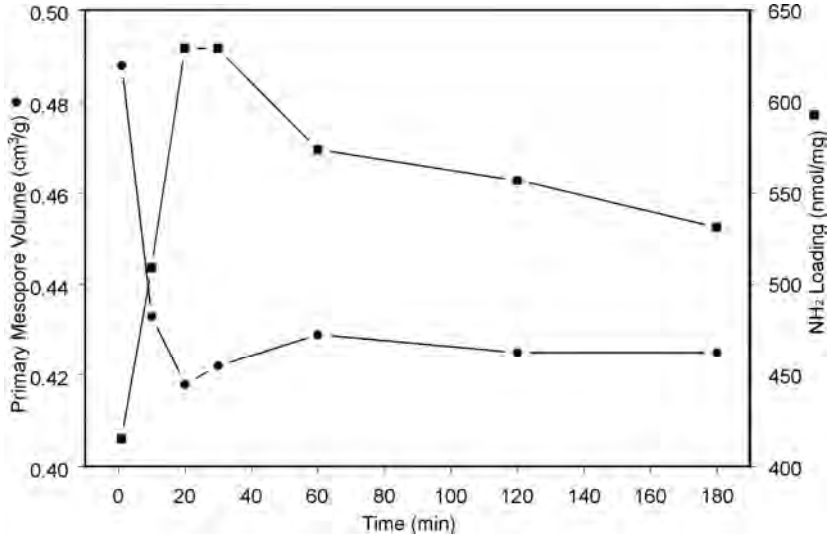

Figure 6.5. Development of the primary mesopore volume (circles) and amino loading (squares) upon deposition of APTES from toluene in presence of one theoretical monolayer of water.

Table 6.3. Primary mesopore volume in % of the initial volume.

Time / Sample	1 min	10 min	20 min	30 min	60 min	120 min	180 min
APTES +H_2O	80.8	71.7	69.2	69.9	71.0	70.4	70.4
APTES	91.3	81.4	77.8	73.4	72.9	70.0	71.3

6.2 Other Solvents

Depending on the solvent, the amino groups are either aggregated or distributed in a more isolated fashion over the surface. The polarity and the dielectric constant of the solvent have an influence on the outcome of the grafting reaction.[68]

Figure 6.6 shows the PSDs after APTES grafting in ethanol and in n-butanol. In the more polar solvent, the silane is grafted more uniformly over the mesoporous silica surface, which leads to a narrow PSD at small pore diameter. This is in agreement with the results of a recent publication by Sharma et al.[68].

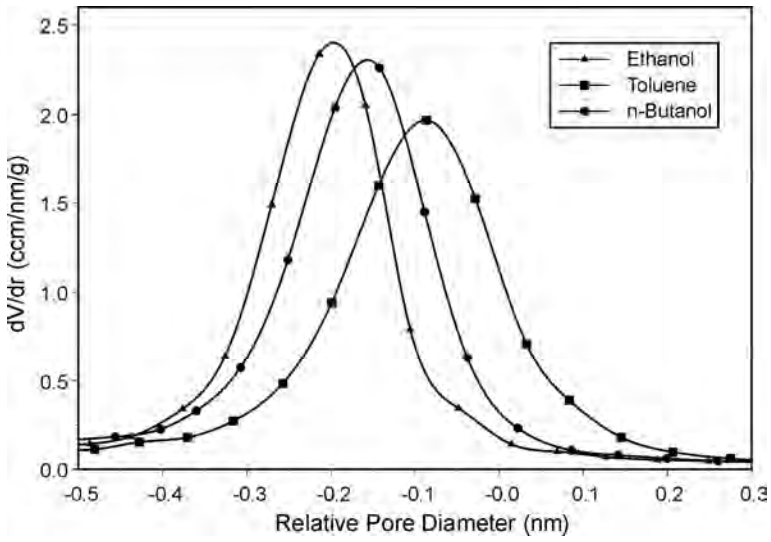

Figure 6.6. Comparison of relative PSDs of APTES (400 µmol/g MCM-41) grafted in toluene, n-butanol and ethanol at 80 °C for 3 h.

6.2.1 Deposition from Ethanol

Water addition to the reaction suspension was also performed with ethanol. Contrary to toluene, the FITC coupling yield increases with increasing water content (Table 6.4). This is most likely due to increased grafting to the outer surface. In contrast to Sharma et al.[69], these experiments did not reveal significant differences in the amino content.

Table 6.4. Amino and FITC loadings (nmol/mg) of APTES grafted samples prepared in ethanol containing different amounts of water.

H_2O (monolayer)	Ethanol		
	NH_2	FITC	Yield %
0	379	131	34.6
½	366	128	35.0
1	336	126	37.5

Figure 6.7 shows the PSDs grafted in ethanol. The PSD shift from "no water" to "½ monolayer" water is much more pronounced than in toluene (see Figure 6.1). The BET surface area as well as pore volume increase with additional water (Table 6.5), this concludes to pore blocking as in grafting from toluene in presence of water.

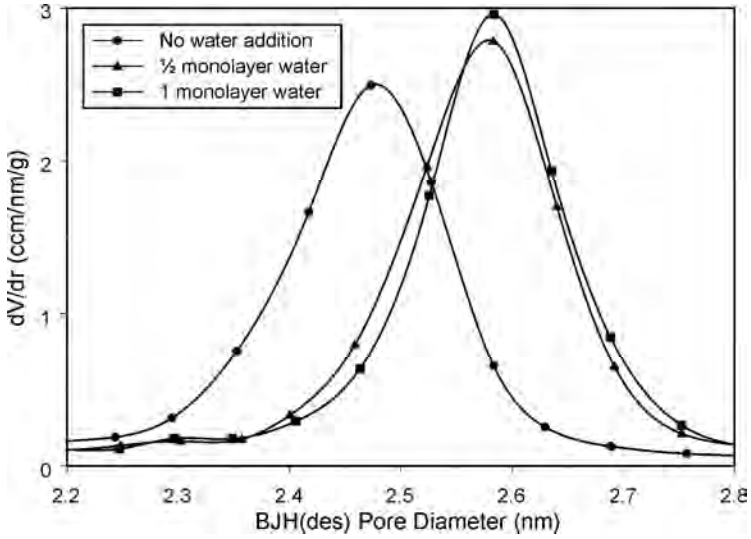

Figure 6.7. PSDs of APTES-grafted samples prepared by deposition from ethanol containing various amounts of water.

Table 6.5. Effect of water on the BET surface area, total pore volume and primary mesopore volume when APTES was grafted from ethanol.

Water (monolayer)	S_{BET} (m^2/g)	V_{tot} (cm^3/g)	V_p (cm^3/g)
0	697	0.55	0.48
½	750	0.60	0.53
1	732	0.59	0.53

6.2.2 Deposition from Water

Grafting was also performed in water. The amino loading (400 nmol/mg) was comparable to the values achieved in toluene. However, the FITC loading (74 nmol/mg) was far lower than for the sample prepared in toluene (130 nmol/mg). The difference of the PSDs was considerable when compared to the blind sample (Figure 6.8). The PSD of the blind sample was practically identical to the parent MCM-41. The basicity of APTES might be the reason for the loss of well-defined mesoporosity.

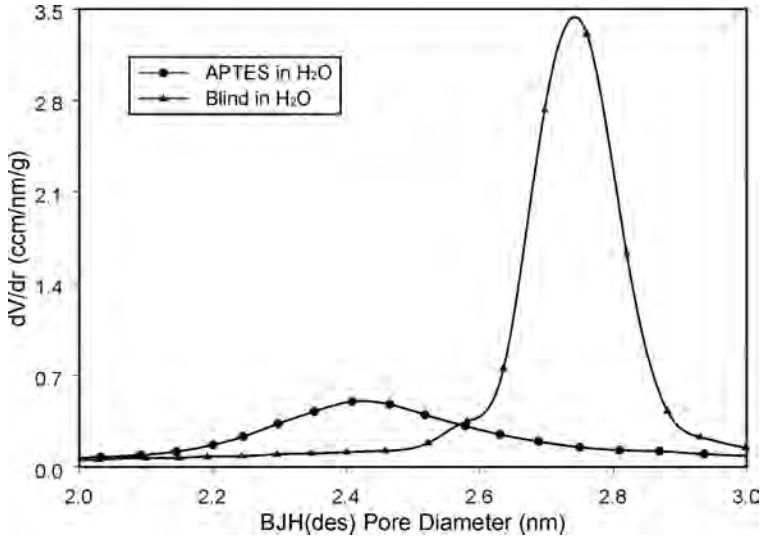

Figure 6.8. PSD after grafting APTES (amino loading 400 nmol/mg) in water compared to the PSD of a corresponding blind sample.

To investigate potential effects of the amino group in terms of silica hydrolysis, APTES was replaced with propylamine (Figure 6.9).

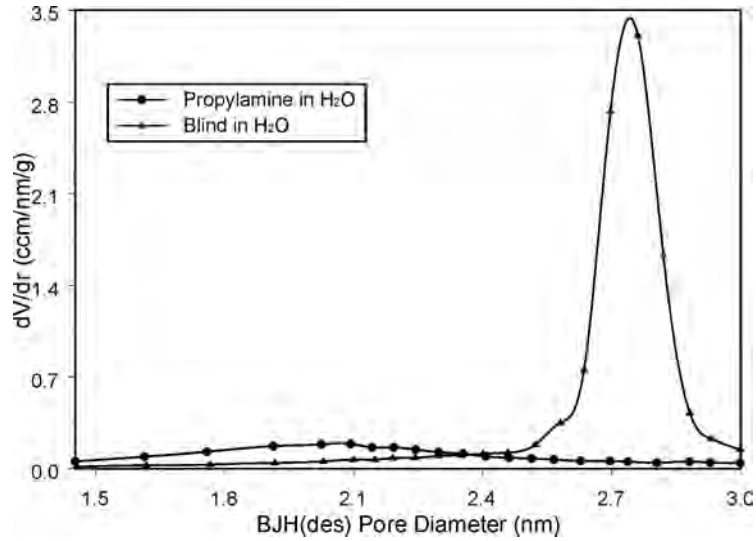

Figure 6.9. PSD after stirring in water containing 400 µmol of propylamine (per 1 g of MCM-41) and PSD of a corresponding blind sample.

Mesoporous silica is stable in water but the stability decreases at high pH[70]. The PSD of the blind samples are similar to those of the parent MCM-41, whereas addition of a base to the grafting suspension decomposes the mesoporous structure.

7. Modification of the External Surface of MCM-41

Different internal and external surface properties are required for applications such as biocatalysis[71] and drug delivery[72]. An important aspect of modifying the outer surface is that the internal surface remains accessible.

The most obvious method would be to graft the silane before removing the SDA from the pores[53]. Figure 7.1 shows the PSD of samples onto which different amounts of APTMS were grafted under reflux in toluene for 3 h before extraction of the SDA. In comparison to the blind sample, the PSDs of the APTMS grafted samples shift to smaller pore sizes. Clearly, this is not an adequate method for modifying the external surface. The SDA is apparently replaced with APTMS resulting in a modified pore surface[73]. Table 7.1 shows the synthesis parameters of all samples made for this chapter.

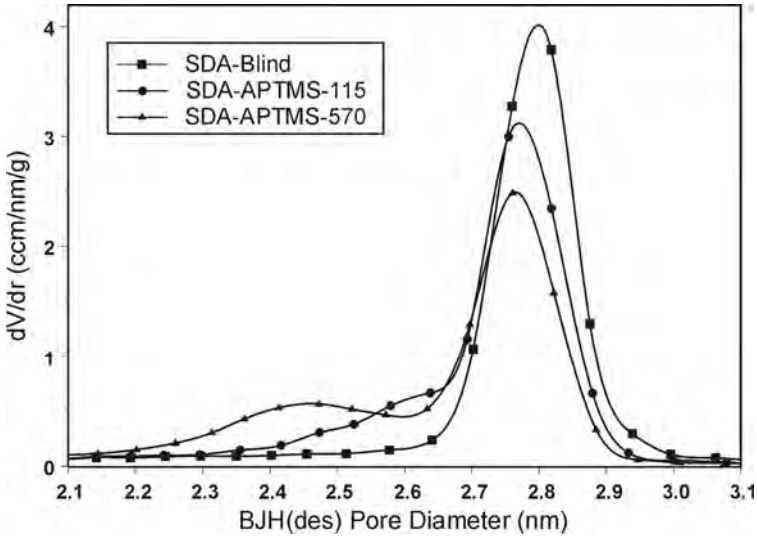

Figure 7.1. PSD of APTMS grafted and blind samples after extraction. Different amounts of APTMS were grafted per 1 g of as-synthesised MCM-41 (Table 7.1).

Table 7.1. Synthesis parameters of functionalised samples. Modification before (+) or after (-) SDA removal. FITC coupling to silane was made before or after MCM-41 surface modification. Pyridine was used in a concentration of 1 mmol per g of MCM-41.

Sample	SDA	Silane precursor	Silane (µmol / g silica)	Reaction temperature	FITC coupling	Base
SDA-blind	+	-	-	125 °C	-	-
SDA-APTMS-115	+	APTMS	115	125 °C	After	-
SDA-APTMS-570	+	APTMS	570	125 °C	After	-
SDA-APTMEES-212-RT	+	APTMEES	212	RT	After	-
SDA-APTMEES-212	+	APTMEES	212	125 °C	After	-
SDA-Fi*APTMS-320-RT	+	APTMS	320	RT	Before	Pyridine
SDA-Fi*APTMS-200-RT	+	APTMS	200	RT	Before	-
MCM-Fi*APTMEES-525	-	APTMEES	525	125 °C	Before	Pyridine
MCM-Fi*APTMEES-36	-	APTMEES	36	125 °C	Before	Pyridine

7.1 Preliminary Experiments

APTMS seems to be too small for the method described above. Therefore, bulkier APTMEES was grafted onto MCM-41 at room temperature and FITC was coupled after extraction, yielding a FITC content of 14 nmol/mg for sample SDA-APTMEES-212-RT. Figure 7.2 shows a minor difference of the PSDs before and after FITC coupling. This would imply that FITC is coupled predominantly on the outer surface of MCM-41. We found that there is always a small shift in PSDs when MCM-41 is stirred in ethanol (blind "FITC coupling" reaction).

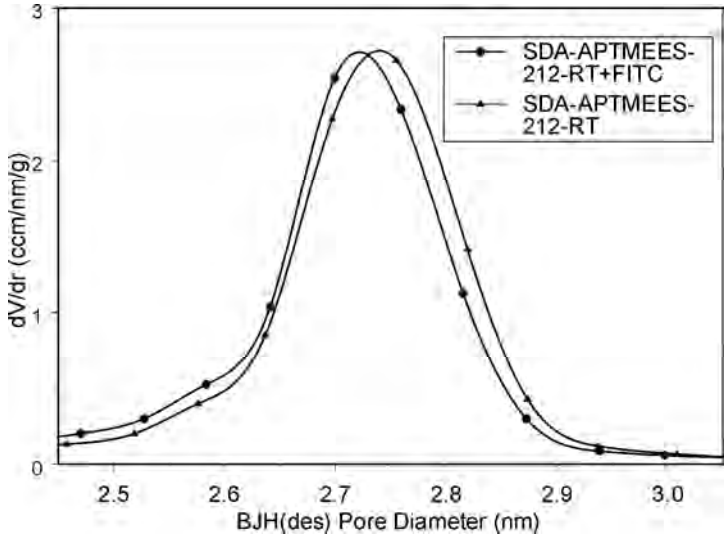

Figure 7.2. PSDs before and after FITC coupling to SDA-APTMEES-212-RT.

When comparing the SDA-APTMEES-212-RT sample to a corresponding blind (Figure 7.3), a shift of almost 0.1 nm is observed. Figure 7.3 also shows the PSD of sample SDA-APTMEES-212 which was grafted at 125 °C. The FITC content of this sample is slightly higher (20 nmol/mg).

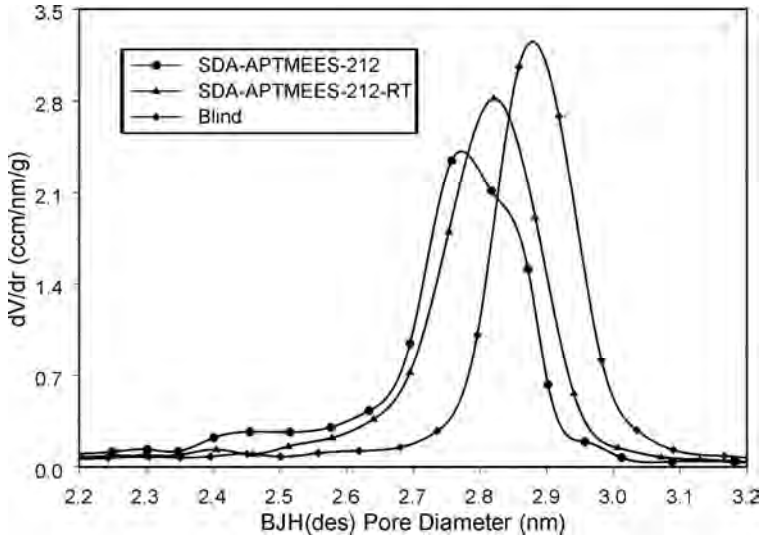

Figure 7.3. PSDs of the FITC coupled samples SDA-APTMEES-212-RT and SDA-APTMEES-212 compared to a blind sample.

Apparently bulkier molecules than APTMEES are required. One possibility we have investigated includes coupling of FITC to the silane before grafting. Experiments started with coupling FITC to APTMS over night at room temperature in THF and pyridine. Grafting was performed at room temperature onto as-synthesised MCM-41. A FITC loading of 22 nmol/mg was obtained for SDA-Fi*APTMS-320. Reactions without additional base and less APTMS (SDA-Fi*APTMS-200) surprisingly resulted in a slightly higher FITC content of 25 nmol/mg. Unfortunately, the PSDs were not satisfactory due to significant pore surface grafting. These samples did not fluoresce under UV-light probably due to cross-linking of APTMS or dense grafting at the pore entrances.

In a further experiment, APTMS was replaced with APTMEES, which was grafted directly to calcined MCM-41 after coupling to FITC. The FITC content for sample MCM-Fi*APTMEES-525 was 100 nmol/mg yielding a fluorescent material. The PSD of MCM-Fi*APTMEES-36 with a FITC content of 20 nmol/mg is shown in Figure 7.4 and compared to the parent MCM-41. This is a promising result that forms the basis for the experiments with protecting groups described in the following chapter.

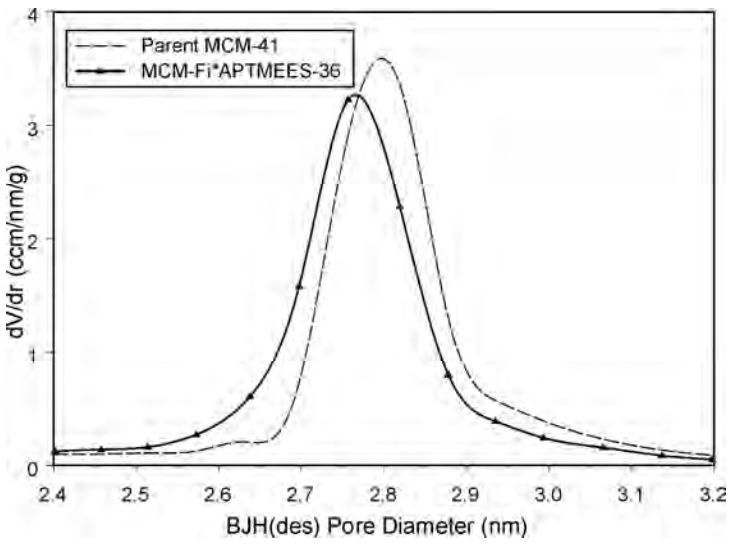

Figure 7.4. MCM-Fi*APTMEES-36 compared to the respective parent MCM-41.

7.2 Experiments using FMOC*

FMOC* (2,7-di-tert-butyl-9-fluorenylmethylchloroformate) is a modification of the widely used protecting group FMOC. Figures 7.5 and 7.6 show the reaction of FMOC* with a primary amino group and the corresponding deprotection steps.[74]

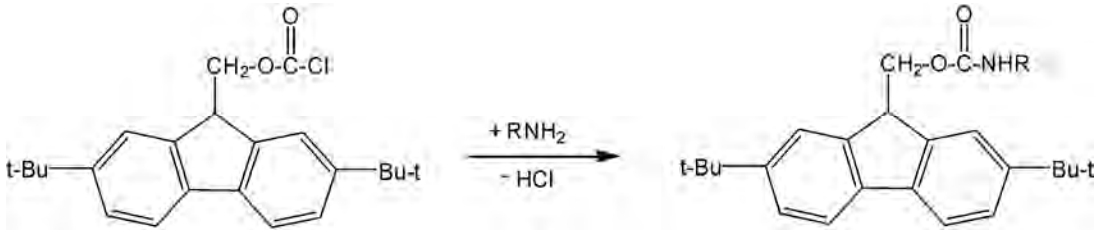

Figure 7.5. Reaction of FMOC* with a primary amino group.

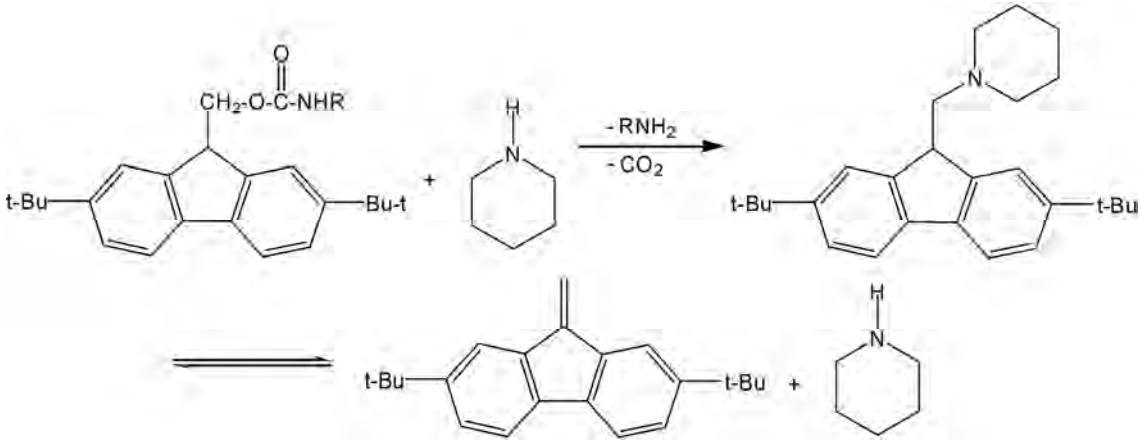

Figure 7.6. Deprotection of the FMOC*-protected amino group.

7.2.1 Experimental Details

In a first step, FMOC* (Aldrich) was dissolved in toluene or THF (containing pyridine) and a calculated amount of silane was added. For complete coupling, the mixture was stirred over night at room temperature or refluxed. The solution was added to the oven-dried (1 h at 80 °C) MCM-41 and the resulting suspension was stirred at room temperature or refluxed for 3 h. After filtering and washing with of 100 ml ethanol, the product was oven-dried at 80 °C for one hour. Experiments were performed with as-synthesised and calcined MCM-41.

Deprotection was conducted by using a 2 % piperidine solution in DMF and stirring at 40 °C for 4 h. The mixture was filtered and washed with 25 ml of DMF and 50 ml of ethanol. The sample was oven-dried (80 °C, 1 h). [75]

In the case of as-synthesised MCM-41, the SDA was removed in a final step by stirring in a solution of NH_4NO_3 (1.0 g) in 100 ml of ethanol at 60 °C for 20 min. After filtration and washing with ethanol, the procedure was repeated one more time for complete extraction. [76]

The degree of deprotection was analysed by dissolving 50 mg of the sample in 15 ml of a 0.33 M aqueous NaOH solution. The FMOC* loading was calculated from a UV-vis measurement at 270 nm (10 000 M^{-1}/cm)[77]. Water was used as reference.

7.2.2 Results

It is essential to work with a certain concentration of piperidine in the deprotection reaction. After finding a report by Cheng and Landry[75], progress was made towards more efficient deprotection.

We have found that it is advantageous to deprotect before removing the SDA, otherwise incomplete extraction is obtained. Samples which were extracted before deprotection were indeed found to have smaller pores.

The most promising results were obtained as follows: APTMS (570 µmol/g MCM-41) was coupled to FMOC* (400 µmol) in toluene over night at room temperature. Grafting to as-synthesised MCM-41 was performed at under reflux in toluene for 3 h. The sample was first deprotected, then extracted followed by FITC coupling resulting in a loading of 40 nmol/mg. Figure 7.7 shows the PSD of the sample before and after FITC coupling.

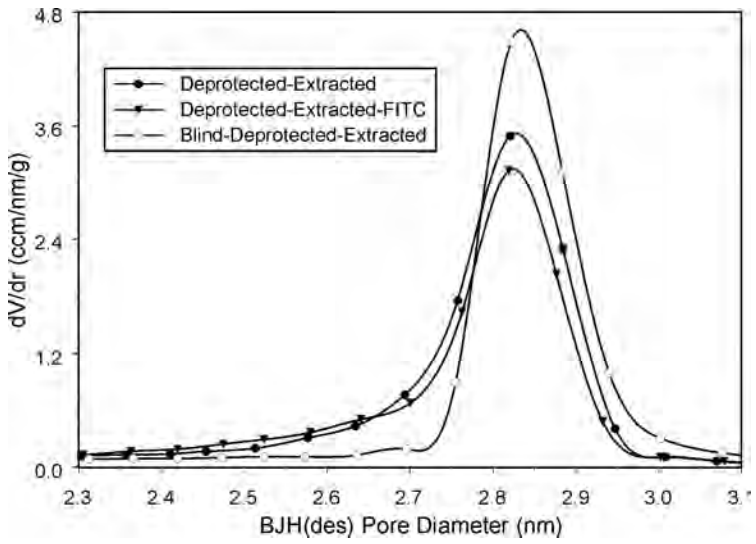

Figure 7.7. APTMS was protected with FMOC* and grafted to as-synthtesised MCM-41. The SDA was extracted after deprotection. Amino groups were subsequently labelled with FITC (40 nmol/mg of coupled FITC). A corresponding blind sample is shown for comparison.

It is worth mentioning that FMOC* can directly react with the MCM-41 surface in toluene and THF suspension under reflux as well as at room temperature. FMOC* and silane therefore have to be coupled in a 1:1 molar ratio.

7.3 Discussion

Selective external surface functionalisation is a challenging task. Our best results were obtained with APTMEES which was coupled to FITC before grafting.

FMOC* is apparently not bulky enough to avoid penetration into the 3.5 nm pores of MCM-41. One possibility might be to use BTESPA instead of APTMEES to increase the reactivity of the precursor.

8. Summary and Outlook

The main goal of this work was the investigation of postsynthetic methods for the functionalisation of mesoporous silicas with amino groups. A convenient method for the synthesis of MCM-41 including scaling possibility to large batches and aging at room temperature was developed. Furthermore, the devised mesoporous silica synthesis procedure comparable to the conventional MCM-41 procedures allows the reduction of the resulting pore diameter (MCM-41(12), 3.1 nm).

The outcome of grafting reactions of different aminopropylalkoxysilanes depends on the nature of the amino group (primary or secondary) and the number of alkoxy substituents. Monoalkoxysilanes graft uniformly over the surface, whereas dipodal trialkoxysilanes react preferably with sites on the external surface and at the pore entrances. Secondary amines have a higher tendency to graft to the external surface as compared to their primary analogues. The modification of silica surfaces is usually made in a solvent. An important aspect in grafting reactions is the solvent polarity. Increasing the polarity minimises clustering and the distribution becomes more uniform as the APAS molecules are able to reach less accessible sites on the internal surface. FITC coupling to the anchored amino groups was used for analysis, as it amplifies the pore size changes of differently modified samples.

A new method for analysing amino groups grafted on the surface of mesoporous silica was developed. It can be applied to a wide range of grafting densities in the case of samples prepared by postsynthetic modification, as well as to co-condensed samples. The advantage of this method is that all amino groups, including those in the pore walls, are analysed. The method is based on the reaction of fluorescamine with the dissolved amino-functionalised samples.

Trace water has an effect on the outcome of grafting reactions. Aminopropyl-monoalkoxysilanes have an increasing tendency to graft into the pores, whereas aminopropyltrialkoxysilanes cause significant pore blocking as a consequence of cross-linking.

Functionalisation of the silica surface via deposition from the vapour phase was compared to the conventional solvent based techniques. The use of vapour phase deposition eliminates trace water-induced silane cross-linking and subsequent pore blocking. The vapour phase deposition method is of interest due to both economical and ecological reasons, especially when large scale synthesis is concerned, as it avoids the use of dry solvents.

One-dimensional channel systems with large pore diameter (SBA-15) or small (MCM-41, MCM-41(12)) pore diameters and three-dimensional channel systems (MCM-48)

behave differently in the grafting reactions with APASs and subsequent FITC labelling. The non-uniform distribution of amino groups obtained after postsynthetic functionalisation with APTMS promotes pore blocking upon FITC coupling. In terms of providing accessible pore surface sites, a three-dimensional channel system is superior to a one-dimensional channel system with similar pore diameter. High amino contents increase the probability of bottleneck formation by coupling of FITC to densely grafted amino groups located at the pore entrances. Micropore grafting of APTMS was observed in SBA-15.

Selective external surface functionalisation is a challenging task. It was found that coupling a protecting group (FITC or FMOC*) to the APAS before grafting results in a higher selectivity for the outer surface. Deprotection of the anchored amines is, however, not straightforward. The best results were obtained with APTMEES which were coupled to FITC before grafting. FMOC*, on the other hand, is apparently not bulky enough to avoid penetration into the pores of MCM-41. One possibility might be to use BTESPA to increase the reactivity of the protected precursor.

9. References

1 Kresge, C. T., Leonowicz, M. E., Roth, W. J., Vartuli, J. C., Beck, J. S., *Nature* **359** (1992) 710.

2 Galarneau, A., Iapichella, J., Bonhomme, K., Di Renzo, F., Kooyman, P., Terasaki, O., Fajula, F., *Adv. Funct. Mater.* **16** (2006) 1657.

3 Vallet-Regi, M., Balas, F., Arcos, D., *Angew. Chem. Int. Ed.* **46** (2007) 7548.

4 Wang, Q., Shantz, D. F., *J. Solid State Chem.* **181** (2008) 1659.

5 Gabaldon, J. P., Bore, M., Datye, A. K., *Top. Catal.* **44** (2007) 253.

6 Fryxell, G. F., Mattigod, S. V., Lin, Y., Wu, H., Fiskum, S., Parker, K., Zheng, F., Yantasee, W., Zemanian, T. S., Addleman, R. S., Liu, J., Kemner, K., Kelly, S., Feng, X., *J. Mater. Chem* **17** (2007) 2863.

7 Sing, K. S. W., Everett, D. H., Haul, R. H. W., Moscou, L., Pierotti, R. A., Rouquérol, J., Siemieniewska, T., *Pure Appl. Chem.* **57** (1985) 603.

8 Beck, J. S., Vartuli, J. C., Roth, W. J., Leonowicz, M. E., Kresge, C. T., Schmitt, K. D., Chu, C. T.-W., Olson, D. H., Sheppard, E. W., McCullen, S. B., Higgins, J. B., Schlenker, J. L., *J. Am. Chem. Soc.* **114** (1992) 10834.

9 Wan. Y., Zhao, D., *Chem. Rev.* **107** (2007) 2821.

10 Bois, L., Bonhomme, A., Ribes. A., Pais, B., Raffin, G., Tessier, F., *Colloids Surf. A* **221** (2003) 221.

11 French, S. A., Sokol, A. A., Catlow, C. R. A., Kornherr, A., Zifferer G., *Chem. Commun.* (2004) 20.

12 Yates, E. A., Jones, M. O., Clarke, C. E., Powell, A. K., Johnson, S. R., Porch, A., Edwards, P. P., Turnbull, J. E., *J. Mater. Chem.* **13** (2003) 2061.

13 Jaroniec, C. P., Kruk, M., Jaroniec, M., Sayari, A., *J. Phys. Chem. B* **102** (1998) 5503.

14 O`Gara, J. E., Walsh, D. P., Phoebe Jr., C. H., Alden, B. A., Bouvier, S. P., Iraneta, P. C., Capparella, M., Walter, T. H., *LC-GC* **19** (2001) 632.

15 Yokoi, T., Yoshitake, H., Tatsumi, T., *J. Mater. Chem.* **14** (2004) 951.

16 Lim. M. H., Stein, A., *Chem. Mater.* **11** (1999) 3285.

17 Barbe, C., Barlett, J., Kong, L., Finnie, K., Lin, H. Q., Larkin, M., Calleja, S., Bush, A., Calleja, G., *Adv. Mater.* **16** (2004) 1959.

18 Lelong, G., Bhattacharyya, S., Kline, S., Cacciaguerra, T., Conzalez, M. A., Saboungi, M.-L., *J. Phys. Chem. C* **112** (208) 10674.

19 Muñoz, B., Rámila, A., Pérez-Pariente, J., Díaz, I., Vallet-Regí, M., *Chem. Mater.* **15** (2003) 500.

20 Song, S. W., Hidajat, K., Kawi, S., *Langmuir* **21** (2005) 9568.

21 Brühwiler, D., Frei, H., *J. Phys. Chem. B* **107** (2003) 8547.

22 Zhao, D., Huo, Q., Feng, J., Chmelka, B. F., Stucky, G. D., *J. Am. Chem. Soc.* **120** (1998) 6024.

23 Ravikovitch, P. I., Neimark, A. V., *J. Phys. Chem. B* **105** (2001) 6817.

24 Galarneau, A., Cambon, H., Di Renzo, F., Fajula, F., *Langmuir* **17** (2001) 8328.

25 Galarneau, A., Cambon, H., Di Renzo, F., Ryoo, R., Choi, M., Fajula, F. *New J. Chem.* **27** (2003) 73.

26 Jun, S., Joo, S. H., Ryoo, R,; Kruk, M., Jaroniec, M., Liu, Z., Ohsuna, T., Terasaki, O., *J. Am. Chem. Soc.* **122** (2000) 10712.

27 Ying, J. Y., Mehnert, C. P., Wong, M. S., *Angew. Chem. Int. Ed.* **38** (1999) 56.

28 Suzuki, K., Ikari, K., Imai, H., *J. Am. Chem. Soc*. **126** (2004) 462.

29 Xu, J., Luan, Z., He, H., Zhou, W., Kevan, L., *Chem. Mater.* **10** (1998) 3690.

30 Shenderovich, I. G., Buntkowsky, G., Schreiber, A., Gedat, E., Sharif, S., Albrecht, J., Golubev, N. S., Findenegg, G. H., Limbach, H.-H., *J. Phys. Chem. B* **107** (2003) 11924.

31 Vrancken, K. C., Possemiers, K., Van Der Voort, P., Vansant, E. F., *Colloids. Surf. A* **98** (1995) 235.

32 Suntola, T., Antson, J., U.S. Patent No 4 058 430 (1977).

33 Ek, S., Iiskola, E. I., Niinistö, L., *Langmuir* **19** (2003) 3461.

34 Wirnsberger, G., Scott, B. J., Stucky, G. D., *Chem. Commun*. (2001) 119.

35 Kawski, A., *Photochem. Photobiol*. **38** (1983) 487.

36 Martin, M. M., Lindquist, L., *J. Lumin.* **10** (1975) 381.

37 Brunauer, S., Emmett, P. H., Teller, E., *J. Am. Chem. Soc.* **60** (1938) 309.

38 Barrett, E. P., Joyner, L. G., Halenda, P. P., *J. Am. Chem. Soc.* **73** (1951) 373.

39 Ravikovitch, P. I., Dommhanaill, S. C. O., Neimark, A. V., Schüth, F., Unger, K. K., Langmuir, 11 (1995) 4765.

40 Lastoskie, C., Gubbins, K. E., Quirke, N., *J. Phys. Chem.* **97** (1993) 4786.

41 Kruk, M., Jaroniec, M., Sayari, A., *J. Phys. Chem. B* **101** (1997) 583.

42 Kruk, M., Jaroniec, M., Ryoo, R., Kim, J. M., *Microporous Mater*. **12** (1997) 93.

43 Sayari, A., Liu, P., Kruk, M., Jaroniec, M., *Chem. Mater.* **9** (1997) 2499.

44 Rouquerol, F., Rouquerol, J., Sing, K. S. W., Adsorption by Powders & Porous solids, Academic Press, London 1999.

45 Lippens, B., de Boer, J. H., *J. Catal* **4** (1965) 319.

46 Kaiser, E., Colescott, R. L., Bossinger, C. D., Cook, P. I., *Anal. Biochem.* **34** (1970) 595.

47 Weigele, M., DeBernando, S. L., Tengi, J. P., Leimgruber, W., *J. Am. Chem. Soc.* **94** (1972) 5927.

48 Udenfriend, S., Stein, S., Böhlen, P., Dairman, W., Leimgruber, W., Weigele, M., *Science* **178** (1972) 871.

49 Brand, M., Frings, A., Jenkner, P., Lehnert, R., Metternich, H. J., Monkiewicz, J., Schram, J. Z., *Naturforsch. B: Chem Sci.* **54** (1999**)** 155.

50 Suppan, P., Chemistry and Light, the Royal Society of Chemistry, Cambridge 1994.

51 Gartmann, N., Master thesis, Mesoporous Hybrid Materials: Tools for the Analysis of Functional Group Distributions, Zürich 2008.

52 Liu, H.-M., Wu, S.-H., Lu, C.-W., Yao, M., Hsiao, J.-K., Hung, Y., Lin, Y.-S., Mou, C.-Y., Yang, C.-S., Huang, D.-M., Chen, Y.-C., *Small* **4** (2008) 619.

53 Mal, N. K., Fujiwara, M., Tanaka, Y., *Nature* **421** (2003) 350.

54 Kanan, S. M., Tze, W. T. Y, Tripp, C. P., *Langmuir* **18** (2002) 6623.

55 Tripp, C. P., Hair, M. L., *Langmuir* **11** (1995) 1215.

56 Ek, S., Iiskola, E. I., Niinistö, L., Vaittinen, J., Pakkanen, T., Root, A., *J. Phys. Chem. B* **108** (2004) 11454.

57 Zhuravlev, L. T., *Colloids Surf. A* **173** (2000) 1.

58 Cassiers, K., Linssen, T., Mathieu, M., Benjelloun, M., Schrijnemakers, K., Van Der Voort, P., Cool, P., Vansant, E. F., *Chem. Mater.* **14** (2002) 2317.

59 Kim, J. M., Kwak, J. H., Jun, S., Ryoo, R., *J. Phys. Chem.* **99** (1995) 16742.

60 Chen, C.-Y., Li, H.-X., Davis, M. E., *Microporous Mater.* **2** (1993) 17.

61 Ek, S., Iiskola, E. I., Niinistö, L., Vaittinen, J., Pakkanen, T. T., Keränen, J., Auroux, A., *Langmuir* **19** (2003) 10601.

62 Kallury, K. M. R., Macdonald, P. M., Thompson, M., *Langmuir* **10** (1994) 492.

63 Burleigh, M. C., Markowitz, M. A., Spector, M. S., Gaber, B. P., *J. Phys. Chem. B* **105** (2001) 9935.

64 Li, C., Yang, J., Shi, X., Liu, J., Yang, Q., *Microporous Mesoporous Mater.* **98** (2007) 220.

65 Melde, B. J., Schroden, R. C., Stein, A., *Adv. Mater.* **12** (2000) 1403.

66 Bellocq, N., Abramson, S., Lasperas, M., Brunel, D., Moreau, P., *Tetrahedron: Asymmetry* **10** (1999) 3229.

67 Engelhardt, H., Orth, P., *J. Liq. Chromatogr.* **10** (1987) 1999.

68 Sharma, K. K., Anan, A., Buckley, R. P., Ouellette, W., Asefa, T., *J. Am. Chem. Soc.* **130** (2008) 218.

69 Sharma, K. K., Asefa, T., *Angew. Chem. Int. Ed.* **46** (2007) 2879.

70 Corma, A., *Chem. Rev.* **97** (1999) 2373.

71 Bornscheuer, U. T., *Angew. Chem. Int. Ed.* **42** (2003) 3336.

72 Lai., C.-Y., Trewyn, B. G., Jeftinija, D. M., Jeftinija, K., Xu, S., Jeftinija, S., Lin, V. S.-Y., *J. Am. Chem. Soc.* **125** (2003) 4451.

73 Antochshuk, V., Jaroniec, M., *Chem. Mater.* **12** (2000) 2496.

74 Stigers, K. D., Koutroulis, M. R., Chung, D. M., Nowick, J. S., *J. Org. Chem.* **65** (2000) 3858.

75 Cheng, K., Landry, C. C., *J. Am. Chem. Soc.* **129** (2007) 9674.

76 Lang, N., Tuel, A., *Chem. Mater.* **16** (2004) 1961.

77 Neuenschwander, M., Vögeli, R., Fahrni, H.-P., Lehmann, H., Ruder, J.-P., *Helv. Chim. Acta* **60** (1977) 1073.

Appendix

- Distribution of Amino Groups on a Mesoporous Silica Surface after Submonolayer Deposition of Aminopropylsilanes from an Anhydous Liquid Phase

  H. Salmio, D. Brühwiler, *J. Phys. Chem. C* **111** (2007) 923-929.

- A Comparative Study of the Functionalization of Mesoporous Silica MCM-41 by Deposition of 3-Aminopropyltrimethoxysilane from Toluene and from the Vapor Phase

  H. Ritter, M. Nieminen, M. Karppinen, D. Brühwiler, *Microporous Mesoporous Mater.*, in press.

- Accessibility of Grafting Sites in Postsynthetically Modified Mesoporous Silica

  H. Ritter, D. Brühwiler, submitted.

Distribution of amino groups on a mesoporous silica surface after submonolayer deposition of aminopropylsilanes from an anhydrous liquid phase

*Hanna Salmio and Dominik Brühwiler**

Institute of Inorganic Chemistry, University of Zurich, Winterthurerstrasse 190, 8057 Zurich, Switzerland

Abstract. The reaction of mesoporous silica MCM-41 with various aminopropylsilanes was investigated. The distribution of grafted amino groups after submonolayer deposition from anhydrous toluene was probed by fluorescein labeling in conjunction with photoluminescence spectroscopy and pore size analysis. Monoalkoxysilanes generally distributed more uniformly than monopodal and dipodal trialkoxysilanes. The outcome of the grafting reaction additionally depended on the nature of the amino group. Secondary amines grafted more efficiently than their primary analogues. Further, it could be shown that the polarity of the solvent considerably affects the distribution of the amino groups in the case of strongly interacting aminopropylsilanes.

Keywords. MCM-41, grafting, silane, site isolation, clustering, cross-linking

*Corresponding Author. E-mail: bruehwi@aci.unizh.ch

Introduction

Since the discovery of the remarkable features of the M41S mesoporous silica family,[1] considerable effort has been directed towards functionalization of these materials. Catalysis[2], optical sensing[3], photonics[4], adsorption[5], and drug delivery[6] are fields in which functionalized mesoporous silica opens new prospects. For many potential applications based on mesoporous silica a homogeneous distribution of site isolated functional groups is desired. In this perspective, co-condensation would be the method of choice, as postsynthetic modification often leads to preferential functionalization of the most readily accessible sites (external surface and pore entrances).[7] However, postsynthetic grafting provides various advantages: Through passivation of the external surface, the internal surface can be selectively functionalized (and vice versa).[8] High densities of functional groups are achievable without unfavorable effects on the stability and the periodic ordering of the mesoporous silica framework. Site isolation can be obtained even for dense grafting by a molecular spacer approach.[9] Control of the pore size and particle morphology is

straightforward, and hierarchic structures can be produced by post-synthetic molecular imprinting.[10]

Aminopropylsilanes are among the most widely used precursors for the modification of silica surfaces. In anhydrous medium, reaction with surface hydroxyl groups proceeds via exchange of the silane alkoxy group (usually methoxy or ethoxy) for the silanol oxygen with concurrent loss of the corresponding alcohol. It is shown in this study, that the choice of the aminopropylsilane precursor is essential for controlling the amount, the distribution, and the stability of the grafted aminopropyl moieties on the mesoporous silica surface.

Experimental Section

Synthesis of MCM-41. Purely siliceous mesoporous silica MCM-41 was synthesized as follows:[11] An amount of 2.20 g of CTAB (hexadecyltrimethyl-ammonium bromide, Fluka) was dissolved under slight warming in a mixture of 52 mL of distilled H_2O and 24 mL of aqueous ammonia (28 %, Fluka). After cooling to room temperature, 10 mL of TEOS (tetraethoxysilane, Fluka) was slowly added under stirring to the clear solution and the resulting gel was further stirred for 3 h at room temperature. The mixture was then transferred to a Teflon lined autoclave and heated at 110 °C for 48 h. The product was obtained by filtration, washed with copious amounts of distilled H_2O (at least 800 mL) and dried in air at room temperature. The template was removed by first heating at 300 °C for 2 h and subsequent calcination in air at 550 °C for 16 h. Heating rates of approximately 2 °C/min were applied.

Grafting of Aminopropyl-silanes. (3-aminopropyl)dimethyl-methoxysilane (APDMMS, Acros), (3-aminopropyl)di-isopropylethoxysilane (APDIPES, Gelest), (3-aminopropyl)-trimethoxysilane (APTMS, Fluka), [3-(methylamino)-propyl]trimethoxysilane (MAPTMS, Gelest), (3-aminopropyl)-triethoxysilane (APTES, Fluka), bis(trimethoxysilyl)propylamine (BTMSPA, Fluka), bis(tri-ethoxysilyl)-propylamine (BTESPA, Gelest), and [3-(methylamino)propyl]methyldimethoxy-silane (MAPMDMS, Gelest) were used as received. Polymerization of the liquid amino-propylsilanes is initiated by the presence of water, leading to hydrolysis and cross-linking. All aminopropylsilanes were therefore kept under inert atmosphere. Experiments with freshly vacuum distilled aminopropylsilanes showed that polymerization was not a concern under our storage conditions. In a typical grafting experiment, an amount of 500 mg of calcined MCM-41 was oven-dried at 80 °C for 1 h and dispersed in 30 mL of dry toluene (puriss., H_2O < 0.005 %). After the addition of a calculated amount of a specific aminopropylsilane, the suspension was heated to 125 °C over a period of 15 min, refluxed for 3 h and subsequently allowed to cool for 30 min. The functionalized product was recovered by

filtration, washed with 100 mL of ethanol, and oven-dried at 80 °C for 1 h.

Fluorescein Labeling. An amount of 250 mg of amino-functionalized mesoporous silica was dispersed in 25 mL of absolute ethanol containing an at least 1.5-fold excess of FITC (fluorescein 5-isothiocyanate, isomer I, Fluka). The amount of FITC was calculated assuming quantitative grafting of the respective aminopropylsilane (15 mg of FITC for a batch prepared with a theoretical aminopropylsilane loading of 100 µmol per gram of MCM-41). After stirring the suspension in the dark at room temperature for 24 h, the colored product was recovered by filtration and washed with 50 mL of ethanol. Prolongation of the FITC coupling time did not lead to further fluorescein binding, indicating that complete labeling of amino groups is obtained after 24 h. To ensure removal of unreacted FITC, the product was redispersed in 50 mL of ethanol and stirred for 15 min at room temperature. After filtration and washing with 50 mL of ethanol, the product was finally oven-dried at 80 °C for 1 h. To determine the amount of coupled fluorescein, a weighed quantity (typically 15 to 30 mg) of the product was dispersed in 25 mL of a 0.2 M aqueous solution of NaOH and stirred for 3 h at room temperature. After dissolution of the silica, the clear solution was diluted with water and the fluorescein concentration was determined by measuring the UV-Vis absorption spectrum (λ_{max} = 490 nm, ε_{max} = 88'000 $Lmol^{-1}cm^{-1}$).

Characterization. Powder X-ray diffraction (XRD) measurements were performed on a Siemens D-500 diffractometer with CuKα radiation, a 2θ step size of 0.05°, and a counting time of 3 s per step. Photoluminescence (PL) spectra were recorded with a Perkin Elmer LS50B spectrofluorometer equipped with a front surface accessory for the measurement of powdered samples. Nitrogen sorption isotherms were collected at 77 K using a Quantachrome NOVA2200 surface area and pore size analyzer. Samples were vacuum-degassed at 353 K for 5 h. The total surface area was obtained using the standard BET method for adsorption data in a relative pressure range from 0.05 to 0.20.[12] The total pore volume was estimated from the amount of nitrogen adsorbed at a relative pressure of 0.95. The primary mesopore volume V_p (the volume of the uniform mesopores) was determined by the α_S-plot method.[13] Mesopore size distributions were evaluated from the desorption branches of the nitrogen isotherms using the BJH method and are plotted relative to the maximum pore diameter of the corresponding parent MCM-41.[14] All samples exhibited type IV isotherms and condensation in primary mesopores was not accompanied by hysteresis. It should be noted that the standard BJH method underestimates the absolute pore size. In order to obtain a more reliable estimate, the method proposed by Kruk et al. was applied:[15]

$$w = 1.2125 \cdot d_{100}\left(\frac{\rho V_p}{1+\rho V_p}\right)^{1/2} \qquad (1)$$

The lattice spacing d_{100} was obtained from XRD data. The density of the pore walls ρ was set to be equal to the density of amorphous silica (2.2 g/cm^3).

Results and Discussion

Blank Test. The investigation of submonolayer coverages requires the evaluation of subtle variations in the pore size distribution (PSD). It is therefore crucial to analyze the pore size changes under the applied reaction conditions without the addition of an aminopropylsilane. We observed a minor shift of the PSD to smaller pore size up to the point of FITC coupling (refluxing in toluene, washing, drying), and a similar shift under FITC coupling conditions (stirring for 24 h in an ethanolic solution of FITC, washing, drying). No fluorescein was detected in the samples at this stage, indicating that binding of FITC only occurs on aminopropylsilane modified MCM-41. The total shift of the PSD of the blank samples was typically 0.04 nm (diameter), with the distribution retaining its width and symmetrical shape. This minor change is attributed to a slight esterification of the surface during the washing treatments in ethanol and subsequent drying.[16]

General Tendencies. We have investigated the reaction of various commercial aminopropylsilanes with calcined MCM-41 in toluene. Structures and abbreviations are given in Figure 1. The pore diameter of our parent MCM-41 was calculated to be 3.6 nm using eq (1), resulting in a pore wall thickness of 0.8 nm. BET surface areas varied slightly from batch to batch in the range of 810 to 890 m^2/g. An external surface area (secondary mesopores and macropores) of approximately 65 m^2/g was estimated from the high pressure part of the α_S-plots. Although the preparation of MCM-41 proved to be well reproducible in terms of the PSD, comparative studies were only conducted on samples synthesized from the same batch of parent MCM-41.

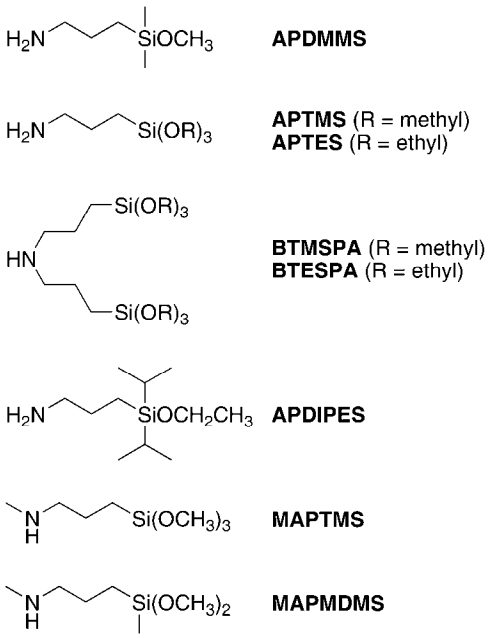

Figure 1. Structures and abbreviations of aminopropylsilanes.

It is instructive to investigate the grafting behavior of a monomethoxy-silane, trimethoxysilane, and a dipodal silane featuring two trimethoxysilyl groups. Taking into account a surface silanol concentration of approximately 3 mmol/g,[17] a charge of 100 µmol aminopropylsilane per gram of MCM-41

ensures an excess of silanol groups. Figure 2 shows the PSDs of MCM-41 after reaction with 100 µmol/g APDMMS, APTMS, or BTMSPA. A shift towards smaller pore size is observed for all samples. However, the extent of this shift strongly depends on the type of silane. For the dipodal silane BTMSPA, the PSD maximum is only slightly shifted relative to the parent MCM-41. Shifts of similar magnitude were observed for the blank samples. The distinctive tail extending towards smaller pore size suggests a nonuniform distribution of the amine sites. The monomethoxysilane APDMMS, on the other hand, grafts more uniformly to the mesoporous silica surface, resulting in a larger shift and a symmetrical PSD. The APTMS grafted sample features properties lying between those two extremes.

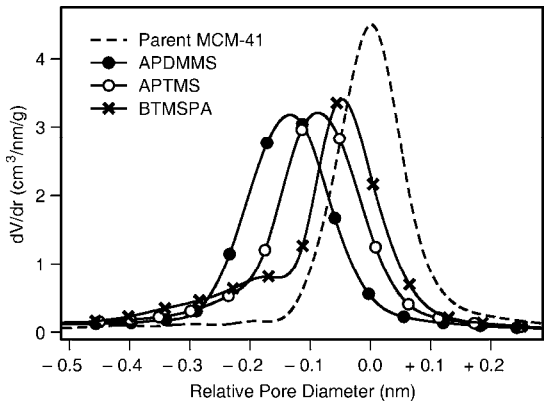

Figure 2. PSDs of MCM-41 after reaction with 100 µmol/g of APDMMS, APTMS, or BTMSPA.

FITC is one of the most popular labeling reagents, forming a thiourea upon reaction with an amine (see Figure 3). Apart from being used to modify proteins, peptides, synthetic

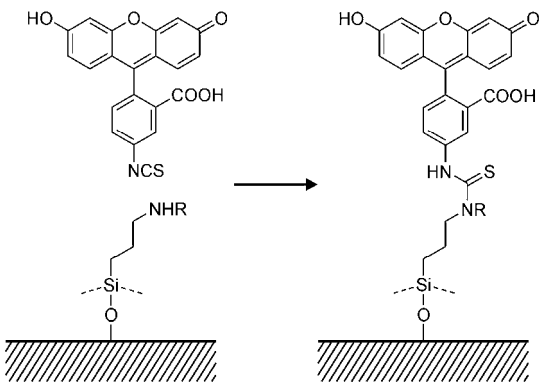

Figure 3. Coupling of FITC to surface bound primary (R=H) and secondary aminopropylsilanes. The number of possible siloxane bonds depends on the type of silane.

oligonucleotides and other biomolecules, FITC has recently been applied in the preparation of mesoporous thin films with pH sensing ability.[18] Coupling of FITC is expected to amplify the differences between the APDMMS, APTMS, and BTMSPA grafted samples. The reaction of FITC with amino groups located on the internal surface changes the PSD, while the coupling of FITC to amino groups anchored to the external surface has no effect in this regard. In the case of the APDMMS grafted sample, the PSD is further shifted to smaller pore size. This is in contrast to the BTMSPA grafted sample, for which a significantly smaller shift of the maximum pore diameter is observed (see Figure 4). Shifts of this magnitude also occurred for blank samples. The PSD of the BTMSPA grafted material remains unsymmetrical, with uneven contributions of smaller pore sizes. Again, intermediate behavior is

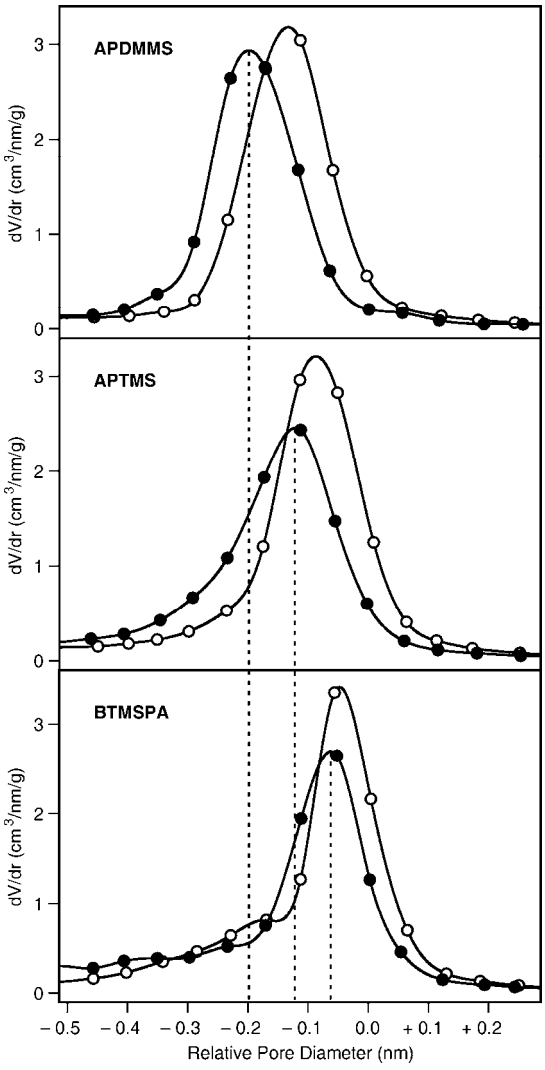

Figure 4. PSDs of APDMMS, APTMS, and BTMSPA grafted samples before (open circles) and after (filled circles) FITC coupling. Fluorescein contents are 20 µmol/g (APDMMS), 36 µmol/g (APTMS), and 52 µmol/g (BTMSPA). The samples were prepared from the same batch of MCM-41 by reaction with 100 µmol/g of the corresponding aminopropylsilane.

found for APTMS. The relatively large pore size shift of the APDMMS grafted sample is surprising considering the fluorescein contents, which amounted to 20 µmol/g for APDMMS, 36 µmol/g for APTMS, and 52 µmol/g for BTMSPA. These results clearly indicate that BTMSPA preferably binds to sites on or close to the external surface. The distinct tail of the PSD suggests clustering of BTMSPA at pore entrance sites. For APTMS and APDMMS, increased grafting in the pores is observed, with APDMMS yielding the most homogeneous distribution of grafting sites. The amount of coupled fluorescein can be taken as a measure of the grafting efficiency of the respective aminopropylsilane.

Further information on the distribution of the amine sites is obtained by examining the photoluminescence of the FITC coupled samples. In order to allow for comparison of the luminescence intensities, samples containing equal amounts of fluorescein were synthesized by adjusting the aminopropylsilane concentration in the reaction mixtures. The resulting luminescence spectra and PSDs are shown in Figure 5. Additional nitrogen adsorption analysis data is compiled in Table 1. At this point it is helpful to briefly discuss the pH dependence of the fluorescein luminescence in solution.[19] Three different fluorescence spectra are typically observed in H_2O when the pH is varied. The cation emission (λ_{max} = 475 nm) appears only in strongly acidic solution. with prominent shoulders around 555 and 595 nm. The fluorescence spectrum of the dianion

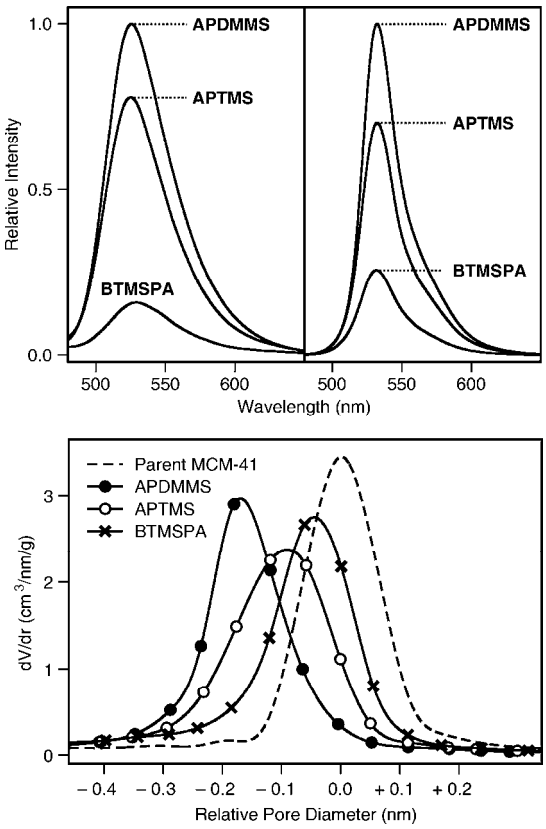

Figure 5. Top: PL spectra of FITC coupled samples grafted with different aminopropylsilane precursors (excitation at 450 nm). The spectra in the left panel were measured on dry samples. The right panel shows the corresponding spectra measured on equally concentrated suspensions in toluene/triethylamine. Bottom: PSDs of the same samples. Fluorescein contents are (20.0 ± 1.0) µmol/g.

features the same maximum, but is narrowed compared to the spectrum of the monoanionic and neutral species. Furthermore, the dianion exhibits a higher fluorescence yield (0.93)[20] than the neutral/monoanionic species (0.20 – 0.35)[19]. Inspecting the luminescence spectra in Figure 5, we can immediately rule out the presence of cationic fluorescein species. To assure that the intensity differences of the samples are not due to varying ratios of neutral, monoanionic, and dianionic fluorescein, PL measurements were performed on toluene suspensions which were titrated with triethylamine until maximum luminescence intensity was observed. Addition of triethylamine leads to narrowing of the luminescence bands, yielding samples exclusively containing dianionic fluorescein. For both dry samples and toluene/triethylamine suspensions, the luminescence intensity increases in the series BTMSPA < APTMS < APDMMS. These remarkably different luminescence intensities are attributed to various degrees of self-quenching. The self-quenching of fluorescein is due to resonance energy transfer between fluorescein molecules, with a Förster distance of 42 Å.[21] Efficient self-quenching therefore implies short distances between the grafted amine sites. Since the investigated coverages lie well within the submonolayer regime, a diminished luminescence intensity suggests clustering of amine sites.

Table 1. Nitrogen adsorption data after FITC coupling.[a,b]

silane	V_{tot} (cm^3/g)	V_p (cm^3/g)	S_{BET} (m^2/g)
BTMSPA	0.635	0.567	780
APTMS	0.625	0.557	770
APDMMS	0.601	0.536	746

[a] V_{tot} = total pore volume; V_p = primary mesopore volume; S_{BET} = BET surface
[b] fluorescein content = (20.0 ± 1.0) µmol/g

Methoxy vs. Ethoxy. Methoxysilanes are generally more reactive than ethoxysilanes.[22] On the other hand, ethoxysilanes are more bulky than the corresponding methoxysilanes. The comparison of the grafting behavior of BTMSPA/BTESPA and APTMS/APTES revealed only minor differences. The yield of FITC coupling was similar for the BTMSPA/BTESPA and APTMS/APTES pairs. However, the tendency to graft to the internal surface was slightly more pronounced in the case of the ethoxysilanes. This difference, while reproducible, is admittedly subtle and much smaller than what we observed when comparing APDMMS, APTMS, and BTMSPA. After FITC coupling, the materials grafted with APTES and BTESPA also showed slightly stronger luminescence compared to the materials grafted with the corresponding methoxysilanes, suggesting a lower degree of clustering.

APDMMS vs. APDIPES. Our results so far indicate that in terms of obtaining a homogeneous distribution of grafting sites, APDMMS is superior to APTMS and BTMSPA. On the minus side, APDMMS grafted samples suffer from reduced stability against solvolysis.[23] Stirring a APDMMS grafted sample (30 mg, 20 µmol/g of coupled fluorescein) in 0.2 M sodium phosphate buffer (20 mL, pH 7.5) for 24 h at room temperature resulted in a loss of (53 ± 3) % of fluorescein. This problem is solved by replacing APDMMS with APDIPES. APDIPES grafted samples feature pore sizes resembling those of the corresponding APDMMS grafted samples (see Figure 6). Taking into account the similar luminescence properties of FITC coupled APDMMS and APDIPES samples, we can conclude that an equally homogeneous distribution of amine sites is obtained. Moreover, APDIPES grafted samples are as stable as their APTMS counterparts. Under the hydrolysis conditions described above, leaching of only (18 ± 3) % of fluorescein was observed. Apparently, the bulky isopropyl groups protect the single siloxane link. This is in agreement with the improved low pH hydrolytic stability of common bonded-phase silicas treated with monofunctional silanes containing bulky groups at the silicon atom.[24] It is interesting to note that despite being more bulky than APTMS, APDIPES is able to bind to less accessible sites on the internal surface and thus produces a more uniform distribution of grafted amino groups.

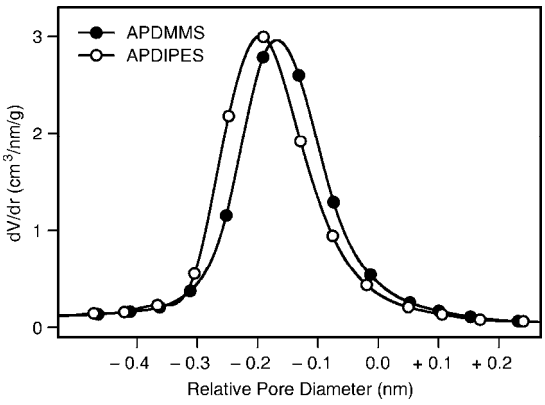

Figure 6. PSDs of APDMMS and APDIPES grafted samples after FITC coupling. Fluorescein contents are (20.0 ± 1.0) µmol/g.

Primary vs. Secondary Amines. To study the role of the amino functionality in the grafting process, it is instructive to compare the reactivity of APTMS and MAPTMS. Despite the fact that both molecules are trimethoxysilanes, the grafting of MAPTMS was found to be considerably more efficient. The reaction of 50 µmol of the respective silane with 500 mg of MCM-41 and subsequent FITC coupling resulted in fluorescein contents of 52 µmol/g for MAPTMS and 36 µmol/g for APTMS. In terms of grafting efficiency, MAPTMS apparently resembles BTMSPA, emphasizing the important role of the amino functionality in the self-catalyzed grafting process.[25] However, when compared to BTMSPA, MAPTMS showed a higher tendency to graft to the internal surface, although not surpassing APTMS grafted samples of the same loading (see Figure 7). The luminescence properties of MAPTMS grafted samples after FITC coupling are comparable to APTMS grafted samples of the same fluorescein content. Under identical reaction conditions, the degree of clustering therefore seems to be determined mainly by the number of methoxy groups per molecule.

Grafting Mechanism. Apparently there is a correlation between the tendency to yield a homogeneous distribution of grafting sites and the number of alkoxy groups (methoxy or ethoxy) per aminopropylsilane molecule. Furthermore, secondary amines give higher grafting yields (estimated from

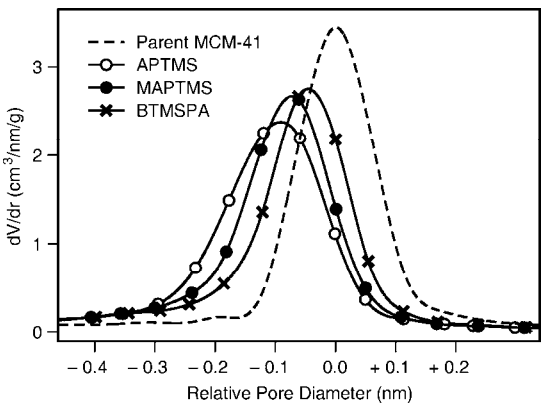

Figure 7. PSDs of APTMS, MAPTMS, and BTMSPA grafted samples after FITC coupling. Fluorescein contents are (20.0 ± 1.0) µmol/g.

the amount of coupled fluorescein) than primary amines. In view of these results, the following mechanism for the reaction of aminopropylsilanes with mesoporous silica is proposed. In a first step, the aminopropylsilane is adsorbed on the mesoporous silica surface forming hydrogen bonds with surface silanol groups. The amino groups thereby function as hydrogen bond acceptors. There is evidence in the case of APTES that this first step reaches an equilibrium within one minute.[25] This initial adsorption concerns accessible silanols, that is, sites on the external surface and sites close to the pore entrances. Note that we have used maximum aminopropylsilane amounts of 100 µmol per gram of MCM-41. Adsorption of a submonolayer is therefore possible even without access to the entire MCM-41 surface. BTMSPA and BTESPA exhibit the strongest interaction with the surface, since their secondary amines are better acceptors

for hydrogen bonds than the primary amines of APTMS, APTES, APDMMS, and APDIPES. Additionally, six alkoxy groups per molecule are available for siloxane bond formation. On the other hand, the monoalkoxysilanes (APDMMS and APDIPES) are more mobile due to a weaker interaction with the surface and are thus able to reach less accessible sites located in the pores. Furthermore, silanes with more than one alkoxy group per molecule have the tendency to form aminopropylsilane islands. This contributes to a nonuniform distribution of the grafting sites, manifesting itself in low luminescence intensities after FITC coupling.

The mechanism leading to the formation of aminopropylsilane islands is subject to speculation. The activation of surface silanols by hydrogen-bonded aminopropylsilanes might advance the formation of islands,[25] especially in regions of high silanol density on the rough MCM-41 surface.[26] Cross-linking between aminopropylsilane molecules is also expected to promote clustering. However, this process requires the presence of water for the preceding hydrolysis step. The actual amount of water on a silica surface depends on the thermal pretreatment.[27] In order to provide reproducible conditions, all our calcined MCM-41 materials were treated at 80 °C before use. This temperature was chosen because of its compatibility with organic modifications introduced by postsynthetic grafting or co-condensation. Total release of physisorbed water usually requires temperatures above 100 °C.[27] The solvent is another potential source of trace water, regardless of careful dehydration treatments. This problem is associated with the fact that silica behaves as a drying agent, adsorbing even minute quantities of water.[28] We can therefore conclude that traces of water are present and that cross-linking most likely contributes to the clustering of the dipodal and (to a smaller extent) the monopodal trialkoxysilanes. Previous studies on the reaction of APTES with silica gel have shown that hydrolysis and cross-linking take place on the silica surface, that is, after the initial adsorption of the silane monomers.[29] Small amounts of water thereby not only promote cross-linking of adsorbed aminopropylsilanes, but also enhance the reactivity of the silanes towards surface silylation.[30] In order to minimize cross-linking, complete dehydration of MCM-41 would be necessary. This requires temperatures where dehydroxylation occurs simultaneously[27] and decomposition of organic functionalities introduced into the MCM-41 framework becomes an issue. As will be shown below, clustering of aminopropylsilanes on the MCM-41 surface can be conveniently minimized by increasing the polarity of the solvent used for the grafting reaction.

The relatively large size of the BTMSPA and BTESPA molecules might contribute to a nonuniform distribution by partial pore blocking. Considering the initial pore diameter of 3.6 nm and the low aminopropylsilane loadings, we expect that such effects are of minor importance under our conditions. This is

supported by the observation that APDIPES distributes more uniformly than the less bulky APTMS. Further evidence that the grafting reactions are not governed by pore blocking was obtained by substituting MCM-41 with fumed silica, which is essentially non-porous while still featuring a large surface area (200 m^2/g). Grafting of BTMSPA, APTMS, and APDMMS to fumed silica and subsequent FITC coupling resulted in fluorescein contents comparable to analogous samples based on MCM-41. More importantly, the luminescence properties of the FITC coupled fumed silica samples resembled those of the corresponding MCM-41 materials.

Prediction of Grafting Behavior.

Our interpretation of the results can be put to a test by attempting to predict the grafting behavior of MAPMDMS (see Figure 1). Being a secondary amine, we anticipate a high grafting yield. In accordance with our expectation, fluorescein contents similar to MAPTMS grafted samples were observed. The presence of only two methoxy groups should lead to an increased mobility of MAPMDMS when compared to MAPTMS. The PSDs of the FITC coupled samples indeed support this hypothesis (see Figure 8). However, when compared to APTMS, the ability of MAPMDMS to graft to internal surface sites is less pronounced, emphasizing the strong interaction of the secondary amino group with the silica surface. Clustering of MAPMDMS molecules is less likely than clustering of the trimethoxysilanes APTMS and MAPTMS. The strong luminescence of FITC coupled samples grafted with MAPMDMS effectively provides evidence for a low tendency to form islands (see Figure 8). Comparison of the relative luminescence intensities in Figures 5 and 8 indicates similarities between MAPMDMS and APDMMS grafted samples. We can therefore conclude that clustering in MAPMDMS grafted samples is virtually absent.

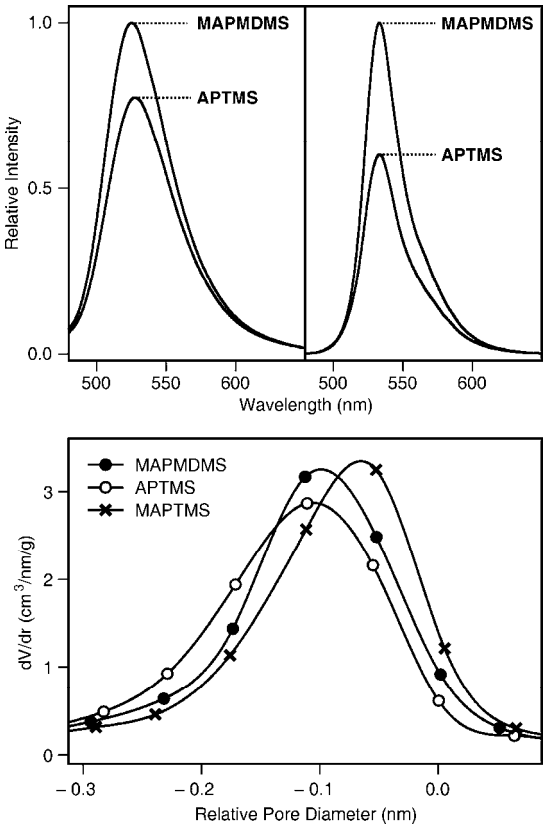

Figure 8. Left: PL spectra of FITC coupled samples grafted with APTMS and MAPMDMS (excitation at 450 nm). The spectra in the left panel were measured on dry samples. The right panel shows the corresponding spectra measured on equally concentrated suspensions in toluene/triethylamine. PSDs are given in the right panel. Fluorescein contents are (20.0 ± 1.0) µmol/g.

Solvent Effects. As a further implication of the proposed grafting mechanism, it is to be expected that the use of a more polar solvent than toluene will generate a more uniform distribution of grafting sites by increasing the mobility of the aminopropylsilane molecules. We have tested this hypothesis by comparing the grafting behavior of BTMSPA in toluene and THF. The results are shown in Figure 9. While the grafting yield remains essentially unchanged when THF is used as a solvent, the strong luminescence of the FITC coupled BTMSPA/THF sample suggests decreased clustering. Furthermore, the PSD of the BTMSPA/THF sample is shifted to smaller pore size by a considerable amount, comparable to APTMS/toluene samples.

The inhibition of clustering in polar solvents bears important consequences. Site isolated grafting is favored and the formation of multilayer coverages becomes less likely in the case of excess silane. The latter was observed for the room temperature functionalization of an external zeolite surface with APTES.[31] For a given aminopropylsilane it is therefore possible to tune the distribution of the grafting sites and the degree of silane clustering by choosing an appropriate solvent. Such solvent effects are less distinct in the case of weakly interacting aminopropylsilanes, that is, primary aminopropylsilanes with small numbers of alkoxy groups.

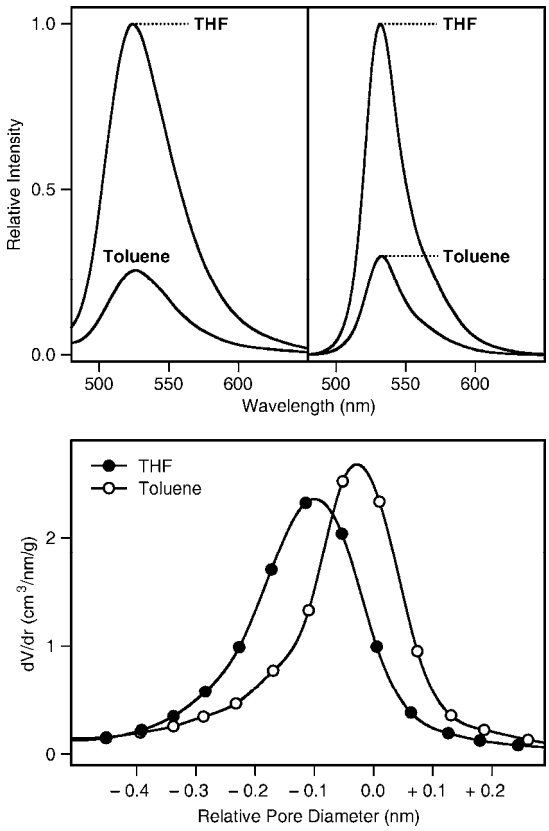

Figure 9. Top: PL spectra of FITC coupled samples grafted with BTMSPA in THF and toluene, respectively (excitation at 450 nm). The spectra in the left panel were measured on dry samples. The right panel shows the corresponding spectra measured on equally concentrated suspensions in toluene/triethylamine. PSDs are given in the bottom panel. Fluorescein contents are (20.0 ± 1.0) µmol/g.

Conclusions

The structure of an aminopropylsilane determines its grafting behavior. Grafting yields strongly depend on the type of amine, while the uniformity of the amine site distribution on the mesoporous silica surface is mainly determined by the number of alkoxy groups. Consequently, the brightness of

FITC coupled samples can be maximized by employing monoalkoxysilanes instead of the widely used trialkoxysilanes as postsynthetically applied surface anchors. Dipodal trialkoxysilanes react preferably with sites on the external surface and at the pore entrances and are therefore candidates for selective external surface modification. Finally, the polarity of the solvent is essential for controlling the grafting site distribution and the degree of clustering. Clustering is minimized with increasing polarity, while the distribution becomes more uniform as the aminopropylsilane molecules are able to reach less accessible sites on the internal surface. Means to control the distribution of grafting sites on mesoporous silica are essential for a variety of potential applications. Optical sensing and cell marking applications rely on a high brightness of the luminescent silica particles, thus requiring site isolated chromophores.[18,32] On the other hand, the accumulation of grafted molecules on the external surface and at the pore entrances is of interest for the design of advanced drug delivery systems.[6c]

Acknowledgments.

Financial support was provided by the Swiss National Science Foundation (project 200021-109185).

References

(1) Beck, J. S.; Vartuli, J. C.; Roth, W. J.; Leonowicz, M. E.; Kresge, C. T.; Schmitt, K. D.; Chu, C. T. W.; Olson, D. H.; Sheppard, E. W.; McCullen, S. B.; Higgins, J. B.; Schlenker, J. L. *J. Am. Chem. Soc.* **1992**, *114*, 10834.

(2) (a) Taguchi, A.; Schüth, F. *Microporous Mesoporous Mater.* **2005**, *77*, 1. (b) De Vos, D. E.; Dams, M.; Sels, B. F.; Jacobs, P. A. *Chem. Rev.* **2002**, *102*, 3615.

(3) Wark, M.; Rohlfing, Y.; Altindag, Y.; Wellmann, H. *Phys. Chem. Chem. Phys.* **2003**, *5*, 5188.

(4) Scott, B. J.; Wirnsberger, G.; Stucky, G. D. *Chem. Mater.* **2001**, *13*, 3140.

(5) (a) Yoshitake, H.; Yokoi, T.; Tatsumi, T. *Chem. Mater.* **2002**, *14*, 4603. (b) Liu, J.; Feng, X.; Fryxell, G. E.; Wang, L.-Q.; Kim, A. Y.; Gong, M. *Adv. Mater.* **1998**, *10*, 161.

(6) (a) Lai, C.-Y.; Trewyn, B. G.; Jeftinija, D. M.; Jeftinija, K.; Xu, S.; Jeftinija, S.; Lin, V. S.-Y. *J. Am. Chem. Soc.* **2003**, *125*, 4451. (b) Muñoz, B.; Rámila, A.; Pérez-Pariente, J.; Diaz, I.; Vallet-Regi, M. *Chem. Mater.* **2003**, *15*, 500. (c) Mal, N. K.; Fujiwara, M.; Tanaka, Y. *Nature* **2003**, *421*, 350.

(7) (a) Yokoi, T.; Yoshitake, H.; Tatsumi, T. *J. Mater. Chem.* **2004**, *14*, 951. (b) Lim, M. H.; Stein, A. *Chem. Mater.* **1999**, *11*, 3285. (c) Singh, U. G.; Williams, R. T.; Hallam, K. R.; Allen, G. C. *J. Solid State Sci.* **2005**, *178*, 3405.

(8) Shephard, D. S.; Zhou, W.; Maschmeyer, T.; Matters, J. M.; Roper, C. L.; Parsons, S.; Johnson, B. F. G.; Duer, M. J. *Angew. Chem. Int. Ed.* **1998**, *37*, 2719.

(9) Hicks, J. C.; Jones, C. W. *Langmuir* **2006**, *22*, 2676.

(10) Shin, Y.; Liu, J.; Wang, L.-Q.; Nie, Z.; Samuels, W. D.; Fryxell, G. E.; Exarhos, G. J. *Angew. Chem. Int. Ed.* **2000**, *39*, 2702.

(11) Brühwiler, D.; Frei, H. *J. Phys. Chem. B* **2003**, *107*, 8547.

(12) Brunauer, S.; Emmett, P. H.; Teller, E. *J. Am. Chem. Soc.* **1938**, *60*, 309.

(13) Kruk, M.; Jaroniec, M.; Ryoo, R.; Kim, J. M. *Microporous Mater.* **1997**, *12*, 93.

(14) Barrett, E. P.; Joyner, L. G.; Halenda, P. P. *J. Am. Chem. Soc.* **1951**, *73*, 373.

(15) Kruk, M.; Jaroniec, M.; Sayari, A. *J. Phys. Chem. B* **1997**, *101*, 583.

(16) Kimura, T.; Kuroda, K.; Sugahara, Y.; Kuroda, K. *J. Porous Mater.* **1998**, *5*, 127.

(17) Zhao, X. S.; Lu, G. Q.; Whittaker, A. K.; Millar, G. J.; Zhu, H. Y. *J. Phys. Chem. B* **1997**, *101*, 6525.

(18) Wirnsberger, G.; Scott, B. J.; Stucky, G. D. *Chem. Commun.* **2001**, 119.

(19) Martin, M. M.; Lindqvist, L. *J. Lumin.* **1975**, *10*, 381.

(20) Weber, G.; Teale, F. W. J. *Trans. Faraday Soc.* **1958**, *54*, 640.

(21) Kawski, A. *Photochem. Photobiol.* **1983**, *38*, 487.

(22) Brand, M.; Frings, A.; Jenkner, P.; Lehnert, R.; Metternich, H. J.; Monkiewicz, J.; Schram, J. *Z. Naturforsch., B: Chem. Sci.* **1999**, *54*, 155.

(23) Waddell, T. G.; Leyden, D. E.; DeBello, M. T. *J. Am. Chem. Soc.* **1981**, *103*, 5303.

(24) Kirkland, J. J.; Glajch, J. L.; Farlee, R. D. *Anal. Chem.* **1989**, *61*, 2.

(25) Vrancken, K. C.; Possemiers, K.; Van Der Voort, P.; Vansant, E. F. *Colloids Surf. A* **1995**, *98*, 235.

(26) Sonwane, C. G.; Jones, C. W.; Ludovice, P. J. *J. Phys. Chem. B* **2005**, *109*, 23395.

(27) Ek, S.; Root, A.; Peussa, M.; Niinistö, L. *Thermochim. Acta* **2001**, *379*, 201.

(28) Kanan, S. M.; Tze, W. T. Y.; Tripp, C. P. *Langmuir* **2002**, *18*, 6623.

(29) Vrancken, K. C.; Van Der Voort, P.; Gillis-D'Hamers, I.; Vansant, E. F.; Grobet, P. *J. Chem. Soc. Faraday Trans.* **1992**, *88*, 3197.

(30) Caravajal, G. S.; Leyden, D. E.; Quinting, G. R.; Maciel, G. E. *Anal. Chem.* **1988**, *60*, 1776.

(31) Brühwiler, D.; Calzaferri, G. *Comptes Rendus Chimie* **2005**, *8*, 391.

(32) Lin, Y.-S.; Tsai, C.-P.; Huang, H.-Y.; Kuo, C.-T.; Hung, Y.; Huang, D.-M.; Chen, Y.-C.; Mou, C.-Y. *Chem. Mater.* **2005**, *17*, 4570.

A comparative study of the functionalization of mesoporous silica MCM-41 by deposition of 3-aminopropyltrimethoxysilane from toluene and from the vapor phase

Hanna Ritter[a], Minna Nieminen[b], Maarit Karppinen[b], Dominik Brühwiler[a,*]

[a] Institute of Inorganic Chemistry, University of Zurich, Winterthurerstrasse 190, CH-8057 Zurich, Switzerland

[b] Laboratory of Inorganic Chemistry, Department of Chemistry, Helsinki University of Technology, P.O. Box 6100, FI-02015 TKK, Finland

* Corresponding author. Tel.: +41 44 635 4630; fax: +41 44 635 6802. E-mail address: bruehwi@aci.uzh.ch (D. Brühwiler)

Abstract

The postsynthetic functionalization of mesoporous silica MCM-41 by vapor phase deposition of 3-aminopropyltrimethoxysilane is investigated as an alternative to the common practice of depositing from toluene. Particular emphasis is given to the possibility of eliminating the influence of trace water upon deposition from the vapor phase. The comparative study of samples prepared by different deposition methods requires identical degrees of functionalization. To obtain reliable information on the amount of surface-grafted aminopropyl groups, we have developed an analysis procedure based on the fluorogenic amine-derivatization reaction of fluorescamine.

Keywords: Mesoporous silica, Functionalization, Vapor phase deposition, Aminopropyltrimethoxysilane, Fluorescamine

1. Introduction

Aminopropyltrialkoxysilanes are among the most frequently used precursors for the modification of mesoporous silica surfaces, allowing subsequent coupling to a variety of functional groups, such as isothiocyanate or sulfonyl chloride [1]. Amino-functionalized mesoporous silica furthermore plays an important role in the development of materials for a wide range of potential applications, including adsorption of metal ions [2], protein sequestration and release [3], enzyme immobilization [4], drug delivery [5], and catalysis [6]. Despite considerable progress in the development of advanced methods for the one-pot synthesis of functionalized mesoporous silica [7], approaches based on postsynthetic functionalization remain popular due to the fact that the separation of the silica synthesis and functionalization steps allows an independent and more straightforward control of pore size, periodicity, particle size, and particle morphology.

The reaction of surface silanol groups with aminopropylalkoxysilanes is usually conducted by refluxing in toluene. Due to the high accessibility of the sites on the external particle surface and on the pore surface close to the channel entrances, the distribution of anchored amino groups in the final product is typically inhomogeneous [8]. We have recently shown that aminopropyl-monoalkoxysilanes produce a more homogeneous distribution than the corresponding trialkoxysilanes [9]. The presence of only one reactive group increases the mobility of the silane on the silica surface, while excluding the possibility of cross-linking.

It is difficult to avoid hydrolysis and cross-linking when depositing trialkoxy- or trichlorosilanes from a solvent. Even when working in dry solvents, trace water is efficiently adsorbed on the silica surface such that hydrolysis becomes possible [10]. It has been proposed that the employment of vapor phase deposition techniques might facilitate the elimination of silane cross-linking, thus minimizing clustering and multilayer formation [11]. In the case of mesoporous silica, this should ultimately lead to a more uniform distribution of the grafted moieties, resulting in a well-defined pore size of the functionalized material. In order to assess the validity of this hypothesis, we have in the present contribution investigated the postsynthetic functionalization of mesoporous silica MCM-41 with 3-aminopropyltrimethoxysilane (APTMS) by deposition from toluene and from the vapor phase. In the latter case, the atomic layer deposition (ALD) technique based on self-limiting surface reactions was employed, which is known to enable the deposition of vaporized precursor molecules in a highly reproducible and homogeneous manner [11].

2. Experimental

2.1. Synthesis of MCM-41

As large batch sizes are required for comparative studies, we have used a scale-up friendly room temperature procedure based on the synthesis reported in reference 12. Briefly, 17.6 g of the structure directing agent CTAB (hexadecyltrimethylammonium bromide, Fluka, purum, ≥ 96 %) was dissolved under slight warming in a mixture of 416 mL of distilled H_2O and 192 mL of aqueous ammonia (25 % NH_3, Fluka). To this clear solution, 80 mL of TEOS (tetraethoxysilane, Fluka, puriss., ≥ 99 %) was slowly added under stirring. After further stirring for 3 h, the gel was aged at room temperature for 24 h in a closed container. The product was obtained by filtration, washed with copious amounts of distilled H_2O, and dried in air at room temperature. The structure directing agent was removed by first heating at 300 °C for 2 h and then calcining in air at 550 °C for 16 h. Heating rates of approximately 2 °C/min were used. The procedure yielded 19.3 g of calcined MCM-41.

2.2. Vapor phase deposition

Reactions were performed in an ALD reactor (F-120 ASM Microchemistry Ltd.) at a pressure of 35 to 50 mbar. A 2.0 g sample of calcined MCM-41 was pretreated in the ALD reactor in nitrogen atmosphere at 180 °C for 3 h to remove physisorbed water [13]. An amount of 2.5 mL (14.2 mmol) of APTMS (Fluka, purum, ≥ 97 %) was subsequently vaporized at 100 °C and deposited onto the MCM-41 bed during 3 h at a selected reaction temperature in the range of 110 to 300 °C. Finally, physisorbed APTMS molecules were purged from the surface by flowing nitrogen for 2 h. Amino group analysis (see below) yielded a final amino loading of 1.2 mmol per gram of parent MCM-41. A further increase of the amount of vaporized APTMS did not lead to an increase in the final amino group content, indicating that the value of 1.2 mmol/g corresponds to the maximum loading which could be achieved by this deposition method.

2.3. Deposition from toluene

In a typical experiment, 0.5 g of calcined MCM-41 was pretreated at 180 °C for 2 h and dispersed in 30 mL of dry toluene (Fluka, puriss., $H_2O \leq 50$ ppm). After the addition of a calculated amount of APTMS (160 µL for the targeted functionalization degree of 1.2 mmol per gram of parent MCM-41), the suspension was refluxed for 3 h. The functionalized product was recovered by filtration, washed with 100 mL of ethanol, and oven-dried at 80 °C for 1 h.

2.4. Amino group analysis

15 mg of amino-functionalized MCM-41 was stirred in 30 mL of a 0.02 M aqueous solution of NaOH until completely dissolved. 100 µL of this

solution was transferred into a quartz cuvette and 2 mL of phosphate buffer (0.2 M, pH 8.0) was added. After the addition of 1 mL of fluorescamine (Sigma, > 97 %) solution (1 mM in acetone), the fluorescence spectrum was measured with a Perkin-Elmer LS50B spectrofluorometer by excitation at 366 nm. The emission intensity at 480 nm was taken as the datum point. A calibration line was prepared accordingly by using 100 µL aliquots of differently concentrated solutions of APTMS in 30 mL of 0.02 M aqueous NaOH (containing 15 mg of dissolved parent MCM-41).

2.5. Characterization

Nitrogen sorption isotherms were collected at 77 K using a Quantachrome NOVA 2200 surface area and pore size analyzer. Samples were vacuum-degassed at 80 °C for 5 h. The total surface area was calculated by the BET method [14], whereas the external surface area and the primary mesopore volume (the volume of the uniform mesopores) were determined from the linear part of the α_S-plot (α_S > 1) [15]. Mesopore size distributions were evaluated from the desorption branches of the nitrogen isotherms by means of the BJH method [16]. In order to obtain a more reliable estimate of the pore size of the parent MCM-41, the NLDFT method developed for silica exhibiting cylindrical pore geometry was also applied (NOVAWin2 software, Version 2.2, Quantachrome Instruments) [17]. In this case, the adsorption branch was used for the calculations [18]. The total pore volume was calculated from the amount of nitrogen adsorbed at a relative pressure of 0.95. All samples exhibited type IV isotherms [19] and condensation in the primary mesopores was not accompanied by hysteresis. Diffuse reflectance infrared Fourier transform spectroscopy (DRIFTS) was performed using a Nicolet Magna IR 750 spectrometer equipped with a Spectra Tech diffuse reflectance accessory. Spectra were collected in the 400-4000 cm^{-1} range at a 2 cm^{-1} resolution over 64 scans. The spectrum obtained from a steel mirror was used as a background. Powder X-ray diffraction (XRD) measurements were performed on a STOE STADI P with Cu$K\alpha_1$ radiation, a 2θ step size of 0.1°, and a counting time of 30 s per step.

3. Results and Discussion

3.1. Parent MCM-41

Fig. 1 shows the nitrogen sorption isotherms, pore size distribution (PSD), and XRD pattern of a typical mesoporous silica MCM-41 synthesized at room temperature. The four XRD peaks, which can be indexed on a hexagonal lattice (*hk*0 reflections only), are indicative of well ordered MCM-41 type materials [20]. Due to its narrow PSD and the fact that the material can be made available in relatively large batches without necessitating costly lab equipment, we have found this material to be ideal for

comparative studies such as the present one.

The standard BJH analysis is known to underestimate the absolute pore size [18]. A more reliable estimate is obtained by the DFT method [17] (d_{DFT} = 3.54 nm vs. d_{BJH} = 2.47 nm, Fig. 1) or by using the geometrical approach proposed by Kruk et al. [21]. Based on the latter formalism, our parent MCM-41 is characterized by an average pore diameter of 3.41 nm and an average wall thickness of 0.93 nm. Typical values for BET surface area and total pore volume are 910 m^2/g and 0.71 cm^3/g (with a primary mesopore volume of 0.58 cm^3/g), respectively. The external surface area accounts for approximately 12 % of the total surface area. The particle size ranges from 0.5 to 2 µm with irregular morphology.

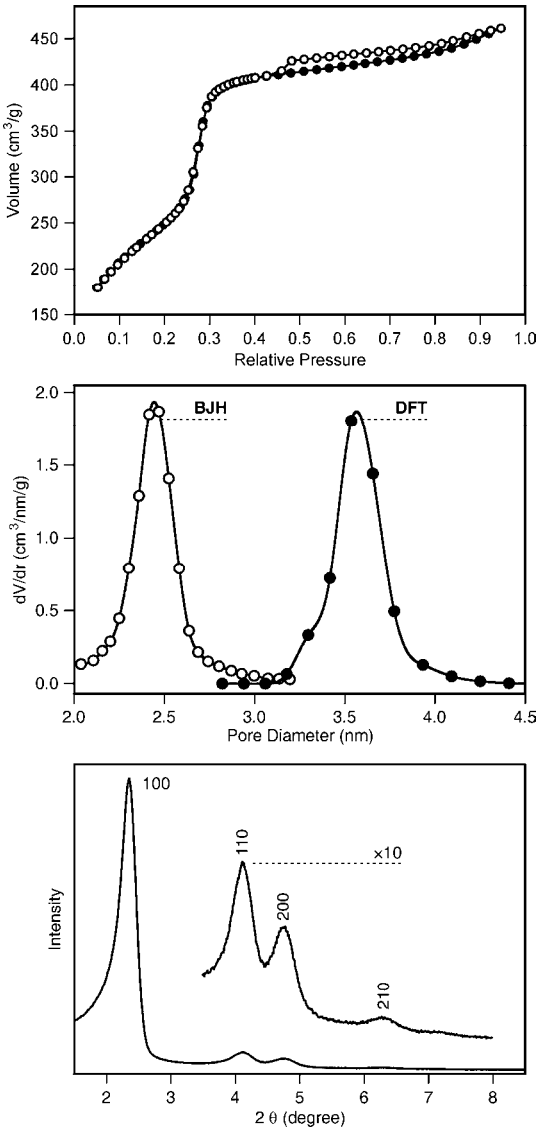

Fig. 1. Characterization data of calcined mesoporous silica MCM-41 synthesized at room temperature. Top: Nitrogen adsorption (solid circles) and desorption (empty circles) isotherm. The high pressure hysteresis loop is due to secondary mesoporosity. Middle: Pore size distributions calculated by BJH and DFT methods. Bottom: XRD pattern.

3.2. Amino group analysis

In order to compare different deposition techniques, it is essential to work under conditions which yield a defined degree of functionalization. This calls for a method that is capable of providing accurate information on the amount of grafted amino groups. Analytical data obtained with ninhydrin (Kaiser test [22]) were found to be unsatisfactory and difficult to reproduce. Samples with identical amounts of amino groups but different distributions of grafting sites (external surface vs. pore surface) produced different results in terms of the actual amount of detected amino groups. We believe that the reason for this discrepancy is the diminished accessibility of the sites deep inside the pores. Problems of this kind are

common for analytical methods employing mesoporous silica with intact pore structure. Methods based on the elemental analysis of amino groups obviously do not suffer from this drawback, however, sufficient precision can only be expected for samples featuring high grafting densities [23]. We have therefore developed a method that affords a reliable determination of the amount of grafted amino groups independent of the pore size and grafting site distribution, while covering a wide range of functionalization degrees. The key reaction of this method is based on the fluorometric quantitation of primary amines with fluorescamine [24]. To eliminate the effect of the grafting site distribution, the mesoporous framework is decomposed prior to the addition of fluorescamine. Reaction of the intrinsically non-fluorescent fluorescamine with the now fully accessible primary amines yields a fluorescent derivative. The fluorescence intensity is then used to determine the initial amino group content by means of a calibration line (Fig. 2).

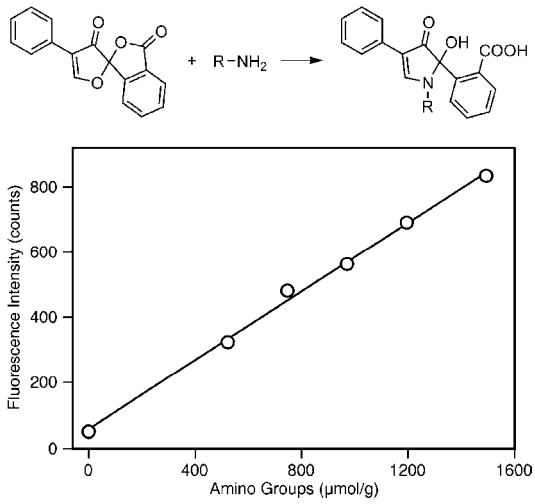

Fig. 2. Fluorogenic amine-derivatization reaction of fluorescamine and a corresponding calibration line prepared with APTMS.

3.3. Deposition temperature

Previous studies on the vapor phase deposition of 3-aminopropyltriethoxy-silane (APTES) on silica have shown that the deposition temperature is an important parameter in terms of determining the binding mode of the silane to the silica surface, revealing that unwanted secondary reactions involving the formation of Si–N bonds occur at temperatures higher than 150 °C [25]. We observed a similar effect in our preliminary vapor phase depositions of APTMS on MCM-41 carried out at selected temperatures (see Fig. 3 for the DRIFT spectra of these samples). Stretching frequencies of the primary amino groups are observed at 3305 and 3373 cm^{-1}. Additional bands at 3437 and 3470 cm^{-1} assigned to Si–NH–C moieties develop at deposition temperatures higher than 150 °C. The contribution of Si–NH–C binding modes is significant already at 250 °C. In order to avoid the reaction of amino groups with surface silanol groups or strained siloxane bridges, as well as with the methoxysilyl groups of other APTMS molecules, the deposition temperature was fixed at 150 °C for the final experiments. Under these conditions, the reaction of methanol,

which is formed upon grafting of APTMS, with surface silanol groups is unlikely [11,26]. No secondary reactions involving the formation of Si–N bonds occurred upon deposition of APTMS from toluene under reflux.

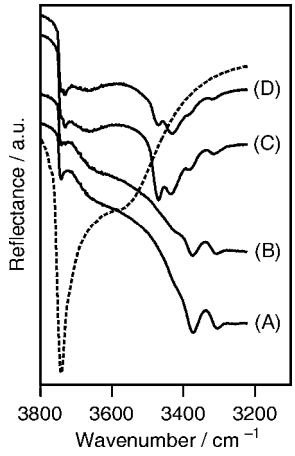

Fig. 3. DRIFT spectra of MCM-41 after vapor phase deposition of APTMS at 110 °C (A), 150 °C (B), 250 °C (C), and 300 °C (D). The dashed curve represents the spectrum of calcined MCM-41 before APTMS deposition.

3.4. Comparison of the deposition methods

It is worth mentioning at this point that the investigated samples, assuming a homogeneous distribution and an initial BET surface area of 910 m^2/g, were synthesized with a surface coverage of 0.79 $–NH_2$ per nm^2 (corresponding to a functionalization degree of 1.2 mmol/g). Fig. 4A compares the PSDs of MCM-41 after deposition of APTMS from the vapor phase (sample Vap-APTMS) and from toluene (sample Tol-APTMS), the former producing a material with a

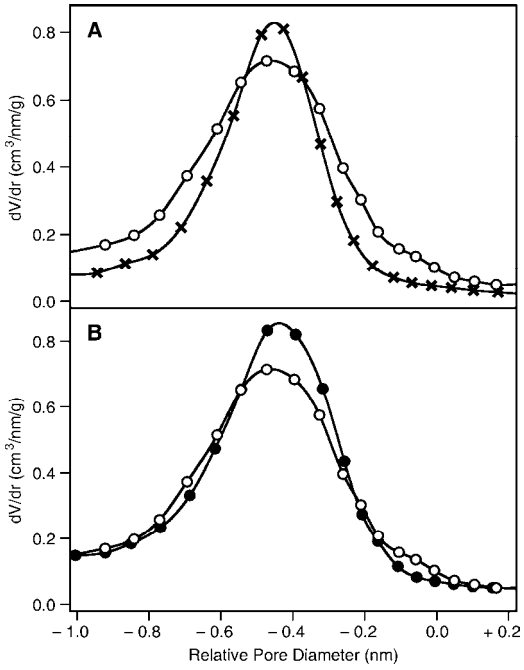

Fig. 4. A: PSD of MCM-41 after deposition of APTMS from the vapor phase (Vap-APTMS, crosses) compared to the PSD of MCM-41 after deposition of APTMS from toluene (Tol-APTMS, empty circles). **B**: PSD of MCM-41 after deposition of APTMS from toluene without (Tol-APTMS, empty circles) and with prior vacuum distillation of APTMS (Tol-APTMS-d, solid circles). Pore diameters are given relative to the average pore diameter of the parent MCM-41. Amino group contents are 1.2 mmol/g for each sample.

narrower PSD (full width at half maximum FWHM = 0.30 nm, compared to FWHM = 0.42 nm for Tol-APTMS). To remove potential APTMS oligomers, we have repeated the deposition from toluene using freshly vacuum distilled APTMS (sample Tol-APTMS-d). As can be seen from Fig. 4B, the PSD of the resulting functionalized MCM-41 is slightly more uniform and narrower

(FWHM = 0.37 nm) compared to the sample prepared without distillation.

The differences between the PSD of Vap-APTMS and Tol-APTMS seem minor at first sight. However, it should be noted that the samples contain the same amount of surface-grafted amino groups. The differences can therefore be attributed to different surface distributions of the functional groups, as we have recently shown for amino-functionalized samples prepared with various aminosilane precursors [9]. Interestingly, there is a considerable contribution of relatively large pores to the PSD of the samples grafted in toluene. This is most likely a consequence of pore blocking due to cross-linking of APTMS. If clustering of APTMS occurs close to the entrance of a given pore, diffusion of additional APTMS molecules into this pore is hindered, leaving part of the pore surface unmodified. In the PSD derived from nitrogen sorption, such a partially blocked pore is consequently recorded with a comparatively large pore diameter.

Upon deposition from the vapor phase, the primary mesopore volume decreased by 0.31 cm^3/g, whereas a less pronounced reduction of 0.25 cm^3/g was observed after deposition from toluene (1.2 mmol/g of grafted amino groups for each sample). The accompanying changes of the BET surface area (–419 m^2/g for Vap-APTMS, –306 m^2/g for Tol-APTMS, and –287 m^2/g for Tol-APTMS-d) support the conclusion that different distributions of grafted amino groups were obtained. A recent study by Asefa and co-workers [6b] has shown that the deposition of APTMS from toluene produced aggregated grafted groups, while Tatsumi and co-workers [8a] found that the surface-bound amino groups were concentrated near the pore entrances and on the external surface. Our results indicate that the tendency towards aggregation and external surface grafting is less pronounced in the vapor phase deposition method. In this context, it is worth mentioning that toluene is not an ideal solvent for producing site isolation of grafted amino groups. Less aggregation and increased site isolation has for example been obtained upon deposition from alcohols [6b] or THF [9].

3.5. Influence of trace water

To investigate the influence of water on the degree of pore blocking, we conducted the following experiment: A 0.5 g sample of calcined MCM-41 was dispersed in 30 mL of toluene containing different amounts of H_2O. After short ultrasonication and additional stirring for 15 min, 160 µL of APTMS was added. Reaction, recovery, and analysis were performed as described above. The resulting PSDs of two representative samples are shown in Fig. 5. While the water content seems to have no effect on the yield of grafted amino groups, the PSDs are clearly different. Pore blocking is obviously strongly promoted by the presence of trace water. This is in agreement with an earlier study by

Walcarius et al. [27] observing slower proton and metal uptake of aminopropyl-grafted MCM-41 prepared by postsynthetic functionalization with APTES (deposited from toluene) in the presence of trace water. The effect shown in Fig. 5 occurs already at relatively low water contents. Under our experimental conditions, a water content of 400 ppm results in a H_2O/APTMS ratio of approximately 0.6. Assuming complete surface adsorption of H_2O with an area of 0.1 nm^2 per molecule, a water content of 400 ppm corresponds to only about 1/13 of a monolayer. We can therefore conclude that the presence of small quantities of water in toluene considerably affects the grafting behavior of APTMS by promoting cross-linking of silane molecules. To obtain a narrow PSD and a high fraction of pore surface grafting, it is therefore crucial to work with dry toluene.

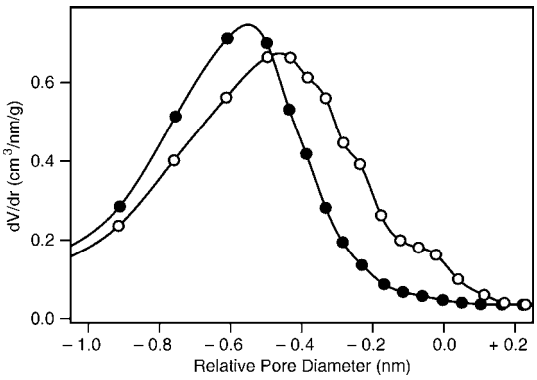

Fig. 5. PSD of MCM-41 after deposition of APTMS from toluene containing approximately 400 ppm of H_2O (empty circles) and less than 50 ppm of H_2O (solid circles). Pore diameters are given relative to the average pore diameter of the parent MCM-41. Amino group contents are 1.2 mmol/g.

4. Conclusions

Functionalization of mesoporous silica by vapor phase deposition of APTMS is a viable alternative to reactions carried out in solvents. The use of vapor phase deposition eliminates trace water-induced silane cross-linking and subsequent pore blocking. As the separation of APTMS monomers from potential oligomers present in liquid APTMS is an inherent property of the vapor phase deposition method, distillation of APTMS prior to the grafting reaction is not necessary. Furthermore, the vapour phase deposition method is of interest for economical and ecological reasons, especially concerning large scale syntheses, as it avoids the use of (dry) solvents. In future work, the vapor phase deposition of APTMS needs to be examined in terms of its potential to provide site isolation, specifically in relation to optimized solvent based deposition techniques [28]. Such comparative studies are particularly meaningful when samples of similar functionalization degree are examined. This requires an analysis method which yields accurate and reproducible results for a wide range of grafting densities independent of the distribution of the functional groups on the mesoporous silica surface. The determination of the

amino groups by reaction with fluorescamine after decomposition of the mesoporous framework provides a sound basis for further research in this field.

Acknowledgement. Financial support was provided by the European Commission through the Human Potential Program (Marie-Curie RTN Nanomatch, Grant No. MRTN-CT-2006-035884) and by the Swiss National Science Foundation (Project 200020-117591).

References

[1] (a) Y. Rohlfing, D. Wöhrle, J. Rathouský, A. Zukal, M. Wark, Stud. Surf. Sci. Catal. 142 (2002) 1067; (b) V. Antochshuk, O. Olkhovyk, M. Jaroniec, I.-S. Park, R. Ryoo, Langmuir 19 (2003) 3031; (c) E. J. Acosta, C. S. Carr, E. E. Simanek, D. F. Shantz, Adv. Mater. 16 (2004) 985; (d) I. Slowing, B. G. Trewyn, V. S.-Y. Lin, J. Am. Chem. Soc. 128 (2006) 14792.

[2] A. M. Liu, K. Hidajat, S. Kawi, D. Y. Zhao, Chem. Commun. (2000) 1145.

[3] Y.-J. Han, G. D. Stucky, A. Butler, J. Am. Chem. Soc. 121 (1999) 9897.

[4] J. F. Díaz, K. J. Balkus, J. Mol. Catal. B: Enzym. 2 (1996) 115.

[5] F. Balas, M. Manzano, P. Horcajada, M. Vallet-Regi, J. Am. Chem. Soc. 128 (2006) 8116.

[6] (a) K. K. Sharma, T. Asefa, Angew. Chem. Int. Ed. 46 (2007) 2879; (b) K. K. Sharma, A. Anan, R. P. Buckley, W. Ouellette, T. Asefa, J. Am. Chem. Soc. 130 (2008) 218; (c) X. Wang, K. S. K. Lin, J. C. C. Chan, S. Cheng, J. Phys. Chem. B 109 (2005) 1763; (d) D. J. Macquarrie, D. B. Jackson, Chem. Commun. (1997) 1781; (e) A. Cauvel, G. Renard, D. Brunel, J. Org. Chem. 62 (1997) 749; (f) D. Brunel, Microporous Mesoporous Mater. 27 (1999) 329.

[7] F. Hoffmann, M. Cornelius, J. Morell, M. Fröba, Angew. Chem. Int. Ed. 45 (2006) 3216.

[8] (a) T. Yokoi, H. Yoshitake, T. Tatsumi, J. Mater. Chem. 14 (2004) 951; (b) M. H. Lim, A. Stein, Chem. Mater. 11 (1999) 3285.

[9] H. Salmio, D. Brühwiler, J. Phys. Chem. C 111 (2007) 923.

[10] (a) C. P. Tripp, M. L. Hair, Langmuir 11 (1995) 1215; (b) S. M. Kanan, W. T. Y. Tze, C. P. Tripp, Langmuir 18 (2002) 6623.

[11] S. Ek, E. I. Iiskola, L. Niinistö, Langmuir 19 (2003) 3461.

[12] D. Brühwiler, H. Frei, J. Phys. Chem. B 107 (2003) 8547.

[13] S. Ek, A. Root, M. Peussa, L. Niinistö, Thermochim. Acta 379 (2001) 201.

[14] S. Brunauer, P. H. Emmett, E. Teller, J. Am. Chem. Soc. 60 (1938) 309.

[15] M. Kruk, M. Jaroniec, R. Ryoo, J. M. Kim, Microporous Mater. 12 (1997) 93.

[16] E. P. Barrett, L. G. Joyner, P. P. Halenda, J. Am. Chem. Soc. 73 (1951) 373.

[17] P. I. Ravikovitch, S. C. O. Domhnaill, A. V. Neimark, F. Schüth, K. K. Unger, Langmuir 11 (1995) 4765.

[18] P. I. Ravikovitch, A. V. Neimark, Colloid Surf. A: Physicochem. Eng. Aspect 187-188 (2001) 11.

[19] K. S. W. Sing, D. H. Everett, R. A. W. Haul, L. Moscou, R. A. Pierotti, J. Rouquerol, T. Siemieniewska, Pure Appl. Chem. 57 (1985) 603.

[20] (a) C. T. Kresge, M. E. Leonowicz, W. J. Roth, J. C. Vartuli, J. S. Beck, Nature 359 (1992) 710; (b) J. S. Beck, J. C. Vartuli, W. J. Roth, M. E. Leonowicz, C. T. Kresge, K. D. Schmitt, C. T.-W. Chu, D. H. Olson, E. W. Sheppard, S. B. McCullen, J. B. Higgins, J. L. Schlenker, J. Am. Chem. Soc. 114 (1992) 10834.

[21] M. Kruk, M. Jaroniec, A. Sayari, J. Phys. Chem. B 101 (1997) 583.

[22] E. Kaiser, R. L. Colescott, C. D. Bossinger, P. I. Cook, Anal. Biochem. 34 (1970) 595.

[23] S. Ek, E. I. Iiskola, L. Niinistö, J. Vaittinen, T. P. Pakkanen, J. Keränen, A. Auroux, Langmuir 19 (2003) 10601.

[24] (a) M. Weigele, S. L. DeBernardo, J. P. Tengi, W. Leimgruber, J. Am. Chem. Soc. 94 (1972) 5927; (b) S. Udenfriend, S. Stein, P. Böhlen, W. Dairman, W. Leimgruber, M. Weigele, Science 178 (1972) 871.

[25] S. Ek, E. I. Iiskola, L. Niinistö, T. T. Pakkanen, A. Root, Chem. Commun. (2003) 2032.

[26] E. A. Wovchko, J. C. Camp, J. A. Glass, J. T. Yates, Langmuir 11 (1995) 2592.

[27] A. Walcarius, M. Etienne, B. Lebeau, Chem. Mater. 15 (2003) 2161.

[28] (a) K. K. Sharma, R. P. Buckley, T. Asefa, Langmuir 24 (2008) 14306; (b) J. C. Hicks, R. Dabestani, A. C. Buchanan III, C. W. Jones, Chem. Mater. 18 (2006) 5022; (c) J. C. Hicks, C. W. Jones, Langmuir 22 (2006) 2676; (d) M. W. McKittrick, C. W. Jones, Chem. Mater. 15 (2003) 1132.

Accessibility of grafting sites in postsynthetically modified mesoporous silica

*Hanna Ritter and Dominik Brühwiler**

Institute of Inorganic Chemistry, University of Zurich,
Winterthurerstrasse 190, 8057 Zurich, Switzerland

E-Mail: bruehwi@aci.uzh.ch (D. Brühwiler)

Abstract. The accessibility of amino groups in postsynthetically functionalized mesoporous silica MCM-41, MCM-48, and SBA-15 is investigated by reaction with fluorescein isothiocyanate (FITC). The quantitative analysis of the surface-grafted amino groups in relation to the amount of coupled FITC over a wide range of loadings affords information about potential pore blocking. In the pore diameter domain of 3 to 4 nm, the actual pore size of materials with a one-dimensional channel system (MCM-41) strongly affects the FITC coupling yield and the distribution of the anchored fluorescein moieties. In the case of SBA-15 (7.6 nm pore diameter), the accessibility of the grafted amino groups is similar to what is expected for a material with a completely open surface. However, grafting in the intrawall micropores of SBA-15 leads to a substantial fraction of inaccessible amino groups. As a direct consequence of short channel lengths and large external surface, excellent accessibility is also observed for nanometer-sized MCM-41 (3.2 nm pore diameter).

1. Introduction

Grafting of a functional group and subsequent coupling of an organic moiety exhibiting the desired property (such as luminescence, sensing, metal coordination) is a popular method for the modification of mesoporous silicas.[1-4] Postsynthetic functionalization techniques are preferably employed when the molecule to be introduced is not sufficiently stable under the conditions of the mesoporous silica synthesis, therefore excluding approaches based on co-condensation, or when a narrow pore size distribution is required. The latter is typically more difficult to obtain by means of co-condensation, especially when high functionalization degrees are desired. A recent study by Rosenholm and Lindén compares the accessibility of amino groups in functionalized SBA-15 prepared by co-condensation, post-synthetic grafting with various amino-silanes, and surface polymerization of a polyethyleneimine, with the important result that the postsynthetic functionalization techniques are superior to co-condensation in terms of

producing a large amount of accessible amino groups.[5]

The accessibility of the binding sites is the key to uniform postsynthetic surface functionalization. Depending on the relation between the pore diameter of the mesoporous material and the size of the moiety to be grafted, sterical hindrance can limit the access to sites deep inside the pores. To evaluate to what extent such pore blocking effects depend on the pore diameter and the dimensionality of the channel system, we have investigated the reaction of fluorescein isothiocyanate (FITC) with amino-functionalized mesoporous silica MCM-41 (one-dimensional channel system),[6,7] MCM-48 (three-dimensional channel system),[6,7] and SBA-15 (one-dimensional channel system, larger pore size than MCM-41, microporous channel walls).[8,9] FITC coupling yields, which are obtained as a result of the combination of a fluorometric quantitation of the grafted amino groups[10] and a UV-Vis spectroscopic detection of the coupled FITC[11], afford information about the accessibility of the surface-grafted amino groups. The accessibility of functional groups on the surface of mesoporous silicas is not only essential for further functionalization by coupling reactions, but also for potential applications such as catalysis[12,13] and adsorption-based separation[14-19].

2. Experimental Section

2.1. Synthesis of Mesoporous Silicas

MCM-41(16) was prepared according to ref. 20. Briefly, 2.20 g of hexadecyltrimethylammonium bromide (CTAB, Fluka) was dissolved under slight warming in a mixture of 52 mL of H_2O and 24 mL of aqueous ammonia (28 %, Fluka). 10 mL of tetraethoxysilane (TEOS, Fluka) was slowly added under stirring and the resulting gel was further stirred for 3 h at room temperature. The mixture was transferred to a Teflon-lined autoclave and heated at 110 °C for 48 h. The product was obtained by filtration, washed with at least 800 mL of H_2O and dried overnight in air at room temperature. The structure directing agent (SDA) was removed by first heating at 300 °C for 2 h and subsequent calcination in air at 550 °C for 16 h. Heating rates of 2 °C/min were applied. The X-ray diffraction (XRD) pattern was in agreement with the pattern reported in ref. 20. MCM-41(12) was prepared accordingly, using 1.86 g of dodecyltrimethylammonium bromide (Fluka) instead of CTAB. The use of a SDA with a shorter alkyl chain reduces the pore size (see Table 1) and shifts the XRD pattern towards larger angles.

MCM-48 was synthesized following a previously reported procedure.[21] An amount of 8.80 g of CTAB was dissolved under slight warming in 80 mL of H_2O. After the addition of 10 mL of 2 M aqueous NaOH, 10 mL of TEOS was added dropwise under stirring. After

further stirring for 30 min, the mixture was transferred to a Teflon-lined autoclave and heated at 100 °C for 72 h. The product was recovered by filtration, washed with at least 1 L of H_2O and oven-dried overnight at 80 °C. The SDA was removed by first heating at 300 °C for 2 h and subsequent calcination in air at 550 °C for 8 h. Heating rates of 2 °C/min were applied.

SBA-15 was prepared according to ref. 9. Briefly, 2.20 g of Pluronic P123 ($EO_{20}PO_{70}EO_{20}$, M_{av} = 5800, Aldrich) was dissolved in a mixture of 49 mL of H_2O and 31 mL of 4 M aqueous HCl. To this clear solution, 5 mL of TEOS was slowly added under stirring. After further stirring for 20 h at approximately 35 °C, the mixture was transferred to a Teflon-lined autoclave and heated at 100 °C for 24 h. The product was obtained by filtration and washed with at least 1 L of H_2O. After drying the material overnight in air at room temperature, the SDA was removed by heating in air at 500 °C for 16 h. A heating rate of 1 °C/min was applied.

Nanoparticles of MCM-41 (nano-MCM-41) were synthesized as follows:[22] First, a clear solution of 2.60 g of hexadecyltrimethylammonium chloride (Fluka) and 2.00 g of Pluronic F-127 (Sigma) in 30 mL of 0.25 M aqueous HCl was prepared. After the dropwise addition of 3.7 mL of TEOS, the mixture was stirred for 20 h at room temperature. Finally, 3.7 mL of aqueous ammonia (28 %, Fluka) was added and the resulting gel was aged without stirring for 24 h. The product was oven-dried at 70 °C for 72 h and subsequently calcined at 600 °C for 3 h with a heating rate of 3 °C/min.

Fumed silica (Sigma, 14 nm primary particle size) was used as received.

2.2. Reaction with APTMS

To ensure reproducible and comparable conditions all of our calcined mesoporous silica materials as well as fumed silica were treated for 1 h at 80 °C before use. This temperature was chosen because of its compatibility with potential organic modifications. It should be noted that the total release of physisorbed water usually requires temperatures above 100 °C. Such temperatures are, however, often not applicable when systems with multiple functional groups are desired, as this typically requires consecutive modification steps, such as co-condensation and subsequent postsynthetic grafting. Experiments conducted with MCM-41(16) dried at 180 °C produced results which were consistent with those obtained for samples dried at 80 °C.

For the functionalization with 3-aminopropyltrimethoxysilane (APTMS, Fluka), 500 mg of fumed silica or calcined mesoporous silica was dispersed in 30 mL of dry toluene (Fluka, puriss., H_2O < 0.005 %). After the addition of a calculated amount (between 0.05 and 1.20 mmol) of APTMS, the suspension was refluxed for 3 h. The functionalized product was recovered by filtration, washed with 100

mL of ethanol, and cured at 80 °C for 1 h. Amino group analysis (Chapter 2.4.) showed that within the error margin of the method, grafting of APTMS was quantitative in the above mentioned range. Samples with low amino content are denoted by A-*x*, where *x* identifies the type of silica. Samples with intermediate and high amino content are identified by B-*x* and C-*x*, respectively. Three independent syntheses were carried out for each data point.

2.3. FITC Coupling

Labeling with fluorescein 5-isothiocyanate (FITC, Fluka) was carried out according to ref. 11. Briefly, a calculated amount of FITC (1.5-fold excess relative to the amount of grafted amino groups) was dissolved in 25 mL of absolute ethanol. After the addition of 250 mg of amino-functionalized silica, the suspension was stirred for 24 h at room temperature. The yellow product was recovered by filtration and washed with 50 mL of ethanol. After redispersion in 50 mL of fresh ethanol and stirring for 15 min, the final product was recovered by filtration, washed with 50 mL of ethanol and oven-dried at 80 °C for 1 h. The amount of coupled fluorescein was determined by dissolving the sample (typically 15 – 30 mg) in 25 mL of 0.2 M aqueous NaOH and measuring the UV-Vis absorption spectrum of the resulting clear solution after appropriate dilution. Repeated analysis of the same sample gave an average relative error of 3 % (for FITC contents in the range of 0.01 to 0.4 mmol/g). The extinction coefficient which was used in the calculations (ε= 75'000 $M^{-1}cm^{-1}$ at λ_{max} = 490 nm) was determined based on a stock solution prepared as follows: FITC was coupled to APTMS in a 1:1 molar ratio by stirring in ethanol for 15 h at room temperature. After removal of the ethanol by evaporation, a weighed amount of the dry residue was dissolved in 50 mL of 0.2 M aqueous NaOH containing 50 mg of dissolved silica.

Adsorption of fluorescein (free acid, Riedel-de Haën) was conducted according to the FITC coupling procedure, using fluorescein instead of FITC.

2.4. Amino Group Analysis

15 mg of amino-functionalized silica was stirred in 30 mL of 0.02 M aqueous NaOH until completely dissolved. 100 µL of this solution was transferred into a cuvette (d = 1 cm) and 2 mL of phosphate buffer (0.2 M, pH 8.0) was added. After the addition of 1 mL of fluorescamine (Sigma) solution (1 mM in acetone), the fluorescence spectrum was measured by excitation at 366 nm. The emission intensity at 480 nm was taken as the data point. A calibration line was prepared accordingly by using 100 µL aliquots of differently concentrated solutions of APTMS in 30 mL of 0.02 M aqueous NaOH (containing 15 mg of the respective dissolved parent silica).[10a] Repeated analysis of the same

sample gave an average relative error of 8 % (for amino contents in the range of 0.09 to 2.4 mmol/g). To allow comparison between materials with different surface area, the amino content was further calculated in units of µmol/m^2 assuming a homogeneous distribution over the entire BET surface area of the parent matieral. Curves depicting the FITC coupling yield as a function of the amino content were additionally verified with at least three control samples per curve.

2.5. Physical Measurements

Nitrogen sorption isotherms were collected at 77 K using a Quantachrome NOVA 2200 surface area and pore size analyzer. Samples were vacuum-degassed at 80 °C for 3 h. The total surface area S_{BET} was calculated by the BET method[23] whereas the external surface area S_{Ext} was determined from the high-pressure linear part of the α_S-plot.[24,25] Pore size distributions were calculated by means of a NLDFT model developed for silica exhibiting cylindrical pore geometry[26] (NOVAWin2 software, Version 2.2, Quantachrome Instruments). Adsorption branches were used for the calculations.[27] Pore size distributions of the functionalized materials are used for comparative purposes only, as the employed NLDFT kernel is not strictly valid for non-siliceous materials. The total pore volume V_{tot} was estimated from the amount of nitrogen adsorbed at a relative pressure of 0.95. The primary mesopore volume V_p (volume of the uniform mesopores) was determined by the α_S-plot method.[24] The de Boer equation was employed for calculating the statistical film thickness *t*.[28] A Perkin-Elmer LS50B spectrofluorometer was used for the fluorescamine assays and UV-Vis spectra were measured with a Cary 1E spectrophotometer. Powder diffraction patterns were collected on a STOE StadiP diffractometer operating with monochromatized Cu$K\alpha_1$ radiation. Scanning electron microscopy (SEM) was performed with a LEO 440.

3. Results and Discussion

3.1. Properties of the Starting Materials

Figure 1 shows the pore size distributions of the investigated mesoporous silicas. Further properties of the unmodified materials are summarized in Table 1.

3.2. FITC Coupling Yields and Accessibility

There are several reasons why FITC is an ideal molecule to probe the accessibility of surface-grafted amino groups: Isothiocyanates are moderately reactive and form robust thioureas with amines, whereas no reaction occurs with surface silanol groups under mild conditions.[11] As the fluorescein moiety is rather bulky (Figure 2), coupled FITC molecules can, depending on the pore

Table 1. Properties of the investigated silica materials.

	d_{DFT}[a] [nm]	Particle Size[b]	S_{BET} [m^2/g]	S_{Ext} [m^2/g]	V_{tot} (V_p) [cm^3/g]
fumed silica	–	14 nm[c]	200	200	– (–)
nano-MCM-41	3.18	20 – 50 nm[d]	590	380	0.81 (0.17)
MCM-41(12)	3.06	1 – 2 µm	820	40	0.48 (0.44)
MCM-41(16)	3.93	1 – 2 µm	870	70	0.74 (0.67)
MCM-48	3.67	1 – 2 µm	1100	160	0.86 (0.75)
SBA-15	7.59	1 – 2 µm	860	50	1.21 (1.09[e])

[a] average pore diameter determined by the NLDFT method
[b] estimated by SEM unless noted otherwise
[c] average size of primary particles, which form branched, chain-like aggregates a few tenths of a micron long (information provided by the supplier)
[d] ref. 22
[e] micropore volume V_μ = 0.09 cm^3/g

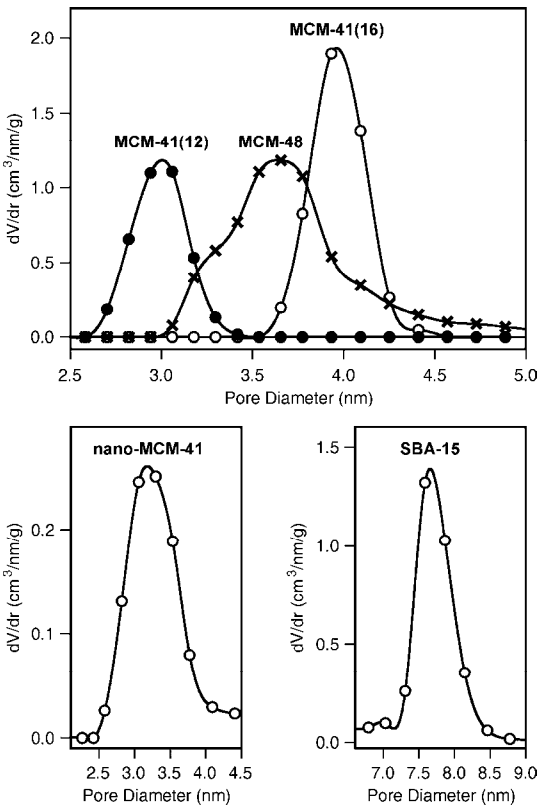

Figure 1. Pore size distributions of the unmodified mesoporous silicas.

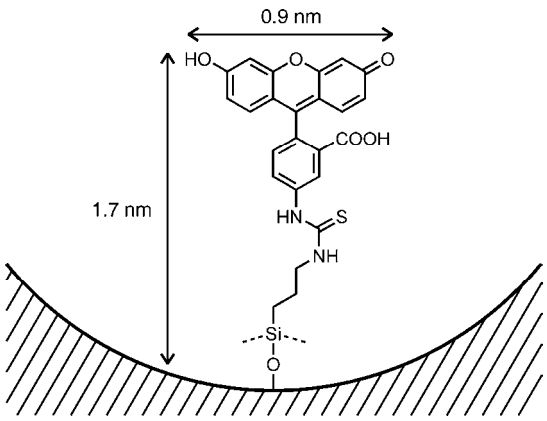

Figure 2. A FITC-labeled grafted amino group. The curvature of the surface corresponds to a circular pore with a diameter of 3.5 nm. The anchored fluorescein moieties are most likely present in various protonation states (neutral, monoanion, dianion).[11]

size and pore system dimensionality, induce pore blocking, thereby rendering amino groups anchored in areas deep inside the pores inaccessible. Upon dissolution of the silica framework in 0.2

M aqueous NaOH, the fluorescein moiety is stable and forms the strongly colored dianion,[29] affording an accurate and convenient determination of the FITC coupling yield by UV-Vis spectroscopy. The FITC coupling yield, which we define as the amount of coupled FITC divided by the amount of grafted amino groups, is a direct measure for the overall accessibility.

When investigating the effect of the pore size on the accessibility, it is important to keep in mind that reactions also occur on the external surface of the particles. Analysis of the high-pressure linear parts of the α_S-plots of the investigated mesoporous silicas reveals that the external surface area typically accounts for less than 15 % of the total BET surface area (Table 1). The nanometer-sized MCM-41 sample (nano-MCM-41) is an obvious exception. Due to the small particle size, the external surface is dominant.

It is instructive to first examine the FITC coupling yields of a non-porous high external surface area sample such as fumed silica. As can be seen in Figure 3, the FITC coupling yield remains relatively constant with increasing amino content. The slight overall decrease of the yield can be explained based on the simple model of two adjacent surface-grafted amino groups. As the distance between the amino groups decreases, the probability increases that, for sterical reasons, only one of the two groups can be labeled with FITC. Note that an amino content of 1.7 µmol/m^2 corresponds to roughly one amino group per nm^2, assuming uniform distribution. Compared to the almost constant FITC coupling yield of the fumed silica samples, the values for MCM-41(16) strongly depend on the amount of grafted amino groups. As MCM-41 features one-dimensional channels, coupling of FITC to amino groups located close to the pore entrances can render large portions of the pore surface inaccessible. MCM-48 of similar pore size exhibits a less pronounced decrease of the FITC coupling yield with increasing amino content. The three-dimensional channel system obviously offers access to a large fraction of the pore surface despite potential pore blocking. MCM-48 and MCM-41(16) feature similar accessibility for amino loadings below 0.5 µmol/m^2.

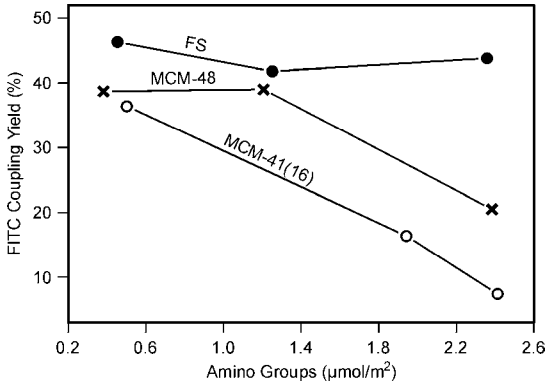

Figure 3. FITC coupling yield as a function of the amino content for fumed silica (FS), MCM-48, and MCM-41(16). Each data point corresponds to the average of three independent syntheses.

Apart from the dimensionality of the pore system, the pore size plays an

important role in defining the access to the amino groups. Whereas strong pore blocking effects are observed in MCM-41(12) and to a lesser extent in MCM-41(16), SBA-15 exhibits almost constant FITC coupling yield (Figure 4). This indicates that virtually no pore blocking due to FITC labeling occurs at an average pore diameter of 7.59 nm. However, while the FITC coupling yield is constant for amino-functionalized SBA-15, the absolute amount of coupled FITC is much lower than in the case of fumed silica. This observation is discussed in more detail in Chapter 3.3.

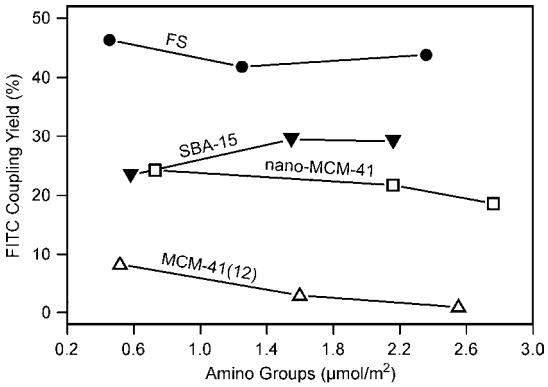

Figure 4. FITC coupling yield as a function of the amino content for fumed silica (FS), SBA-15, nano-MCM-41, and MCM-41(12). Each data point corresponds to the average of three independent syntheses.

Despite their relatively small pore diameter difference (Δd_{DFT} = 0.87 nm), MCM-41(12) and MCM-41(16) feature significantly different FITC coupling yields. This is best illustrated by inspecting the A-*x* samples, i.e., the samples with the lowest amino content (0.5 µmol/m^2, corresponding in this case to approximately 0.4 mmol/g). Whereas 1.0 g of the amino-functionalized MCM-41(16) sample is able to bind 0.13 mmol of FITC, the corresponding MCM-41(12) sample binds only 0.03 mmol, leading to the conclusion that in the latter case, FITC predominantly reacts with amino groups anchored to the external surface. This is in agreement with nitrogen sorption data of the samples before and after FITC coupling (Figure 5, Table 2). In the case of A-MCM-41(12), grafting of 0.4 mmol/g of APTMS led to a reduction of the pore volume, but only to a slight accompanying decrease of the pore diameter, thus indicating preferential functionalization at the pore entrances and a scarcely functionalized pore body. The same observation is made for the MCM-41(12) samples with higher amino contents. It is interesting to note that upon FITC coupling, the pore volume and BET surface area increase for A-MCM-41(12). This effect is due to minor leaching of amino groups upon stirring in ethanol for 24 h. As the amount of coupled FITC is small and most likely concentrated on the external particle surface of MCM-41(12), the loss of pore surface-grafted amino groups is not compensated by intrapore coupling of FITC. For MCM-41(16), on the other hand, a significant reduction of the pore volume was observed over the entire range of investigated amino contents, confirming that even at high amino content (C-MCM-41(16)), FITC is able to couple to amino groups located on the pore surface. However, the pore size distributions before and after FITC coupling (Figure 5) suggest that with increasing amino content, FITC couples

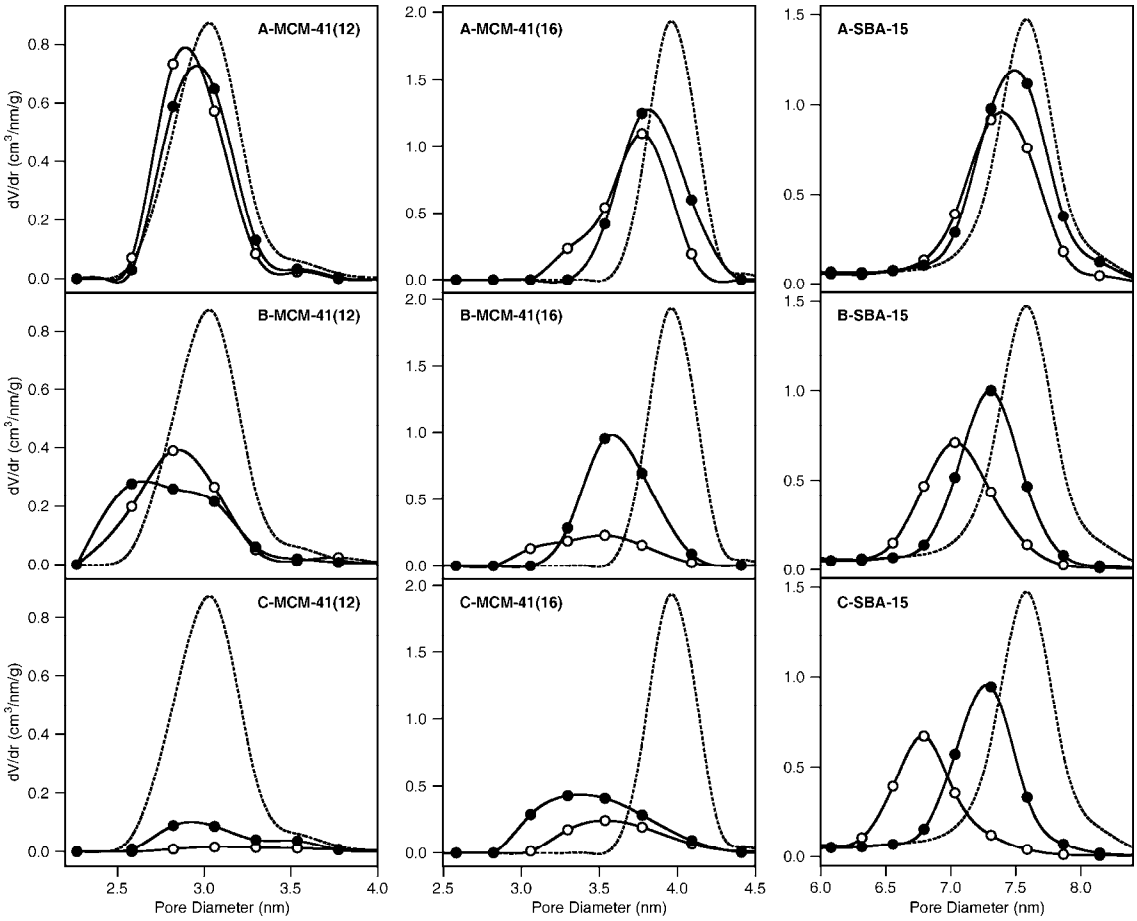

Figure 5. Pore size distributions of selected amino-functionalized MCM-41(12), MCM-41(16), and SBA-15 samples before (filled circles) and after (empty circles) FITC coupling. The dashed lines represent the pore size distributions of the respective unmodified parent materials. The amino content increases from the A- to the C-samples. Additional characterization data is compiled in Table 2.

predominantly to pore entrance sites of MCM-41(16), leading to a reduction of the pore volume while retaining a relatively large pore diameter. The pronounced binding of FITC to pore entrance sites of amino-functionalized MCM-41(16) causes pore blocking with increasing amino content, thereby decreasing the FITC coupling yield (Figure 3). Figure 5 also shows the pore size distributions of the corresponding SBA-15 samples, which illustrate the expected outcome of a comparatively more uniform distribution of amino groups and coupled FITC.

Inspection of the nitrogen sorption isotherms before and after FITC coupling reveals that in some specific cases, the desorption isotherm does not close at lower relative pressure. Such broad hysteresis has been reported for mesoporous organosilicas and has been interpreted as a consequence of bottlenecking of pore openings, clearly

Table 2. Structural data of selected amino-functionalized samples.

	n [mmol/g]		S_{BET} [m^2/g]		V_{tot} (V_p) [cm^3/g]	
	$-NH_2$[a]	FITC[b]	$-NH_2$[c]	FITC[d]	$-NH_2$[c]	FITC[d]
A-MCM-41(12)	0.38	0.03	665	717	0.38 (0.34)	0.40 (0.36)
B-MCM-41(12)	1.09	0.03	–[e]	–[e]	0.22 (0.18)	0.25 (0.22)
C-MCM-41(12)	1.81	0.01	–[e]	–[e]	0.08 (0.07)	0.04 (0.01)
A-MCM-41(16)	0.40	0.13	810	740	0.66 (0.59)	0.57 (0.50)
B-MCM-41(16)	1.43	0.26	664	–[e]	0.51 (0.45)	0.22 (0.17)
C-MCM-41(16)	1.75	0.10	560	–[e]	0.40 (0.36)	0.21 (0.17)
A-SBA-15	0.40	0.09	716	569	1.08 (1.00)	0.86 (0.80)
B-SBA-15	1.02	0.31	541	407	0.79 (0.73)	0.62 (0.57)
C-SBA-15	1.41	0.34	437	316	0.70 (0.64)	0.49 (0.45)

[a] amount of amino groups determined by fluorescamine analysis
[b] amount of coupled FITC
[c] amino-functionalized sample
[d] amino-functionalized sample after FITC coupling
[e] isotherm shows broad hysteresis extending into the BET region

although the existence of a pronounced hysteresis at low relative pressure is not understood.[30,31] Interestingly, we have observed such broad hysteresis for samples where the FITC coupling yields as well as the pore size distributions indicate pore blocking. For MCM-41(16),hysteresis was only observed for B- and C-samples after FITC coupling (see Figure 6 for an example), whereas the sorption isotherms of MCM-41(12) featured a broad hysteresis already after reaction with APTMS (B- and C-samples), suggesting a highly non-uniform distribution of the grafted amino groups with increased concentration at the pore entrances. SBA-15 samples exhibited the typical H1 hysteresis loops, closing at a relative pressure above 0.5, irrespective of the amino and FITC content.

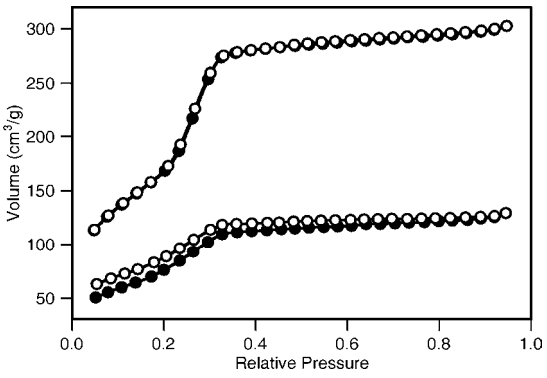

Figure 6. Nitrogen sorption isotherms of B-MCM-41(16) before (top) and after (bottom) FITC coupling. Desorption isotherms are shown by empty circles.

Trace water is a critical factor in the deposition of trialkoxysilanes, because silica acts as a drying agent, adsorbing even minute quantities of water. Even when working under suitably dry conditions, the adsorption of small quantities of water on the silica surface cannot be fully excluded when

depositing silanes from a solvent.[32] As a result, silane cross-linking is to be expected to some degree. The formation of silane clusters can lead to narrow pore sections and promote pore blocking. The degree of silane clustering can therefore be crucial in determining the accessibility of the grafted functional groups, especially when working with small one-dimensional mesopores.

3.3. The Role of Microporosity

It is well known that SBA-15 contains intrawall pores, which may constitute up to 30 % of the total porosity.[33] These intrawall pores include micropores[34-36] which provide connectivity between the primary mesopores.[37] It is reasonable to assume that grafting of APTMS also occurs in these smaller pores. Along the same line of reasoning, one can expect that a high degree of surface roughness leads to a larger fraction of inaccessible amino groups. It has recently been proposed that SBA-15 features a higher degree of pore surface roughness and a larger amount of surface defects than MCM-41.[38-40] Grafting of APTMS in the intrawall pores of SBA-15 is one possible explanation for the comparatively low overall FITC coupling yields. It is worth mentioning that at very low amino content (0.1 µmol/m^2) the FITC coupling yield dropped to 15 % (compared to close to 40 % for a corresponding MCM-41(16) sample). This is most likely a consequence of preferential intrawall micropore adsorption of APTMS.

The presence of micropores in SBA-15 leads to various problems in the determination of textural properties. A large micropore volume renders the standard BET analysis unreliable. Galarneau et al. proposed that in such cases the actual surface areas are much lower than what is obtained by BET analysis.[41] Regarding the results shown in Figure 4, this would imply a higher grafting density for the SBA-15 samples. However, we obtained a C_{BET} value of 120, which is well within the normal range of values expected for silica adsorbents and confirms that the system is in the field of application of the BET equation.[41,42]

Comparison of the *t*-curves of the unmodified SBA-15 and a corresponding amino-functionalized sample (A-SBA-15) reveals that the positive intercept of the *t*-curve of the parent SBA-15, which is an indication of microporosity, is no longer observed after APTMS grafting (Figure 7, top left). A distinct deviation from linearity at low *t*-values provides additional evidence for the presence of micropores in the parent SBA-15. Improved *t*-curve linearity is obtained after APTMS grafting. This effect can already be observed for a relatively low amino content of 0.1 µmol/m^2 (Figure 7, bottom left). In the case of analogous MCM-41(16) samples, the initial linear parts of the *t*-curves approach the origin independent of amino-functionalization, showing only a minor deviation from linearity (Figure 7, right). This is the expected behavior of a purely mesoporous material.

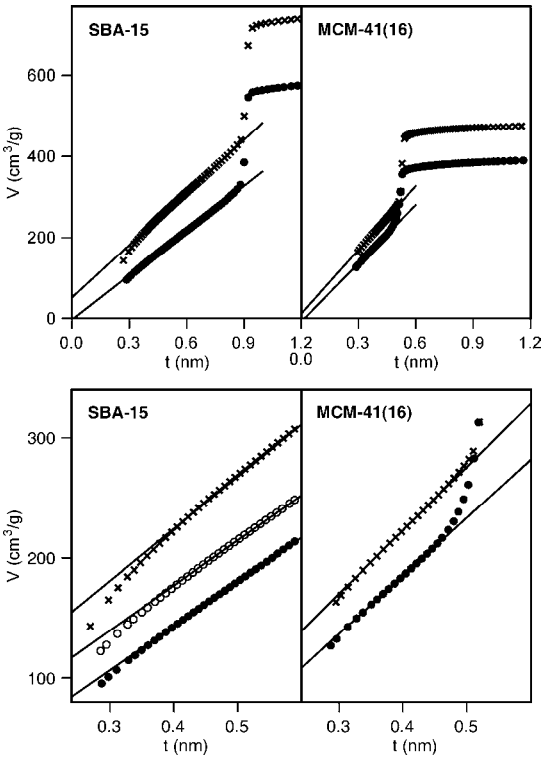

Figure 7. *t*-plots of SBA-15 and MCM-41(16) before (crosses) and after (solid circles) reaction with APTMS. The amino contents are 0.5 µmol/m^2. The bottom panels show a magnified view of the low pressure region. The empty circles represent a SBA-15 sample with an amino content of 0.1 µmol/m^2.

3.4. Nanoparticles of MCM-41

Functionalized mesoporous silica nanoparticles are of interest for medical and biological applications, such as cell labeling and magnetic resonance imaging,[43-45] as well as intracellular controlled-release delivery.[46-51] Due to the short channel lengths and the major contribution of the external surface to the total surface (Table 1), the postsynthetic functionalization behavior of mesoporous silica nanoparticles is substantially different from their micrometer-sized counterparts. Also note that only a small fraction of the total pore volume is attributed to the primary mesopores. The comparatively large value for V_{tot} is mainly due to interparticle spaces.[22] As can be seen from Figure 4, the overall accessibility of the grafted amino groups is excellent in the case of the MCM-41 nanoparticles, decreasing only slightly with increasing amino content.

The FITC coupling yields of fumed silica, SBA-15, MCM-41(12), and nano-MCM-41 remain virtually constant in the investigated range of amino contents (Figure 4). The absolute values of the respective yields are, however, significantly different. In the case of SBA-15, we have attributed the lower absolute yield to the presence of intrawall micropores. In the case of nano-MCM-41, part of the surface is concave, thereby reducing the overall accessibility compared to the non-porous fumed silica samples. Interestingly, the absolute FITC coupling yields are much lower for MCM-41(12) than for nano-MCM-41, despite their almost identical average pore diameter (Δd_{DFT} = 0.12 nm). This is most likely a consequence of the much smaller external surface area and longer channels of MCM-41(12).

3.5. Confinement

We have used the deposition of the free acid of fluorescein in combination

with a defined washing treatment to probe the confinement experienced by the adsorbed molecules. With pK_a values of 4.4 (neutral fluorescein) and 6.7 (fluorescein monoanion),[29] we can expect protonation of surface-grafted amino groups and subsequent electrostatic interaction with fluorescein mono- and dianions. The amount of retained fluorescein after the washing procedure is a measure for the confinement. The results of experiments conducted with B-*x* samples are shown in Figure 8. The samples are arranged according to their FITC coupling yield (white bars). The amount of adsorbed fluorescein (black bars) follows basically the same trend. This is not surprising, as a high accessibility, indicated by a large FITC coupling yield, results in a large number of immediately available adsorption sites for fluorescein. The MCM-41(16) sample is, however, a notable exception, retaining an uncharacteristically large amount of fluorescein after washing. In this case, it is particularly illustrative to compare the respective fluorescein/FITC ratios. With a value of 0.32, the MCM-14(16) sample clearly stands out. This can be explained on the basis that fluorescein molecules adsorbed in the channels are well protected against washing with ethanol, whereas in the case of MCM-41(12) or nano-MCM-41 most of the fluorescein molecules are located on or close to the exposed external surface. Similarly, a large pore diameter (SBA-15) leads to less confinement, rendering the

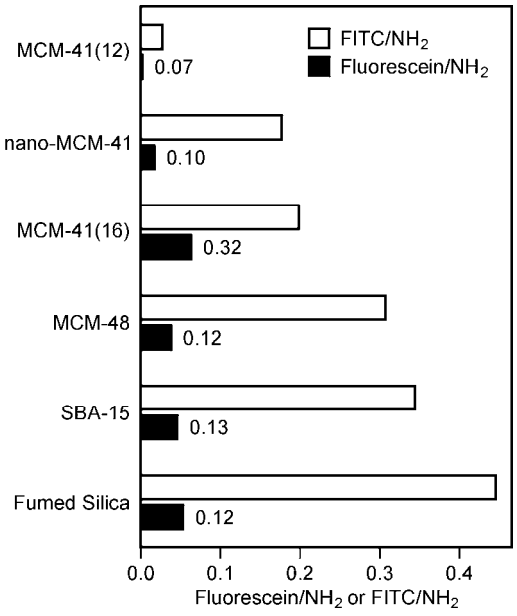

Figure 8. Relative amount of coupled FITC and adsorbed fluorescein for selected B-*x* samples. The respective fluorescein/FITC ratios are given by the values next to the black bars.

adsorbed fluorescein molecules susceptible to removal by washing. Based on the amount of retained fluorescein, adsorption in the intrawall micropores of SBA-15, which would provide strong confinement, is unlikely. Again it is interesting to note the differences between MCM-41(16) and MCM-48. The three-dimensional channel system apparently facilitates the removal of adsorbed fluorescein molecules.

A-*x* samples exhibited the same tendency, but featured smaller absolute amounts of adsorbed fluorescein (due to the smaller amount of grafted amino groups), hence rendering the analysis less reliable. Compared to the respective B-*x* samples, the C-*x* samples contained larger amounts of fluorescein after the

washing treatment. In agreement with the results shown in Figure 8, C-MCM-41(16) featured the highest fluorescein/FITC ratio.

4. Conclusions

Our conclusions concerning the accessibility of amino groups in the one-dimensional channel systems of MCM-41(12), MCM-41(16), and SBA-15 are illustrated by the schematic snapshots shown in Figure 9. The small pore diameter of MCM-41(12) facilitates the formation of blocked pores upon coupling of FITC to amino groups located at the pore entrances. The non-uniform distribution of the amino groups obtained after postsynthetic functionalization with APTMS further promotes pore blocking upon FITC coupling.

A slightly larger pore diameter (MCM-41(16)) provides higher FITC coupling yields, which are, however, extremely sensitive to the total amount of grafted amino groups. High amino contents increase the probability of bottleneck formation by coupling of FITC to densely grafted amino groups at the pore entrances.

The accessibility of the amino groups grafted to the mesopore walls of SBA-15 is comparable to the accessibility on an open surface. The large pore diameter provides access to sites deep inside the pores irrespective of the total amino content. However, the microporosity

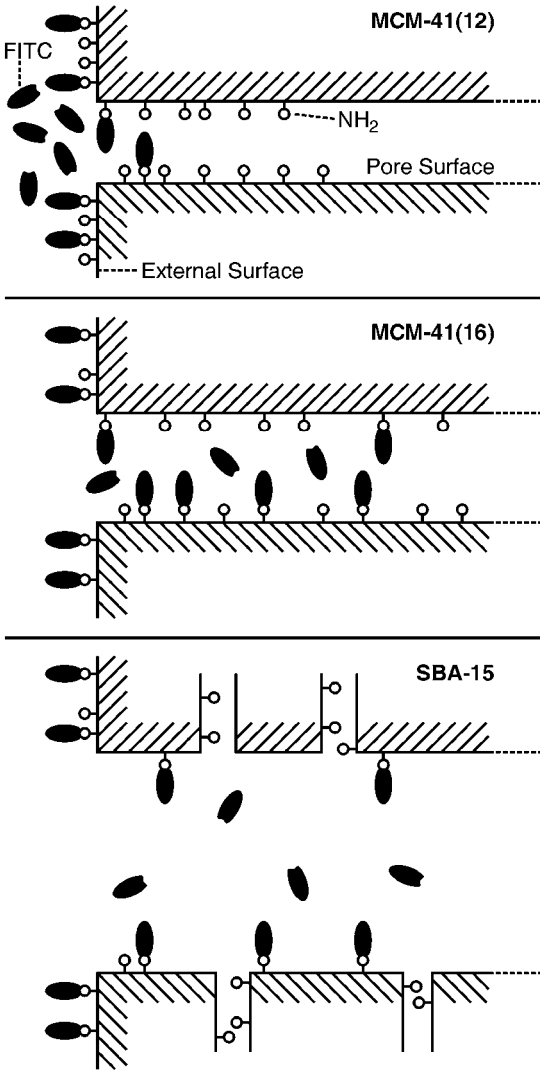

Figure 9. Schematic snapshots illustrating the labeling of functional groups grafted to MCM-41(12), MCM-41(16), and SBA-15.

and surface roughness of SBA-15 renders a considerable fraction of amino groups inaccessible.

When carrying out multistep functionalization reactions, such as grafting a precursor and subsequent coupling of a further functional moiety, the relationship between the amount of grafted precursor and the accessibility has to be taken into account. This is especially critical when the size of the

moiety to be coupled is similar to or larger than the pore radius.

In terms of providing accessible pore surface sites, a three-dimensional channel system is superior to a one-dimensional channel system of similar pore diameter. Contrary to MCM-48, MCM-41 suffers from a lack of alternative paths to a given pore surface site. However, if selective functionalization of the external surface and/or the pore entrances is required, as for example in the design of mesoporous silica based drug delivery devices,[46-56] one-dimensional channel systems are advantageous provided that the initial pore diameter is carefully adapted to obtain the desired functional group distribution. By providing excellent accessibility, short channels, as for example present in nanoparticles of MCM-41, complicate the independent functionalization of external and internal surfaces.

Finding a balance between the accessibility of the adsorption sites and confinement is crucial for the synthesis of mesoporous silica based host-guest systems. A high accessibility facilitates the inclusion of guest species, but the subsequent lack of confinement causes high leaching rates. Low accessibility can similarly lead to high leaching rates, as guest molecules are preferentially adsorbed at sites on the external surface and on the pore surface close to the pore entrances.

Acknowledgement

Financial support was provided by the European Commission through the Human Potential Program (Marie-Curie RTN Nanomatch, Grant No. MRTN-CT-2006-035884) and by the Swiss National Science Foundation (Project 200020-117591). We would like to thank Stefan Ritter (Paul Scherrer Institut) for SEM measurements and Nando Gartmann for the determination of extinction coefficients.

References

(1) Rohlfing, Y.; Wöhrle, D.; Rathouský, J.; Zukal, A.; Wark, M. *Stud. Surf. Sci. Catal.* **2002**, *142*, 1067.

(2) Antochshuk, V.; Olkhovyk, O.; Jaroniec, M.; Park, I.-S.; Ryoo, R. *Langmuir* **2003**, *19*, 3031.

(3) Acosta, E. J.; Carr, C. S.; Simanek, E. E.; Shantz, D. F. *Adv. Mater.* **2004**, 16, 985.

(4) Descalzo, A. B.; Jimenez, D.; Marcos, M. D.; Martínez-Máñez, R.; Soto, J.; El Haskouri, J.; Guillém, C.; Beltrán, D.; Amorós, P.; Borrachero, M. V. *Adv. Mater.* **2002**, *14*, 966.

(5) Rosenholm, J. M.; Lindén, M. *Chem. Mater.* **2007**, *19*, 5023.

(6) Beck, J. S.; Vartuli, J. C.; Roth, W. J.; Leonowicz, M. E.; Kresge, C. T.; Schmitt, K. D.; Chu, C. T.-W.; Olson, D. H.; Sheppard, E. W.; McCullen, S. B.; Higgins, J. B.; Schlenker, J. L. *J. Am. Chem. Soc.* **1992**, *114*, 10834.
(7) Kresge, C. T.; Leonowicz, M. E.; Roth, W. J.; Vartuli, J. C.; Beck, J. S. *Nature* **1992**, *359*, 710.
(8) Zhao, D.; Feng, J.; Huo, Q.; Melosh, N.; Fredrickson, G. H.; Chmelka, B. F.; Stucky, G. D. *Science* **1998**, *279*, 548.
(9) Zhao, D.; Huo, Q.; Feng, J.; Chmelka, B. F.; Stucky, G. D. *J. Am. Chem. Soc.* **1998**, *120*, 6024.
(10) (a) Ritter, H.; Nieminen, M.; Karppinen, M.; Brühwiler, D.*Microporous Mesoporous Mater. in press*. (b) Udenfriend, S.; Stein, S.; Böhlen, P.; Dairman, W.; Leimgruber, W.; Weigele, M. *Science* **1972**, *178*, 871.
(11) Salmio, H.; Brühwiler, D. *J. Phys. Chem. C* **2007**, *111*, 923.
(12) Taguchi, A.; Schüth, F. *Microporous Mesoporous Mater.* **2005**, 77, 1.
(13) Clark, J. H.; Macquarrie, D. J.; Tavener, S. J. *Dalton Trans.* **2006**, 4297.
(14) Cides da Silva, L. C.; dos Santos, L. B. O.; Abate, G.; Cosentino, I. C.; Fantini, M. C. A.; Masini, J. C.; Matos, J. R. *Microporous Mesoporous Mater.* **2008**, *110*, 250.
(15) Fryxell, G. E.; Mattigod, S. V.; Lin, Y.; Wu, H.; Fiskum, S.; Parker, K.; Zheng, F.; Yantasee, W.; Zemanian, T. S.; Addleman, R. S.; Liu, J.; Kemner, K.; Kelly, S.; Feng, X. *J. Mater. Chem.* **2007**, *17*, 2863.
(16) Yoshitake, H. *New J. Chem.* **2005**, *29*, 1107.
(17) Ho, K. Y.; McKay, G.; Yeung, K. L. *Langmuir* **2003**, 19, 3019.
(18) Nooney, R. I.; Kalyanaraman, M.; Kennedy, G.; Maginn, E. J. *Langmuir* **2001**, *17*, 528.
(19) Liu, A. M.; Hidajat, K.; Kawi, S.; Zhao, D. Y. *Chem. Commun.* **2000**, 1145.
(20) Brühwiler, D.; Frei, H. *J. Phys. Chem. B* **2003**, *107*, 8547.
(21) Xu, J.; Luan, Z.; He, H.; Zhou, W.; Kevan, L. *Chem. Mater.* **1998**, *10*, 3690.
(22) Suzuki, K.; Ikari, K.; Imai, H. *J. Am. Chem. Soc.* **2004**, *126*, 462.
(23) Brunauer, S.; Emmett, P. H.; Teller, E. *J. Am. Chem. Soc.* **1938**, *60*, 309.
(24) Kruk, M.; Jaroniec, M.; Ryoo, R.; Kim, J. M. *Microporous Mater.* **1997**, *12*, 93.
(25) Sayari, A.; Liu, P.; Kruk, M.; Jaroniec, M. *Chem. Mater.* **1997**, *9*, 2499.
(26) Ravikovitch, P. I.; Domhnaill, S. C. O.; Neimark, A. V.; Schüth, F.; Unger, K. K. *Langmuir* **1995**, *11*, 4765.
(27) Ravikovitch, P. I.; Neimark, A. V. *Colloid Surf. A: Physicochem. Eng. Aspect* **2001**, *187-188*, 11.
(28) Lippens, B. C.; de Boer, J. H. *J. Catal.* **1965**, *4*, 319.
(29) Martin, M. M.; Lindqvist, L. *J. Lumin.* **1975**, *10*, 381.
(30) Burleigh, M. C.; Markowitz, M. A.; Spector, M. S.; Gaber, B. P. *J. Phys. Chem. B* **2001**, *105*, 9935.
(31) Li, C.; Yang, J.; Shi, X.; Liu, J.; Yang, Q. *Microporous Mesoporous Mater.* **2007**, *98*, 220.

(32) Kanan, S. M.; Tze, W. T. Y.; Tripp, C. P. *Langmuir* **2002**, *18*, 6623.
(33) Ravikovitch, P. I.; Neimark, A. V. *J. Phys. Chem. B* **2001**, *105*, 6817.
(34) Ryoo, R.; Ko, C. H.; Kruk, M.; Antochshuk, V.; Jaroniec, M. *J. Phys. Chem. B* **2000**, *104*, 11465.
(35) Impéror-Clerc, M.; Davidson, P.; Davidson, A. *J. Am. Chem. Soc.* **2000**, *122*, 11925.
(36) Galarneau, A.; Cambon, H.; Di Renzo, F.; Ryoo, R.; Choi, M.; Fajula, F. *New J. Chem.* **2003**, *27*, 73.
(37) Jun, S.; Joo, S. H.; Ryoo, R.; Kruk, M.; Jaroniec, M.; Liu, Z.; Ohsuna, T.; Terasaki, O. *J. Am. Chem. Soc.* **2000**, *122*, 10712.
(38) Ravikovitch, P. I.; Neimark, A. V. *Langmuir* **2006**, *22*, 11171.
(39) Shenderovich, I. G.; Buntkowsky, G.; Schreiber, A.; Gedat, E.; Sharif, S.; Albrecht, J.; Golubev, N. S.; Findenegg, G. H.; Limbach, H.-H. *J. Phys. Chem. B* **2003**, *107*, 11924.
(40) Fenelonov, V. B.; Derevyankin, A. Y.; Kirik, S. D.; Solovyov, L. A.; Shmakov, A. N.; Bonardet, J.-L.; Gedeon, A.; Romannikov, V. N. *Microporous Mesoporous Mater.* **2001**, *44-45*, 33.
(41) Galarneau, A.; Cambon, H.; Di Renzo, F.; Fajula, F. *Langmuir* **2001**, *17*, 8328.
(42) Rouquerol, F.; Rouquerol, J.; Sing, K. *Adsorption by powders & porous solids*; Academic Press, San Diego, CA, 1999.
(43) Wu, S.-H.; Lin, Y.-S.; Hung, Y.; Chou, Y.-H.; Hsu, Y.-H.; Chang, C.; Mou, C.-Y. *ChemBioChem* **2008**, *9*, 53.
(44) Taylor, K. M. L.; Kim, J. S.; Rieter, W. J.; An, H.; Lin, W.; Lin, W. *J. Am. Chem. Soc.* **2008**, *130*, 2154.
(45) Lin, Y.-S.; Tsai, C.-P.; Huang, H.-Y.; Kuo, C.-T.; Hung, Y.; Huang, D.-M.; Chen, Y.-C.; Mou, C.-Y. *Chem. Mater.* **2005**, *17*, 4570.
(46) Lu, J.; Liong, M.; Zink, J. I.; Tamanoi, F. *Small* **2007**, *3*, 1341.
(47) Torney, F.; Trewyn, B. G.; Lin, V. S.-Y.; Wang, K. *Nature Nanotechnol.* **2007**, *2*, 295.
(48) Slowing, I.; Trewyn, B. G.; Lin, V. S.-Y. *J. Am. Chem. Soc.* **2007**, *129*, 8845.
(49) Slowing, I.; Trewyn, B. G.; Giri, S.; Lin, V. S.-Y. *Adv. Funct. Mater.* **2007**, *17*, 1225.
(50) Lu, J.; Liong, M.; Sherman, S.; Xia, T.; Kovochich, M.; Nel, A. E.; Zink, J. I.; Tamanoi, F. *Nanobiotechnol.* **2007**, *3*, 89.
(51) Slowing, I.; Trewyn, B. G.; Lin, V. S.-Y. *J. Am. Chem. Soc.* **2006**, *128*, 14792.
(52) Mal, N. K.; Fujiwara, M.; Tanaka, Y.; Taguchi, T.; Matsukata, M. *Chem. Mater.* **2003**, *15*, 3385.
(53) Mal, N. K.; Fujiwara, M.; Tanaka, Y. *Nature* **2003**, *421*, 350.
(54) Yang, Q.; Wang, S.; Fan, P.; Wang, L.; Di, Y.; Lin, K.; Xiao, F.-S. *Chem. Mater.* **2005**, *17*, 5999.

(55) Hernandez, R.; Tseng, H.-R.; Wong, J. W.; Stoddart, J. F.; Zink, J. I. *J. Am. Chem. Soc.* **2004**, *126*, 3370.
(56) Lai, C.-Y.; Trewyn, B. G.; Jeftinija, D. M.; Jeftinija, K.; Xu, S.; Jeftinija, S.; Lin, V. S.-Y. *J. Am. Chem. Soc.* **2003**, *125*, 4451.

TOC Graphic and Summary:

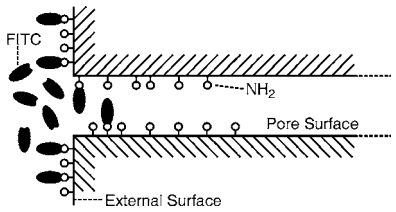

The accessibility of amino groups in postsynthetically functionalized mesoporous silica (MCM-41, MCM-48, SBA-15) is investigated by determining the fluorescein isothiocyanate coupling yields, which are found to depend on the pore diameter, particle size, channel system dimensionality, and channel wall porosity.

Curriculum Vitae

Family name: Ritter (née Salmio)

First names: Hanna Taina Katariina

Born: 28.11.1979 in Espoo, Finland

Nationality: Finnish

Education:

- Tapiolan lukio (High School), Espoo, Finland, 08/1995-05/1998
- Helsinki University of Technology, Espoo, Finland, Department of Chemical Technology, Inorganic Chemistry 09/1998-02/2004
- Master thesis: “Atomic Layer Deposition as Coating Method for Plastic and Metal Parts“
- PhD student at the University of Zürich since 07/2005

List of Publications and Conference Contributions

Publications

Distribution of Amino Groups on a Mesoporous Silica Surface after Submonolayer Deposition of Aminopropylsilanes from an Anhydous Liquid Phase

H. Salmio, D. Brühwiler, *J. Phys. Chem. C* **111** (2007) 923-929.

A Comparative Study of the Functionalization of Mesoporous Silica MCM-41 by Deposition of 3-Aminopropyltrimethoxysilane from Toluene and from the Vapor Phase

H. Ritter, M. Nieminen, M. Karppinen, D. Brühwiler, *Microporous Mesoporous Mater.*, in press.

Accessibility of Grafting Sites in Postsynthetically Modified Mesoporous Silica

H. Ritter, D. Brühwiler, submitted.

Functionalized Silicate Nanochannels: Towards Applications in Drug Delivery and Solar Energy Conversion

D. Brühwiler, H. Ritter, J. H. Ramm, L.-Q. Dieu, C. Bauer, I. Dolamic, N. Gartmann, *Chimia*, in press.

Posters

Swiss Chemical Society Fall Meeting, Zürich 13.10.2006:

Distribution of Grafted Aminopropylalkoxysilanes on the Surface of Mesoporous Silica MCM-41

H. Salmio, D. Brühwiler

Swiss Chemical Society Fall Meeting, Lausanne 12.9.2007:

Positioning of Functional Groups on Mesoporous Silica Surfaces

H. Ritter, D. Brühwiler

Convenient Room Temperature Synthesis of High Quality Mesoporous Silica MCM-41

H. Ritter, D. Brühwiler

Swiss Chemical Society Fall Meeting, Zürich 11.9.2008:

Postsynthetic Modification of Mesoporous Silica: Methods, Tools, and Perspectives,

H. Ritter, J. H. Ramm, N. Gartmann, D. Brühwiler